NASA Contractor Report 3405

An Experimental Investigation of the Aerodynamics and Cooling of a Horizontally-Opposed Air-Cooled Aircraft Engine Installation

Stan J. Miley and Ernest J. Cross, Jr.
Texas A&M University
College Station, Texas

John K. Owens
Mississippi State University
Mississippi State, Mississippi

David L. Lawrence
Turbo West Corporate Aircraft Center
Broomfield, Colorado

Prepared for
Langley Research Center
under Grant NSG-1083

NASA
National Aeronautics
and Space Administration

**Scientific and Technical
Information Branch**

1981

SUMMARY

A flight test based research program was performed to investigate the aerodynamics and cooling of a horizontally-opposed aircraft engine installation. Specific areas investigated were the internal aerodynamics and cooling mechanics of the installation, inlet aerodynamics, and exit aerodynamics. The applicable theory and current state-of-the-art are discussed for each area. Flight test and ground test techniques for the development of the cooling installation and the solution of cooling problems are presented.

The results show that much of the internal aerodynamics and cooling technology developed for radial engines are applicable to horizontally-opposed engines. Correlation is established between engine manufacturer's cooling design data and flight measurements of the particular installation. Also, a flight test method for the development of cooling requirements in terms of easily measurable parameters is presented. The impact of inlet and exit design on cooling and cooling drag is shown to be of major significance.

INTRODUCTION

The research program, which is reported herein, was established to perform an exploratory investigation of the cooling drag associated with reciprocating engine powered

general aviation aircraft. As work progressed, it became apparent that attention should be focused on the engine cooling installation aerodynamics which are manifested as cooling drag. An associated area of concern, inadequate engine cooling, particularly for supercharged engines at altitude, is also related to installation aerodynamics. Poor aerodynamic design not only results in excessive cooling drag, but also can result in poor cooling. The standard cure for inadequate cooling is to operate the engine at higher-than-necessary fuel flows. Consequently, both situations result in reduced fuel efficiency.

Cooling installation aerodynamics is concerned with the behavior of the airflow system required for cooling by air-cooled reciprocating aircraft engines. The components which make up the system are dependent on the particular engine geometry. Figure 1 illustrates four basic engine geometries and the associated cooling airflow system configurations. Three of the four geometries, the in-line, the vee, and the horizontally-opposed, use the same system, consisting of an inlet, high pressure plenum, low pressure plenum, and exit. The first three components are necessary because the engine geometry requires the cooling airflow to pass through the engine perpendicular to the flight path. The radial engine geometry, however, requires a relatively simpler system consisting primarily of a cylindrical cowl. The airflow

passing through the engine remains parallel to the flight path. The cowl functions as an external baffle, forcing the captured airflow through the cooling fins. It also incorporates the cooling flow exit in its structure.

Cooling installation aerodynamics involve two problem areas. The first is concerned with the character of the flow through the engine's cooling fins and the resulting heat transfer to this flow. The technology developed for radial engines in this area is also applicable to horizontally-opposed engines as well as in-line and vee geometries. The second problem area is concerned with the external and internal flow of the installation system. The existing technology here is applicable only to similar geometries. The large amount of data regarding radial engine cowl/nacelle design is of little use to horizontally-opposed installations.

As part of the research program, an extensive literature survey was performed to identify material applicable to the cooling flow/heat transfer aerodynamics and cowl external internal aerodynamics problem areas. Over five hundred references have been collected. The results of the literature survey will be published as a separate report.

The literature is dominated by the development of radial engines and mainly encompasses the period 1930-1945. After this time, interest turned to the development of gas turbine powerplants, and air-cooled engine related technology essentially disappeared from print. All aspects of the problem

areas are well covered except for the cowl aerodynamics of the non-radial geometries. Of the five hundred plus citations during the radial development period, only six (references 1-6) concern in-line or vee cowl aerodynamics. These are, for the most part, also applicable to the horizontally-opposed cowl geometry. In recent years, attention has been given to horizontally-opposed installations (references 7-11).

Except for the literature survey, the research program was experimental and involved a series of flight test investigations. One ground test investigation on the test aircraft was also conducted. The first test program attempted to measure the cooling drag of a single engine aircraft. The remaining programs investigated various aspects of the installation aerodynamics utilizing a twin engine aircraft.

The investigators wish to acknowledge the important contributions by the general aviation industry to this research program. In particular, the donation of the aircraft and propulsion system for use in this program by Piper Aircraft, Avco Lycoming, and Hartzell Propeller is greatly appreciated. Also, the participation by engineering representatives from Avco Lycoming, Beech, Cessna, Grumman American, Mooney, Piper, Rockwell, and Teledyne Continental for program critique and review was an important asset.

SYMBOLS

a	effective orifice area, m^2
$a_{1,2,3}$	coefficients of least squares surface used in equation (5)
b	exponent of orifice power law
$c_{1,2,3,4}$	constants of heat transfer power laws used in equations (8) - (11)
C_p	pressure coefficient $\frac{p - p_\infty}{q_\infty}$
H	heat transferred per unit time, joule/sec
I	indicated engine power, kw
k,l,m,n	exponents of power laws in development of cooling correlation relation, equations (8) - (13)
p	static pressure, N/m^2
p_∞	free stream static pressure, N/m^2
q_∞	free stream dynamic pressure, N/m^2
T_a	ambient (free stream) temperature, °C
T_{EGT}	exhaust gas temperature, °C
T_{ex}	temperature of cooling flow exiting the engine, °C
T_g	effective combustion gas temperature, °C
T_h	cylinder head temperature, °C
T_{h_A}	average of the 6 engine cylinder head temperatures, °C
T_{h_6}	cylinder head temperature of cylinder number 6, °C

T_{up}	temperature of cooling flow in upper plenum, at rear of engine, °C
T^*	heat transfer temperature ratio
T^*_A	heat transfer temperature ratio based on use of T_{h_A} for cylinder head temperature
T^*_6	heat transfer temperature ratio based on use of T_{h_6} for cylinder head temperature
V_i	inlet velocity, m/sec
V_o	flow velocity approaching inlet, m/sec
w	cooling air mass flow, kg/sec
W_c	charge flow of fuel and air through the engine, kg/sec
x,y	coordinates used for integration in the determination of cooling air mass flow, equation (5), m
Δp	engine baffle pressure drop, N/m^2
ρ	air density, kg/m^3
σ	density ratio relative to standard sea level
σ_{ex}	density ratio of cooling air flow exiting the engine relative to standard sea level

MEASUREMENT OF COOLING DRAG

The objective of this program was to ascertain if reliable measurements of cooling drag could be obtained using flight test techniques. If so, then follow-on testing would attempt to identify the contributions of specific installation components to the cooling drag.

The aircraft used for this program was a Beech T-34B (Figure 2) obtained on loan from the U.S. Navy. The cooling installation of the aircraft is unique by current practice in that exhaust ejector pumps, or augmentors, are used at the exit. The ejector tubes are visible in the figure extending through the bottom of the fuselage, near the leading edge of the wing. The drag measurements were made using the technique of feathered sinks, i.e., engine stopped, propeller feathered, gliding flight. A special full-feathering propeller was installed for this program.

All flights were performed in the early morning and in calm air. Airspeed deviations for good data runs were kept to within one knot. A stabilized glide of at least 1,500 meters in altitude was required for an acceptable data run. Configurations which were tested included inlets open, inlets closed, ejector tubes open, tubes restricted, and tubes closed. The results of the drag measurements are given in Table I.

The drag associated with the cooling flow through the installation is indicated to be seven percent of the no-flow aircraft drag. Drag calculations based on the momentum loss of the internal flow yielded a value of six percent of the no-flow drag. These values are similar to those of reference 11 for a twin engine configuration.

As a result of this first drag measurement program, it became evident that the drag levels of interest were barely resolvable through flight test. The follow-on program to investigate the drag contributions of specific installation system components was abandoned in favor of studying the associated aerodynamics. The point-of-view here is that cooling drag can be reduced to the minimum necessary level by good aerodynamic design of the cooling installation. The emphasis of the research program thus shifted from a traditional trial-and-error drag clean-up approach, to a more scientific approach of investigating and understanding the various aerodynamic effects involved in the operation of the cooling installation.

COOLING INSTALLATION AERODYNAMICS PROGRAM

Test Aircraft and Cooling Installation

The test aircraft used in the program was a Piper PA-41P prototype pressurized Aztec. The aircraft is shown in Figure 3. The engines were turbosupercharged with a sea level rating of 201 kw. The aircraft was capable of operating at altitudes in excess of 7,000 meters. The starboard power plant was used for the various studies of the program.

A schematic of the cooling installation of the PA-41P test aircraft is shown in Figure 4. Particular points of

reference are denoted by numbers. This arrangement is typical of most horizontally-opposed engine installations. The source of cooling flow is represented by point (1). The flow has been acted on by the propeller and is no longer at free stream conditions. The cooling air enters the inlet (2) and is conveyed to the upper plenum (3). It then flows through the cooling fin passages into the lower plenum (4) and is exhausted through the exits (5). This configuration, where the cooling air flows from the upper to the lower plenum, is known as downdraft cooling. Updraft cooling configurations are also available, where the air flows from bottom to top. The location of exits is generally on the lower surface of the cowl, although some arrangements exist with the exits on the upper surface.

Cooling Installation Operation and Design

Cooling requirements. The function of the cooling installation is to conduct sufficient air flow to cool the engine under specified operating conditions. The airflow requirements and engine orifice characteristics are normally supplied by the engine manufacturer in a form similar to Figure 5. The cooling requirements are determined from the right side of the graph. The operation condition is specified in terms of air temperature, engine power, and cylinder head temperature (CHT); the required airflow is then read from the ordinate. The engine orifice characteristics refer to the

relationship between the rate of flow through the cooling fin passages and the decrease in pressure which accompanies this. This pressure decrease is called the baffle pressure drop, which relates to the intercylinder baffle plates used on most air-cooled engines.

Theory of operation. Figure 6 gives a schematic of the cooling installation model. The source of the cooling air (1) is the free stream with a dynamic pressure head corresponding to the airspeed of the aircraft. In actuality, the pressure head is modified by the propeller. The inlet (2) captures the cooling air, partially converts the dynamic head to static pressure, and conveys the flow to the upper plenum. The upper plenum (3) serves as a reservoir for the engine and auxiliary cooling flow. The cooling air at this point should be at stagnation conditions with full recovery of the dynamic head. The flow then proceeds through the cooling fin passages of the engine into the lower plenum (4). If the upper plenum is used to supply auxiliary cooling (7), then part of the air flow takes this path. In passing from region (3) to region (4), the air is heated and the density changes accordingly. The heated air then accelerates through the exit (5) such that its static pressure is equal to the local external (6) static pressure of the flow. Through the use of a hinged flap, both the exit area and the external exit pressure can be varied to control the flow rate.

In actuality, the pressure recovery in the upper plenum may be as low as fifty percent of the free stream dynamic pressure, due to flow losses through the inlet. Also, insufficient plenum volume results in finite velocities, consequently, the flow is not evenly distributed over the engine face nor is the transition from horizontal flow to vertical flow through the cooling passages accomplished efficiently.

Cooling installation design. Procedures for the design analysis are given in references 7 and 12. They are summarized here.

The design of the cooling installation is based on one-dimensional subsonic compressible flow theory. Starting with the dynamic pressure head in front of the inlet [point (1) in Figure 6], the upper plenum pressure (3) is determined by applying a pressure recovery factor which accounts for the amount of diffusion developed by the inlet (2) and the flow losses incurred between (1) and (3). There is a question as to whether the plenum static pressure or the total pressure should be used here. This will be addressed in a later section. The lower plenum pressure (4) is determined by the baffle pressure drop associated with the required cooling air flow rate. As indicated in Figure 5, the pressure drop is altitude dependent. The flow density in the lower plenum is determined from the temperature rise across the engine. This information heretofore has not been supplied by engine

manufacturers, and estimates based on experience must be used. Typical values range from 50°C to 70°C. The exit area (5) is then sized to accelerate the flow so that its static pressure is the same as the local external flow (6). The exit area acts as the system throttle in that the flow rate and associated pressure drops will adjust so that the exit pressure matches the external pressure. For a given flight condition, expanding the exit area increases the flow rate, and conversely.

The design problem is made difficult by the wide variation in horizontally-opposed aircraft engine configurations. Of prime concern here are the upper and lower plenum volumes. With the oil sump located on the bottom of the engine, installations tend to have relatively large plenum volumes below and relatively small plenum volumes on top. The character of the flow in these respective regions is affected by the location and configuration of the induction and exhaust lines, and the presence of an inter-cooler, alternator, and/or propeller governor. This leads to some engine dependent empiricism in the determination of pressure recoveries and flow losses. Also, the differences between the test configuration, for which the cooling requirements are determined, and the installation configuration create uncertainties as to the application of the requirements data. A typical cooling requirements test configuration is shown in Figure 7. This

is the ideal cooling configuration in that a true plenum exists on top of the engine and the cooling air is distributed uniformly across the upper engine face. The temperature of the cooling air is uniform and the plenum pressure is a true measure of the baffle pressure drop. For the installation configuration in Figure 4, the flow is highly nonuniform, the temperature of the flow rises as it progresses towards the rear, and the relationship between this plenum pressure and that of Figure 7 is open to question.

Cooling Installation and Aerodynamics Investigations

The objective of the Installation Aerodynamics Program was to investigate the various aerodynamic effects involved in the operation of the cooling installation. This was done in the context of the aforediscussed design problems in the previous section. Three areas were studied: internal flow mechanics, inlet effects, and exit effects. The internal flow investigation dealt with two problem areas. The first consisted of an evaluation of the various methods of installation flow pressure measurement in current use by the general aviation industry. The second problem area dealt with the engine orifice characteristics and the correlation between installation measurements and test cell measurements. Much was drawn from the radial engine cooling correlation work performed by NACA.

The inlet and exit studies investigated the effects of some basic design parameters on installation performance. Four different inlet configurations were studied in terms of both the external flow and internal flow. Exit design parameters investigated included exit area, location, and cowl flap geometry.

INTERNAL FLOW STUDIES

Internal Flow Instrumentation Investigation

The objectives of the internal flow instrumentation investigation were to measure the flow temperature and pressure distributions and pressure losses through the installation, and to evaluate different techniques for measuring the engine baffle pressure drop. Total pressure surveys, utilizing Kiel tubes, were taken at several longitudinal stations in the high pressure plenum. These locations, illustrated in Figure 8, were at the rear of the inlet duct in front of the leading cylinders, and above each cylinder on its center line. Total pressure Kiel tubes were also located in the exit ducts. The inlet Kiel tubes are shown in Figure 9, and the cylinder mounted tubes are shown in Figure 10. Also shown in Figure 10 are the plenum temperature probes which consist of a thermocouple sensor and radiation shield. The temperature probe locations are

given in Figure 8.

The pressure distribution on the upper engine face and the baffle pressure drop across the engine were measured by a number of different probes and methods. Representative techniques of both airframe and engine manufacturers were included. Figure 11 illustrates the various probe configurations and locations. All probes shown in Figure 11(a), except the baffle button probe (1), are 1.6 mm diameter open-end total pressure tubes. The tube opening was internally chamfered to a 60 degree included angle. This increased the probe angularity insensitivity to approximately 30 degrees. The vertical positions of these probes are shown in Figure 11(b). The cylinder barrel tubes (2) and cylinder head tubes (3) were located vertically on the center line of the cylinder. Cylinder head tubes (4) were located 9.5 mm below the local fin height on the exhaust stack side of the cylinder. Cylinder head tubes (5) were located between adjacent cylinders, flush with the top of the local fins. Referring to Figure 10, the (5) tubes were exposed to the engine face pressure without fin passage losses. The "baffle button" probes (1), Figure 11(c), consist of a brass roundhead machine screw inserted through the intercylinder baffle at the base of barrels. The screw is drilled for, and fitted with, a 1.6 mm tube for connection to pressure measuring instrumentation. The head of the screw

is filled and smoothed. Piccolo tubes, Figures 8 and 11(d), were mounted in the upper and lower plenums to provide an integrated or averaged measurement of the static pressure. The upper plenum static pressure was also measured by multi-element pressure belts. As shown in Figure 11(e), the belts were attached to the inside upper surface of the cowl. Hole spacing between belt elements was 5 cm.

The pressure in the lower plenum was measured by four different probe configurations. Common practice here is to use total pressure tubes located so that they are shielded from any local high flow velocities. The total probe configurations used are shown in Figures 11(c) and 11(f). A set of baffle-shield probes was located in the lower plenum at each of the baffle button positions (1) in Figure 11(a). Fin-shield probes were located adjacent to each of the cylinder head upper plenum pressure probes (5). All lower plenum pressure probes, of the same configuration, were manifolded together to give a single averaged measurement for that configuration. The fourth probe configuration used was the aforedescribed piccolo.

The thermocouple temperature probe locations in the upper plenum are shown in Figure 8. Two additional probes were positioned in the lower plenum, one at each exit.

The pressure and temperature data were recorded on an analog tape recorder using a serial multiplexing format. A

total of 144 channels of pressure data and 48 channels of temperature data were available. An 80-tube photomanometer system was also used for additional pressure data when required.

The purpose of this study was to evaluate different probes and techniques for measuring the engine face, upper plenum and lower plenum pressures. A fundamental problem involved in these measurements is the question of whether one is measuring a static or a total pressure. If the plenum volume is large, then for the range of cooling air flow rates encountered, the two pressures are the same. If, however, one side of the engine is tightly cowled and the plenum volume is correspondingly small, there will be a distinct difference between static and total pressure. For the PA-41P test aircraft, the lower plenum was large and the upper plenum was relatively small. The results should be interpreted accordingly.

Figure 12 presents a comparison of the different lower plenum pressure measurements. The data represent different airspeeds, altitudes, and cowl flap settings. All pressures are referenced to free-stream total pressure. As indicated in Figure 12, all methods give essentially the same measure. The fin-shield probes give a reading 3% below the piccolo and the baffle-shield-down probes give a reading 2% above. The baffle-shield-up probes read the same as the piccolo. The

differences are felt to be due to position error type effects, i.e., effects associated with the location and orientation of the open end of the probe. From the standpoint of simplicity, the piccolo tube appears to be the best method of measuring the lower plenum pressure. However, as will be shown, if the plenum volume were small, consideration should be given to the baffle-shield-up probes.

The volume of the upper plenum is measurably smaller than the lower plenum. The cross-sectional area of the upper plenum is approximately 650 cm^2, and this combined with the cooling air flow rate results in flow velocities in the neighborhood of 15 m/sec. There is correspondingly a difference between static and total pressure in the region. Pressure data from the engine face probes and the belts are presented in Figure 13 for two different inlets. The data are given in pressure coefficient form referenced to free-stream static pressure. The abscissa represents the longitudinal coordinate referenced to the cylinder number. The ordinate intersection is the front of the engine; to the right is progressing towards the rear down the right bank of cylinders, and to the left is progressing down the left bank of cylinders.

Several observations can be made regarding the data in Figure 13. All pressure measurement methods were subject to position error effects. This is due to having finite flow velocities of irregular directions in the plenum. The

increased scatter for the climb condition is believed to be due to the corresponding change in the propeller slipstream flow. The scatter pattern also varies according to the different inlets tested. Again, this indicates a change in the character of the flow through the plenum.

Since the pressure belt measures the static pressure variations, it is evident that the pressure at the engine face is also static. There is no effective recovery of the plenum dynamic pressure. The increase in static pressure from front to rear is consistent with the diffusion effect accompanying the progressive passage of the flow through the engine to the lower plenum. The left side of the plenum (cylinders 2-4-6) behaves differently from the right side (cylinders 1-3-5). This asymmetrical behavior showed itself in a number of different measurements and is believed to be due to inlet flow blockage by the propeller governor. The governor is visible inside the inlet shown in Figure 9.

The baffle button probes (1) provide the most reliable measure of the engine face pressure. The piccolo tube indicates low. It is possible that the piccolo reading may be raised through biasing the tube by cutting it short so that it does not extend to the front cylinders where the flow velocity is highest.

In summary, results of this investigation show that the baffle button probe gives the most reliable measure of engine

face pressure. If the engine is not equipped with inter-cylinder baffles, then a shortened piccolo tube will work equally well. The pressure in the lower plenum is measured accurately by the piccolo. However, if this volume is small, then the baffle-static-up probe configuration should be considered.

Engine Orifice Characteristics

Background. Engine orifice characteristics relate the cooling air mass flow through the engine's fin passages to the pressure drop across the engine. The relationship is similar to orifice flow, which is described by

$$w = a\sqrt{\rho \Delta p}. \qquad (1)$$

A more general form of this relationship is given by the power law

$$w = a\ (\rho \Delta p)^{b} \qquad (2)$$

In equation (1), "b" has the value of b = 0.5.

A study of air-cooled engine development shows that the power law relationship of equation (2) is a valid representation of engine orifice characteristics. The constant of proportionality "a" functions as an equivalent orifice area

in that it tends to vary directly with cooling fin spacing and total passage area. The exponent "b" is a function of fin spacing and intercylinder baffling. Fin spacing tests reported in reference 13 show "b" ranging from b = 0.78 for 0.5 mm spacing to b = 0.50 for 5 mm spacing. Available data for current horizontally-opposed aircraft engines has "b" ranging from b = 0.52 to b = 0.58. Values of "a" vary over a much wider range, depending on geometric engine size and number of cylinders.

The values of "a" and "b" for a particular engine model are determined by ground test, using a system similar to that shown in Figure 7. Cooling air mass flows and corresponding baffle pressure drops are measured over the range of interest. The coefficients "a" and "b" are then determined by rewriting equation (2) in logarithmic form,

$$\ln (w) = b \cdot \ln (\rho \Delta p) + \ln (a) \qquad (3)$$

and applying linear regression techniques.

Once determined, the coefficients can be used with equation (2), in theory, to measure the cooling air flow through the engine in flight. This approach is necessary because aircraft engine installations do not lend themselves to direct cooling air mass flow measurements, whereas the corresponding engine baffle pressure drop is readily

measureable. For the purpose of flight cooling flow measurements then, the engine is used as an orifice meter. The validity of such measurements depend on two considerations: altitude and engine heating effects on the ground test determined orifice characteristics; and correlation between the baffle pressure drop measurements of the cooling flow for the aircraft installation configuration and for the ground test configuration. The first of these concerns will be discussed in the following paragraphs, while the second will be dealt with in a later section.

Altitude and heating influences on engine orifice characteristics were investigated as part of the cooling correlation research effort associated with radial air-cooled engine development. The objective of this effort was to extrapolate ground test determined cooling requirements data to operational altitudes and different power and mixture settings. Summaries of the engine orifice characteristics investigations are given in references 14 and 15. The method which has emerged from this work replaces the entering cooling flow density term in equations (2) and (3) with the density of the heated air leaving the cylinders. This exit density is based on the flow static pressure and stagnation temperature. An additional modification which is made is to utilize the density ratio "σ" and absorb the sea level density constant into "a". The engine orifice equation now becomes

$$w = a(\sigma_{ex}\Delta p)^{b}. \qquad (4)$$

Equation (4) has been shown to work effectively up to 12,000 meters in altitude. Figure 14, taken from the results of reference 14, shows a comparison of the extrapolation capabilities of the exit density ratio versus a density ratio based on the average of the ambient and exit densities. The average density ratio parameter works for low mass flows and low altitudes. However, the power law breaks down with increasing mass flows and altitude. This breakdown is caused by compressibility effects which become dominant with higher flow velocities and altitudes. Use of the ambient density ratio parameter solely would result in even greater deviations. The exit density ratio power law, on the other hand, provides a valid extrapolation, unaffected by altitude, up to higher mass flows.

Therefore, in regard to the influence of heating and altitude on ground test determined engine orifice characteristics, there is a well proven relationship [equation (4)] available to provide the necessary extrapolation. Altitude orifice characteristics, derived from ground test data and use of this relationship, should be considered as valid data for flight test use.

Flight test measurements. The flight cooling air mass

flow measurement system is shown in Figure 15. The system consists of an array of total and static pressure probes mounted in each inlet and static pressure ports distributed azimuthally in the inlet ducts. The inlets are axisymmetric designs incorporated into the nose cowl to form the conventional "bug eye" configuration. Previous studies of the aerodynamic behavior of these inlets indicated that the internal flow was well behaved and no adverse effects resulted from the propeller. The static and total pressure distributions across the inlet duct showed some variation; however, these variations were consistent with observed angle of attack and propeller wake influences. No indication of flow separation or stall was observed in the data.

Using the least-squares technique, surfaces of the form

$$P = a_1 z + a_2 y + a_3 x^2 + a_4 y^2 + a_5 x^3 + a_6 y^3. \qquad (5)$$

were fitted to the total and static pressure data. Terms involving products of x and y were not usable in the polynomial because all probe location involved either $x = 0$ or $y = 0$ coordinates. Using the fitted polynomial for the static and total pressure distributions across the inlet duct, the corresponding cooling air mass flow rate was determined by numerical integration. Installation temperature and pressure data on both sides of the engine were also recorded.

Data were taken in altitude increments of 900 m from 1,800 m to 7,200 m. Airspeed and cowl flap settings were used to vary the mass flow. A sample of the data from three different altitudes is given in Figure 16. The baffle pressure drop value used here, and in subsequent graphs, is taken as the difference between upper plenum total and lower plenum static pressures. The reason for this will be discussed in a later section. The results are consistent with the behavior predicted by equation (4). Taking the exit density ratio and placing it with the effective orifice area coefficient "a", one has

$$\ln (w) = b \cdot \ln (\Delta p) + \ln (a \cdot \sigma_{ex}^{b}). \qquad (6)$$

Equation (6) represents a family of straight lines in logrithmic scaled coordinates. The last term on the right is the ordinate intercept which, as shown in Figure 16, varies with altitude. Using the corrected baffle pressure drop parameters, "$\sigma_{ex}\Delta p$", the separated altitude curves collapse onto a single sea level curve as shown in Figure 17. The curve follows

$$\ln (w) = b \cdot \ln (\sigma_{ex}\Delta p) + \ln (a)$$

Figure 18 presents a comparison between the result of Figure

17 and manufacturer's data applicable to the engines of the test aircraft. The difference between the two curves lies with the respective values of the effective orifice areas. The "a" of the installed engine in the test aircraft is significantly larger than that of the manufacturer's test cell engine. The implication drawn was that approximately 55 percent of the cooling air entering the intakes was by-passing the engine and leaking through the external engine baffle system. Flow temperature measurements made directly below the engine and at the cooling flow exit showed a significant reduction, and suggested the mixing of heated and unheated cooling air, lending support to the leakage theory.

The external baffle system about the engine, shown in Figure 19, is typical of current practice. A neoprene rubber tape is used to provide the seal between the high and low pressure sides of the engine. Figure 20 is a view of the high pressure side of the cowled engine looking from front to rear. The neoprene tape is seen laying against the inside of the cowl as it is intended to do. Sealing is assumed to occur when the tape is forced tighter against the cowl by the ram pressure of the cooling flow. A simple and effective method in theory, however, apparently not so in practice.

To test the leakage theory, the neoprene tape was replaced by a cover on top of the engine as shown in Figure 21.

This "dog house" modification provided a positive lock seal in this region, and removed the uncertainty that accompanies passive systems such as the rubber tape. The flight tests were repeated and the results are given in Figure 22. The "dog house" reduced the system orifice area, i.e., decreased the leakage about the engine. With the "dog house", the same engine baffle pressure drop is obtained with 38 percent less cooling flow entering through the inlets.

However, this improved curve still indicated sufficient discrepancy from the manufacturer's curve to warrant additional testing. Also, at this point, the question of the validity of comparing the measurements between the flight installation configuration and the ground test cell configuration came to the forefront. To attack this question, a test technique utilized in reference 4 was employed.

Ground test measurements. If an aircraft related investigation can be validly performed on the ground as well as in flight, ground testing should be strongly considered. This is particularly the case when the investigation involves internal aerodynamics. Flight test investigations of cooling system aerodynamics are required if the concern is directed toward the external flow at the inlet and exit. Between these two points, however, flight serves only as a means of generating an internal air flow, which could be accomplished just as well by a blower on the ground. Ground test investigations of

the internal aerodynamics of cooling installations offer the advantages of unconstrained configurational variations and flow measurements, and perhaps most importantly, the advantage of personal observation of the functioning of the system. A moistened finger or cheek are very effective leak detectors.

The ground test system is shown in Figure 23. The system consists of a variable speed axial flow fan, mass flow metering section, diffuser, and connecting ductwork as required.

The first configuration tested was the "dog house" shown in Figure 21. The purpose of this test was to validate the flight mass flow measurement system in the inlets. Comparisons between the inlet rakes and the duct metering section showed a discrepancy of 17 percent. This correction was applied retroactively to the flight test results. The data in Figures 16, 17, 18, and 22 include this correction. During this test, additional leakage was observed about the valve lifter covers and between the metal external baffle and engine proper. These regions were sealed with duct tape and silicone rubber, and the test was repeated. A reduction in leakage of 8 percent was obtained by this additional sealing. With this configuration, leakage was still detectable, primarily through the front engine baffle and out through the gap between the prop spinner and nose cowl. The presence

of the nose cowl made it impossible to seal this region; accordingly, it was removed and additional ductwork was installed to reach the high pressure plenum of the engine. This arrangement, shown in Figure 24, represents the maximum seal, no leakage, flight configuration case. This configuration was important in that it served as the flight configuration "ideal case" for comparison with the ground test cell configuration. These two test configurations are presented schematically in Figure 25. Testing of the maximum seal flight configuration showed that the front engine baffle was responsible for an additional 9 percent leakage.

Referring to Figure 25, the ground test cell configuration represents the "ideal case" from the standpoint of flow behavior. The flow enters the high pressure side of the engine in a uniform manner and in the same direction as it will move through the cooling fin passages. The high pressure plenum is large and the velocity is low. The baffle pressure drop is measured as the difference between the high pressure plenum static and ambient static. However, in the case of the flight configuration, the cooling air enters at much higher velocities and in a direction perpendicular to the fin passages. In many cases, it must flow about obstacles directly in its path such as alternators, oil coolers, prop governors, intake manifolds, etc. A

significant wake in the internal flow develops immediately, due to the "bug eye" intake configuration. A true flow static pressure is difficult to measure under these circumstances. Total pressures are relatively easy to acquire, particularly with the use of Kiel probes. The point of concern here is whether the engine orifice characteristics determined by ground test cell measurements are comparable to those determined by flight test measurements. To investigate this question, a ground test cell configuration was assembled and flow measurements performed.

The test cell configuration is shown in Figure 26. Turning vanes were utilized in the bend and honeycomb in the vertical duct to achieve an "ideal" uniform flow at the engine. A total pressure survey made at the engine confirmed a uniform flow. The engine baffle pressure drop was measured in the same manner as standard test cell practice. The results from this test are given in Figure 27 along with the results from the maximum seal "ideal" flight configuration test. The engine orifice characteristics as measured by both test configurations are identical if the baffle pressure drop for the flight configuration is based on high pressure plenum total, rather than on high pressure plenum static. Use of the plenum static pressure gives an error of 8 percent. The location of the total pressure probes was at the rear engine baffle. Data presented in a later section show

this region to be the least affected by inlet configuration and blockage. The key finding from this particular test is that ground test cell determined engine orifice characteristics are perfectly valid for flight test utilization if the flight measurements are based on engine plenum total pressure rather than static. Accordingly, all engine orifice characteristic data presented herein utilize upper plenum total and lower plenum static to form the baffle pressure drop parameter. This includes Figures 16, 17, 18, and 22.

In order to achieve a valid comparison between the flight and ground test results, a correction must be introduced to convert the "cold" engine data to "hot" engine data. In order to determine this correction, a flight test was performed to measure the orifice characteristics of both the "hot" and "cold" engine. The "hot" data was taken with the engine operating at normal cruise power settings. The engine was then shut down and allowed to cool to ambient temperature, to obtain the "cold" data. The "hot" and "cold" orifice characteristics are the same if exit density ratio is used for the altitude correction. However, if the ambient density ratio is used, the "hot" curve shifts downward by 10 percent as shown in Figure 28. Therefore, it appears that use of the exit density ratio as a correlation factor, works well for both altitude correction,

and "hot" and "cold" engine correction.

The results from the flight and ground tests are summarized in Figure 29. It is evident from the figure that a significant leakage problem exists with the use of the rubber tape external baffle system. Considering the fact that the test aircraft has very low time and, accordingly, that the external baffles are in relatively good shape, one can visualize the leakage problem which may exist with the number of high time aircraft in service. Leakage produces two adverse effects: increased cooling drag and reduced cooling performance. The first of these is more obvious since the internal flow drag is directly proportional to the mass flow of cooling air through the installation. The second effect results from the reduction in the baffle pressure drop which can be generated across the engine, due to increased losses between the inlet and plenum. The operation of the inlets and the losses immediately downstream are functions of the total air mass flow, regardless of whether it passes through or around the engine. Reducing leakage will produce an increase in cooling flow through the engine and, correspondingly, improved cooling.

Cooling Correlation Investigation

One of the many technological outgrowths of the radial

air-cooled engine development was the NACA Cooling Correlation Analysis procedure. This procedure is well documented in numerous NACA reports (see references 16 and 17). The purpose of the method is to take ground based data of engine cooling requirements and extrapolate these requirements to operational altitudes. The NACA procedure required the development of empirical relationships concerning the heat generated by the engine, which could only be determined by ground test. Consequently, use of the method for flight investigations was always tied to the availability of ground test results. This proved to be of little significance, however, due to the close technological cooperation between the government, airframe manufacturers and engine manufacturers during World War II. This technological cooperation is today much reduced in regard to the general aviation industry. The competitive market situation in conjunction with product liability concerns work against cooperation between airframe and engine manufacturers in the solution of installation cooling problems. The airframe manufacturer, in many instances, must work alone to solve cooling problems armed only with ground test cell data, as represented by Figure 5.

A flight test program was performed to investigate whether an installed engine cooling correlation procedure could be developed to assist in the solution of cooling problems. The objective was a cooling correlation relation

which involved parameters which could be easily measured in flight. The NACA method was used as a basis (see reference 16). The heat generated by combustion which is transferred to the cylinders is given by

$$H = c_1 W_c^1 (T_g - T_h). \tag{8}$$

The air charge flow "W_c" is directly relatable to the indicated engine power "I", and (8) can be rewritten as

$$H = c_2 I^m (T_g - T_h). \tag{9}$$

The heat given up by the cylinders to the cooling air flow is

$$H = c_3 w^k (T_h - T_a). \tag{10}$$

For flight testing, the cooling air mass flow "w" is impractical to measure. The orifice characteristics of the engine are used here and the corrected baffle pressure drop parameter is substituted.

$$H = c_4 (\sigma_{ex} \Delta p)^n (T_h - T_a) \tag{11}$$

For a constant cylinder head temperature, equations (9) and (11) must be equal, giving

$$(T_h - T_a)/(T_g - T_h) = cI^m/(\sigma_{ex}\Delta p)^n \qquad (12)$$

Equation (12) is essentially the NACA Cooling Correlation relation. The effective combustion gas temperature "T_g" was determined by ground testing. Empirical relationships had to be established between it and other heat generating parameters such as fuel/air ratio, exhaust back-pressure, and ignition timing. As all other physical quantities in equation (12) are measurable in flight, it was decided to replace this term with the measured exhaust gas temperature. For the PA-41P test aircraft, the supercharger turbine inlet temperature was used. Equation (12) now becomes

$$(T_h - T_a)/(T_{EGT} - T_h) = T^* = cI^m/(\sigma_{ex}\Delta p)^n \qquad (13)$$

The test program was flown as part of the orifice characteristics study. Altitude ranged from 1,800 m to 7,200 m. At each altitude, a test matrix of four power settings and three mixture settings was run. The mixture settings ranged from full-rich to peak EGT. Due to turbo-supercharging, the same four power settings were obtainable at all test altitudes. The cowl flaps were used to vary the cooling air flow at each test point.

The results are presented in Figures 30 and 31. In Figure 30, the relationships between engine baffle pressure

drop and the temperature ratio, T_A^*, based on the average of the cylinder head temperatures are plotted for a constant indicated power. Each plot represents a range of altitudes and cooling air mass flows. All four curves have the same slope, but different ordinated intercepts, dependent on the power setting. This is in agreement with equation (13). Rewriting (13) in logrithmic form with $(\sigma_{ex}\Delta p)$ as the independent variable,

$$\ln(T^*) = -n \cdot \ln(\sigma_{ex}\Delta p) + \ln(cI^m) \qquad (14)$$

The intercept varies with the indicated engine power I. The resulting cooling correlation relation is given in Figure 31. A separate correlation was performed using the hottest running cylinder temperature, (cylinder number 6), in place of the averaged cylinder temperature. Results similar to those of Figures 30 and 31 were obtained. Both correlations are given below.

$$T_A^* = (T_{h_A} - T_a)/(T_{EGT} - T_{h_A}) = 0.17I^{0.52}/(\sigma_{ex}\Delta p)^{0.29} \qquad (15)$$

$$T_6^* = (T_{h_6} - T_a)/(T_{EGT} - T_{h_6}) = 0.18I^{0.50}/(\sigma_{ex}\Delta p)^{0.28} \qquad (16)$$

Both show excellent agreement with the behavior predicted by equation (13).

The results of this investigation show that a cooling correlation for a particular aircraft installation can be developed in terms of quanitities which are easily measureable in flight. This correlation, once established, provides the basis for the solution of cooling problems, and for relating cooling requirements to aircraft performance. The airframe manufacturer is thus freed from dependency on ground test cell data, for cooling installation flight test investigations.

Internal Flow Temperature Rise

As part of the cooling correlation analyses, correlations were also developed for the temperature rise of the cooling air at the rear of the upper plenum and at the exit. The first of these locations is important in that many installations use a portion of the airflow at this point for auxiliary cooling, such as oil cooling, intercooling, etc. The second location is of interest since it leads to the exit density which is important for future installation design analyses. The correlations were developed using the basic formulation of equation (13). Appropriate temperature terms were changed to represent the heat transfer process. The results are given in Figures 32 and 33. For the range of baffle pressure drop

(cooling air mass flow) developed by the PA-41P test aircraft, the cooling flow temperature rise at the rear baffle is

$$20°C < (T_{up} - T_a) < 30° , \qquad (17)$$

and the temperature rise across the engine is

$$70°C < (T_{ex} - T_a) < 100°C. \qquad (18)$$

The exit temperature rise values are consistent with numbers reported by other sources for horizontally-opposed engines. The upper plenum temperature values, however, should be treated carefully. The heat transfer mechanism here is commonly referred to as velocity cooling. The amount of heat transferred to the cooling air is dependent on the flow velocity and flow turbulence in the plenum, and these, in turn, are dependent on installation and engine configurations.

INLET INVESTIGATION

Background

The function of the inlet is to recover the available dynamic pressure and deliver the cooling flow to the high pressure plenum in a uniform manner. Ideally, this should

be accomplished with no internal or external flow separation. Inlets are classified as either two-dimensional, as in the case of wing leading edge intakes, or three-dimensional, as in the case of axisymmetric intakes. The inlets used on general aviation reciprocating engine aircraft are three-dimensional, and are of relatively complex geometry in comparison to those used for turboprop and turbojet powered aircraft. This is due primarily to the configuration of the horizontally-opposed engine which allows for an installation with minimal frontal area and yet requires cooling air to pass vertically through the engine. Conventional practice is to use two inlets, one on each side of the propeller spinner. The design of the inlet shape heretofore has been accomplished through a combination of styling dictates and intuition. Very little aerodynamic analysis and design is used. The reasons for this are the absence of practical analytical methods and the cost of aerodynamic testing of different candidate shapes. As part of this program, a systematic study of inlets and their effects on the cooling installation was performed.

Inlet Aerodynamic Theory

The theoretical aerodynamic behavior of inlets will be discussed in relation to three-dimensional axisymmetric

configurations. Figure 34 shows an inlet with the pertinent design parameters identified. The purpose of the inlet is to capture the required amount of flow and recover a part of the dynamic head as an increase in static pressure. The desired recovery of the inlet itself is related to the velocity ratio (V_i/V_o), i.e., the ratio of the inlet velocity to the free stream velocity. A large pressure recovery corresponds to a small velocity ratio and vice versa. The diffusion, through which the recovery occurs, takes place externally. If sufficient internal length is available, then an internal diffuser is also possible to increase the recovery.

The ability of an inlet to deliver the desired pressure recovery and, in fact, its ability to function properly over a range of operating conditions, is related to its cross-sectional shape as illustrated in Figure 34. The axisymmetric inlets used in the investigation are from the Kuchemann A-series, detailed in reference 18. They consist of two distinct elliptical segments which join at the nose of the lip contour. The ellipses are in proportion according to the "A" designation. Other inlet families are available for different proportions. Three A-series inlets are shown in Figure 35. The numerical part of the designation

refers to the percentage ratio of the inlet area to maximum external cross-sectional area. Low numbers produce relatively thick lip contours with relatively large radii of curvature and high numbers produce the reverse. In Figure 36, the potential flow pressure distributions about the lip contour are given for different velocity ratios and angles of attack. The distributions were calculated according to the method of reference 19. Both the internal and external pressure distributions exhibit characteristics similar to those of airfoils. For many conditions, there is a suction peak followed by an adverse pressure gradient, which, when the boundary layer response is included, are the necessary conditions for flow separation and stall. The strength of the suction peak and severity of the adverse gradient are dependent on the relative thickness of the lip contour or, correspondingly, on the radii of curvature employed. For larger velocity ratios, the stagnation point is to the outside of the lip nose, the suction peak is formed on the inside, due to the turning angle in combination with the radii of curvature. For small velocity ratios, the stagnation point lies to the inside and the suction peak correspondingly forms to the outside. In general, therefore, inlets designed for large velocity ratios and small external pressure recovery

are subject to the possibility of internal flow separation and stall. Inlets designed for small velocity ratios and large external pressure recovery are likewise subject to the possibility of external flow separation.

The effect of the location of the stagnation point on inlet pressure distributions suggests one fundamental design tenet which should be followed for the reciprocation engine cooling installations. With current technology, the flow field about an arbitrary nose cowl shape is not well defined. Therefore, the locations of the stagnation points on the inlet lip contour are also ill-defined. Accordingly, inlet lip contours should be well-rounded with large radii of curvature to minimize inadvertent suction peaks and following adverse pressure gradients.

Design of the Test Inlets

Five different inlet configurations were investigated in this program. They are shown in Figures 37-41. They consist of the original PA-41P inlet, three axisymmetric configurations, and a conventional design representative of current general aviation practice. The PA-41P inlet, here designated as STD, is a swept configuration, with the purpose of reducing propeller blockage by relieving the frontal area. The propeller hub incorporates a 20 cm shaft extension to

provide the necessary length for this. The aerodynamic effects of sweep for these types of inlets are unknown. The three axisymmetric inlets were investigated because of the existence of an experimental data base and analytical design procedures. While this information applies to true axisymmetric configurations, it provides a point of reference for comparing the results of incorporating these shapes into a cowl nose piece. The inlets are designated according to their respective design velocity ratio (0.3 or 0.6) and longitudinal location (forward or aft). The fifth inlet is a conventional general aviation design incorporating as much of the 0.3F inlet shape as possible. The designation for this inlet is GAC.

Inlet Internal Effects

The STD, 0.3F, 0.6F, and 0.3A inlets were investigated in one program phase. In a later phase, with some modifications to the external engine baffling, the 0.3F and GAC inlets were tested.

The internal effects of the inlets are measurable in terms of the pressure recovery obtained in the upper plenum and the baffle pressure drop developed across the engine. The baffle pressure drop varies directly with the cooling air mass flow, as seen in Figure 5, and therefore is an indication of the volume of cooling flow obtained. The

pressure recovery is important for two reasons. First, it represents one of the two internal losses in the system; the other being the baffle pressure drop. Poor pressure recovery, or large inlet losses, means less pressure head available for moving the cooling flow through the engine. Second, poor pressure recovery results in higher cooling drag for the same cooling flow.

To properly evaluate the inlets, the nature of the flow immediately in front of the inlet needs to be defined. A total pressure survey rake was mounted close to the propeller disk as shown in Figure 37(a). The results from this survey shown are given in Figure 42 in terms of the pressure coefficient referenced to free stream static. Superimposed is a planform view of the nacelle. The effect of the propeller is seen in terms of the distribution of total pressure available at the inlet. This varies from $0.85q_\infty$ at the spinner to approximately $1.1q_\infty$ at the outer edge for cruise, and to $1.2q_\infty$ for climb. The reductions in total pressure near the spinner are attributed to losses associated with the propeller shanks operating in a stalled condition, i.e., the shank angle of attack is too high for the operating condition. On the average, a loss of $0.1q_\infty$ occurs for the inlet flow in cruise.

Figures 43-46 give results for the upper plenum total pressure surveys for four of the test inlets. The survey

points were at the end of the inlet duct and across each row of cylinders (see Figures 8, 9, and 10). The presentation shown is a top view of the engine with the inlets in the upper left and upper right corners of the graph. The respective cylinders are denoted by the numbers 1-6 outside the graph. The propeller governor is located in the lift inlet in front of cylinder number 2.

The 0.3F inlet in Figure 44 gives the highest pressure recovery in the plenum. The inlet ducts are well behaved as indicated by showing a total pressure distribution similar to the propeller rake. The 0.6F, 0.3A, and STD inlets resulted in lower values of upper plenum total pressures. The pressure recovery of the plenum is obtained through a combination of external diffusion by the inlet, internal diffusion by incorporating an expanding area diffuser in the inlet duct, and the diffusion associated with the flow expanding into the plenum volume from the inlets.

The STD inlet in Figure 43 shows a loss in pressure recovery in its left inlet, indicating the presence of an internal stall. This may be due to either the blockage by the propeller governor located in the left inlet, or due to the left inlet operating at a higher angle of attack than the right inlet and consequently exceeding the design's stall angle. The angle of attack asymmetry is due to the swirl component of the propeller flow. Also evident in

the figure is the nonuniformity of the flow entering the plenum as indicated by the variation in total pressure. This again is the result of insufficient diffusion by the inlet.

The 0.3F inlet in Figure 44 results in good pressure recovery in the plenum. The flow is more uniform, indicating that part of the recovery has been accomplished externally by the inlet.

The 0.3A inlet in Figure 45 produces $0.2q_\infty$ less pressure recovery than the 0.3F. This loss is believed to result primarily from the poor interface between the inlet duct and the plenum entrance. The inlet duct is partially obstructed by the front cylinders. The extent to which external diffusion was accomplished is unknown. As the inlet moves aft, its geometry, which controls its aerodynamics, is increasingly compromised by the nose cowl geometry.

The 0.6F inlet in Figure 46 shows similar poor recovery. While the 0.3F inlet was designed for external diffusion, the 0.6F was designed for internal diffusion using an appropriately configured internal duct. For both climb and cruise conditions, the inlet indicates an internal stall by the loss in pressure in the region adjacent to the spinner. This condition is more severe for climb than for cruise. The inlet is operating at a higher velocity ratio in climb

due to the use of cowl flaps to pump additional flow through the system. Referring to the inlet velocity ratio contours in Figure 36, this increases the internal suction peak and following adverse gradient, thereby increasing the tendency towards internal stall.

The GAC inlet was tested at a later time after the "dog house" modification had been made to the external engine baffle. Cooling air mass flow measurements had shown the external baffle to have considerable leakage. The four inlets just discussed were operating at significantly higher velocity ratios than anticipated. This aggravated internal aerodynamic problems. The 0.3F inlet was also operated with the modified baffle and consequently it is used as a reference for comparison purposes. The results are given in Figures 47 and 48. The 0.3F inlet shows a slight improvement over the earlier test. This is due to reducing the flow losses associated with the inlet duct interface with the plenum. These losses were reduced as a result of reducing the cooling air flow by elminating the baffle leakage. The GAC inlet in Figure 48 shows about the same performance as the STD inlet. The absence of the survey rakes at the end of the inlet duct for these tests increases the difficulty of interpreting the results. The indication is that, like the other low performance inlets, little or no external diffusion occurred and significant flow losses were created at the

plenum entrance. Additional information concerning the contour pressure distribution are given in a later section.

The effects of the inlets on cooling installation performance over the complete operating range of aircraft are given in Figures 49-52. The parameters of importance are the plenum pressure recovery and the engine baffle pressure drop, which is directly related to the cooling air mass flow rate. These parameters are presented in Figure 49 for climb at a constant 100 kts equivalent airspeed. Only the three inlets shown were subjected to a climb test. The 0.3A inlet did not allow adequate cooling for this flight condition. The indicated altitude dependencies are due to propeller effects. While maintaining the same engine power in the climb, the propeller survey rake indicated a reduction in slipstream total pressure with altitude. This reduction in slipstream total pressure caused a reduction in plenum pressure recovery and also reduced pumping effectiveness of the cowl flaps.

The 0.3F and STD inlets result in the same baffle pressure drop, i.e., the same cooling air mass flow. The 0.3F inlet, however, accomplished this at a higher pressure recovery which translates into lower internal cooling drag. There is more energy in the flow at the exit than for the

STD inlet. The decrement in baffle pressure drop produced by the 0.6F inlet is due totally to its loss in pressure recovery.

Baffle pressure drop and plenum pressure recovery for cruise conditions are shown in Figures 50 and 51. These parameters are shown to be independent of altitude and only slightly dependent on airspeed. This dependency appears to be due to changes in the external nacelle pressure at the exits which accompanies the angle of attack variation with airspeed. In Figure 50, the 0.3F and STD inlets generate approximately the same baffle pressure drop, while the 0.3A and 0.6F inlets result in somewhat lower capability. The marked distinction is in the pressure recovery, which exerts an important influence on cooling drag as well as cooling air mass flow. The 0.3F and GAC inlet results, in Figure 51, were tested after the modification to the engine baffles to reduce leakage. An increase of $0.2q_{\infty}$ in baffle pressure drop is seen for the 0.3F inlet as a result of this change. The GAC inlet appears to function at the level of the 0.3A and 0.6F inlets.

The effect of propeller operation on inlet performance is shown in Figure 52. Improvements in pressure recovery and baffle pressure drop are obtained for the 0.3F, 0.6F, and 0.3A inlets, while the GAC inlet shows no change, and the STD shows a reduction with propeller running. The

behavior of the STD and GAC inlets is not understood in this regard. It is believed that the answer lies with the interaction between the swirl component of the slipstream and the particular inlet geometry.

External Inlet Effects

Flow visualization. The external flow about the inlets was investigated through the use of in-flight tuft photographs. Pressure distribution data were also obtained for the 0.3F, 0.6F, 0.3A, and GAC inlets. Initially, a wide range of flight conditions, cooling air flows, and propeller operating conditions were run. After observing that the external flow behaved in a systematic manner, the test conditions were reduced to representative climb and cruise conditions, each with propeller running and propeller stopped.

The in-flight tuft studies are presented in Figures 53-57. The STD inlet in Figure 53 is shown with the propeller stopped as well as running. As also indicated in the other figures, the nacelle is operating at a positive angle of attack for the cruise condition. The nose cowl stagnation point appears to be immediately below the propeller spinner. A strong upward flow is indicated aft of the spinner and a strong outward flow is shown below the inlets. The flow into the inlet has an upward component at the spinner. The inlet flow is

separated on the lower intake contour, as a result of the small radii of curvature used there. As will be seen with the pressure distribution results, with propeller stopped, the stagnation point on the upper lip tends to move toward the inside. This produces a suction peak, following adverse gradient and subsequent local separation. This is evident on the outboard inlet. The inboard inlet is already separated with propeller running. Stopping the propeller increases the separated area.

The external flow about the 0.3F and 0.6F inlets in Figures 54 and 55 is well ordered. The flow appears to be primarily in the longitudinal direction with no obvious lateral or azimuthal components, and no flow separation

The 0.3A and GAC inlet configurations in Figures 56 and 57 show behavior similar to the STD configuration. The stagnation point below the spinner causes upward flow on the nose cowl immediately aft of the spinner, and a flow below the inlet. The intake area appears to be stalled for both inlets. The external flow about the inlets is unseparated and orderly.

Inlet pressure distributions. Figure 58 shows the locations where inlet pressure distribution data were taken. The results for the cruise condition for the 0.3F, 0.6F, 0.3A, and GAC inlets are presented in Figures 59-62. Pressure data for the STD inlet were not acquired. For

the cruise condition, data were taken for the propeller running under load, and for propeller stopped and feathered.

The pressure distributions for the 0.3F inlet are given in Figure 59. Referring to Figure 36, the pressure distributions are consistent with the axisymmetric inlet design. The difference between the upper and lower surfaces indicates that the inlets are operating at a positive angle of attack. The difference between the inboard and outboard inlets is believed to be due to blockage of the inboard intake duct by the propeller governor which causes this side to operate at a lower velocity ratio than the outboard. With the propeller stopped, the stagnation points on the inboard inlet move to the inside which is consistent with the reduction in cooling air flow that accompanies this. The outboard inlet shows little response to stopping the propeller, indicating no appreciable movement of the stagnation point. The change in velocity here appears to be small. The side pressure distributions show asymmetry when the propeller is stopped. This behavior is evident on all of the inlets. It is believed that this is due, in part, to side-slip angles which resulted from trimming the aircraft after shutting down the right engine.

The 0.6F inlet in Figure 60 shows similar behavior. While this inlet was designed to operate at a higher velocity ratio than the 0.3F inlet, the pressure distributions

do not reflect this. They are more peaky than the 0.3F, indicating a lower operating velocity ratio. However, the internal total pressure surveys showed this inlet to be stalled in both intake ducts, so that the results of Figure 35 no longer apply. Accordingly, it is impossible to interpret the pressure distributions beyond this point.

The 0.3A inlet in Figure 61 also demonstrates similar behavior. As with the previous inlets, the external pressure distribution is consistent with the axisymmetric geometry, and there is no indication of separation of the external flow.

For the GAC inlet, a more extensive internal pressure distribution was obtained. The results are given in Figure 62. The internal pressure data indicate attached flow and an initial pressure recovery of $0.8q_{\infty}$. The motion of the stagnation point on the upper lip contour is noted with stopping the propeller. Unlike the axisymmetric configurations, both the inboard and the outboard inlets exhibit similar behavior, with some difference showing for the lower contour. The side pressure distributions differ from the axisymmetric models for the stopped propeller case. The stagnation point moves towards the inside for both inlets. The outboard lateral distribution indicates a local stall. Again, because of the complex geometry involved, it is impossible to explain this

behavior further without an appropriate analytical model or additional experimental data.

EXIT INVESTIGATION

Background

The exits of the cooling installation act as the system throttle. Since the flow is subsonic throughout, the quantity of cooling flow will adjust itself so that the pressure at the exit is equal to the local external flow pressure. The relationship between cooling flow volume rate and exit pressure is governed primarily by the exit duct area. Too small an exit area will throttle the flow and lower the volume rate. Too large an exit area may result in mixing problems between the cooling flow and external flow, which can have an adverse effect downstream. An additional function, which must be incorporated into the exit configuration, is a cooling flow pumping mechanism for the climb flight condition, where the flow volume required for cooling at high power settings cannot be generated by the low flight velocity. The mechanism most often utilized is a cowl flap, which is essentially a spoiler, sized to produce a local low pressure wake immediately downstream.

Exit configurations and locations are also well

standardized. The predominant location is on the lower surface of the cowl, well back from the nose. The local external pressure is generally close to free-stream static. Depending on landing gear placement and other related considerations, the exit may be split into two ducts, one on either side of the cowl, or a single duct may be used on the bottom. Periodically, the exits have been located on the upper surface of the cowl, particularly for twin-engine configurations where there is a low pressure region available for pumping. A negative aspect of the upper surface location is the depositing of oil and grime, which is picked up by the cooling flow, on parts of the airframe which may come in contact with the passengers and/or crew.

Exit Test Configurations

The original PA-41P exit configuration is shown in Figure 63. This is a split system located on the lower cowl beneath the leading edge of the wing. The cowl flap is shown fully deployed. The existing installation left little room for configurative variations. The central area of the lower cowl was occupied by the landing gear and oil cooler. This, in combination with the requirement to maintain fire wall integrity, dictated that existing location be used. Three exit system parameters could be varied: exit area, cowl flap deflection, and cowl flap

aspect ratio. The relationship between cowl flap deflection and exit area depends on the location of the flap hinge in relation to the exit duct. Figure 64 shows two examples of this arrangement, one where cowl flap deflection increases the exit area, and the other where exit area remains constant. The restrictions imposed by the PA-41P installation dictated that the first arrangement be used.

The exit design parameters which were investigated consisted of exit area and cowl flap aspect ratio. The test cowl flaps were relocated so that the original PA-41P exit area was increased by fifty percent. Restrictor fairings were then placed in the exit duct which reduced the area to its original value and then to a fifty percent decrease below this. The exit area variation is shown in Figure 65. Three cowl flaps, with aspect ratios of 1.5, 0.75, and 0.55, were tested with each of the exit areas to produce a 3 x 3 configuration matrix. The cowl flaps were installed by relocating the hinge line so that all three produced the same exit areas at the same settings. This, however, resulted in different cowl flap deflection angles with the short, high aspect ratio flap having the largest deflection angle. The three cowl flaps are shown in Figure 66. The range in deflection angles between the long and short flaps is shown in Figure 67.

All pertinent geometric data are presented in Table II.

Exit Area Test Results

The results from the exit area investigation are given in Figure 68. Application of Bernoulli's equation shows that the lower plenum pressure is inversely proportional to the exit area. Since the combined pressure drop from inlet to exit is constant for any specific flight condition, a reduction in lower plenum pressure means an increase in baffle pressure drop can be accommodated, and accordingly, an increase in cooling flow. The variation in lower plenum pressure is seen in this figure. The change in lower plenum pressure is not converted completely into baffle pressure drop, however. With the increased cooling flow the upper plenum pressure also decreases, because the inlet pressure recovery is reduced with the higher velocity ratio and the internal inlet losses increase with increased flow velocity. It is clear from Figure 68, however, that baffle pressure drop, and correspondingly, cooling flow can be increased by increasing exit area. The implication is that poor inlet design of leaky baffles can be compensated by subsequently increasing the exit area to achieve the required cooling. However, internal cooling drag will be increased through

increase in momentum defect, and external drag may be increased through mixing with the external flow and associated deleterious effects downstream.

Cowl Flap Test Results

The results from the cowl flap study are presented in Figure 69. Due to cooling requirements, this study was performed at a low speed cruise condition rather than climb. The prime difference here is the absence of the additional slipstream velocity which influences the effectiveness of the cowl flap. The results show a decrease in lower plenum pressure and an increase in baffle pressure drop with cowl flap deflection. The spread in the curves as the cowl flaps are closed is opposite to what would be expected. In the closed position, the exit area should be the same for all three flaps. During the test, it was observed that as the length of the flap increased, the hinge moments on the flap, in the closed position, also increased. The positioning linkage of the cowl flaps allowed some defection under load. This increased the closed position exit areas somewhat above the values in Table II. It is believed, accordingly, that the spread in the results at the closed position is due to the medium and long cowl flaps deflecting towards the open position due to aerodynamic loads. The

cowl flap airloads vanished as the flaps were deflected towards the open position. The Table II values are correct for the no airload open condition.

In the open position, no difference is seen between the three cowl flaps in Figure 69. Considering the wide deflection angle range, as listed in Table II, it appears that exit area, not deflection angle, is the controlling mechanism here. The deflection of the cowl flap is supposed to generate a low pressure region immediately downstream which acts as a pump for the cooling flow. This effect is not apparent for the configurations tested.

Exit Location Investigation

The interest in the use of upper surface cooling air exits is driven by two basic ideas. First, for engines with updraft cooling, i.e., where the cooling flow enters the bottom and exits the top, upper surface exits are more expedient, rather than requiring the flow to return again to the lower surface for exhausting. Second, particularly for twin engine aircraft, there are obvious regions of low pressure which seem to offer the advantage of additional pumping to increase the baffle pressure drop across the engine. This ignores the fact, however, that the flow in a low pressure region on an aerodynamic body, must ultimately negotiate an adverse pressure gradient to reach

free stream static pressure. Due to boundary layer effects, this is difficult to achieve without flow separation in the most favorable of circumstances. The introduction of a low momentum secondary flow into a low pressure region can well result in severe effects downstream in terms of flow separation and corresponding increases in drag.

Nacelle pressure distribution measurements. Prior to locating the upper surface exits, nacelle pressure distribution measurements were taken. Figure 70 shows the points where static pressure belts were positioned for the longitudinal pressure distribution measurements. The symbols in the figure relate the indicated position to the pressure data given in Figures 71 and 72. The results presented in Figure 71 and 72 show the nacelle external static pressures at the exits, on the lower surface, and at the longitudinal point of lowest pressure on the upper surface. The low pressure point coincided with the suction peak of the wing section near the leading edge. In Figure 71, the results are for cruising flight. A noticeable difference exists between the nacelle pressures on the inboard side and the outboard side. Due to the presence of the fuselage, the flow in this region generally has higher velocities than comparable points

outboard of the nacelle. Also, on the starboard side of the aircraft, the swirl of the propeller slipstream increases the angle of attack of the inboard wing section, and decreases the angle of attack of the outboard wing section. This also contributes to higher velocities and correspondingly lower pressures on the inboard section. Figure 72 presents the results for climb power at different airspeeds. Also included for comparison purposes are the same data for propeller stopped. At the best climb speed of approximately 100 kts, the propeller slipstream amplifies the pressure by about 0.4 q_∞. In both cases, the lowest pressure is found adjacent to the upper wing surface. The pressure increases towards free stream as one moves away from the wing as indicated by the results for the top of the nacelle. In cruise, there is a potential doubling of the suction pressure at the exits by locating them on the upper surface.

Exit location results. The installation of the upper surface exits is shown in Figure 73. The exit area was set at the largest of the three investigated in the lower surface exit investigation (150% of original). Louvers were used at the exits to align the exit flow with the external flow. The final test configuration is shown in Figure 74. During the test program, the lower exits were closed off and all cooling

flow passed through the upper exits. The results are given in Figure 75 for both cruise and climb conditions. Three sets of data are presented: upper surface exits with louvers on, louvers off, and conventional lower surface exits. The upper surface exits increase the baffle pressure drop across the engine by $0.1q_{\infty}$. The louvers contribute some flow resistance which affects the obtainable baffle pressure drop. In the climb condition, the upper and lower exit systems are essentially equal. However, here the lower exits have been modified by deployment of the cowl flaps. The upper surface exits are shown to be superior in cruise and comparable in climb to the conventional lower surface exits. Intuitively, one would expect the upper surface system to offer less drag in climb than the lower surface system with cowl flaps open.

A drag study was performed comparing the upper and lower surface exits in both climb and cruise configurations. Rate of climb was used as the measure for the climb test. The results were inconclusive. No judgement could be rendered concerning the relative drag of the two systems. The generalized speed/power method was used for the cruise configuration. The results are given in Figure 76 in terms of generalized power versus generalized velocity. The upper surface exits result in a definite drag increase for the aircraft. In terms of generalized velocity, there is

approximately a 6 kt decrease in speed for the same power setting. During the test program a mild buffet was felt in the horizontal tail due to the flow from the upper surface exits. With the louvers removed, the buffet increased noticeably, indicating the presence of a well developed wake. Tuft studies did not indicate any significant change in flow patterns. Other than its manifestation through tail buffet, the actual formation and nature of this wake was not determined. However, the indicated presence of the wake lends support to the drag measurement results. For the configuration tested, the cooling installation benefits of the upper surface exits were negated by an associated drag increase. A similar configuration was tested in a full scale wind tunnel (reference 11). The drag results were in agreement with the results reported here. Reference 1 also indicates that locating the exits in a low pressure region does not lead to the best configuration when the resulting drag is included in the evaluation. In summary, the reported results to date, do not support the apparent benefits of cooling air exits in low pressure regions of the aircraft.

CONCLUSIONS

1. With present techniques, reliable measurements of cooling drag are difficult to obtain through flight test. Such investigations should be performed through wind tunnel test whenever practical.
2. Much of the radial engine technology concerning engine orifice characteristics and altitude correlation is directly applicable to horizontally-opposed engines.
3. The differences between ground test cell configurations and flight installation configurations, in regard to internal aerodynamic measurements, are accounted for by using total pressure measurements rather than static pressure measurements. The measurements should be of the oncoming flow from the inlets rather than that of the component passing through the engine.
4. Current design practices of using a rubber tape lap seal for the external engine baffle results in significant leakage, cooling problems, and increased cooling drag.
5. A simple ground test blower system has been shown to be an important tool for the development of aircraft cooling installations.
6. A flight test technique for the determination of the installed engine cooling requirements are determined in

terms of easily measurable parameters, thus freeing the airframe manufacturer from the restrictions imposed by ground test cell data in this regard.

7. The aerodynamic behavior of the inlets are a major factor in the effectiveness of the cooling installation. There is an obvious need for basic inlet design guidance.
8. The design parameter of exit area has been shown to agree with theory in regard to its effect on the cooling installation. The locating of the exits in a low pressure region should not be attempted without a thorough study of the consequences.

TABLE I. - COOLING DRAG FLIGHT TEST RESULTS

Configuration	C_D @ C_L = 0
No cooling flow	0.0226
Augmentor 25% open	0.0234 (+4%)
Augmentor 50% open	0.0226 (+0%)
Augmentor 100% open	0.0242 (+7%)

TABLE II. - COWL FLAP TEST CONFIGURATION DATA

Cowl Flap Position	Exit Area (cm^2)	Cowl Flap Deflection (deg.)		
		Short	Medium	Long
1-closed	214	--	--	--
2	268	13	5	3
3	300	22	10	6
4	326	31	14	9
5-open	366	42	18	13

REFERENCES

1. Hammen, T. F., Jr.; and Rowley, W. H.: Factors Pertaining to Installation of Inverted, In-Line Aircooled Aircraft Engines. SAE Journal (Transactions), Vol. 54, No. 3, March 1946.
2. Ellerbrock, H. H., Jr.; and Wilson, H. A., Jr.: Cowling and Cooling Tests of a Fleetwings Model 33 Airplane in Flight. NACA WR L-632, 1945. (Formerly NACA MR May 1944).
3. Conway, R. N.; and Emmons, M. A., Jr.: An Investigation of the Ranger V-770-8 Engine Installation for the Edo XOSE-1 Airplane. I-Cooling. NACA WR L-561, 1945. (Formerly NACA MR L5I12).
4. Nichols, M. R.; and Dennard, J. S.: An Investigation of the Ranger V-770-8 Engine Installation for the Edo XOSE-1 Airplane. II-Aerodynamics. NACA WR L-562, 1945. (Formerly NACA MR L5I12b).
5. Nichols, M. R.; and Keith, A. L., Jr.: An Investigation of the Cowling of the Bell XP-77 Airplane in the Propeller-Research Tunnel. NACA MR November 1943.
6. Nielsen, J. N.; and Schumacher, L. E.: Analysis of the High-Altitude Cooling of the Ranger SGV-770 D-4 Engine in the Bell XP-77 Airplane. NACA CMR October 1943.

7. Monts, F.: The Development of Reciprocation Engine Installation Data for General Aviation Aircraft. SAE Paper 730325, April 1973.

8. Miley, S. J.; Cross E. J., Jr.; Owens, J. K.; and Lawrence, D. L.: An Investigation of the Aerodynamics and Cooling of a Horizontally-Opposed Engine Installation. SAE Quarterly Transactions, Vol. 86, September 1978.

9. Miley, S. J.; Cross, E. J., Jr.; Owens, J. K.; and Lawrence, D. L.: Aerodynamics of Horizontally-Opposed Aircraft Engine Installations. AIAA Paper 77-1249, August 1977.

10. Miley, S. J.; Cross, E. J.,Jr.; Ghomi, N. A.; and Bridges, P. D.: Determination of Cooling Air Mass Flow for a Horizontally-Opposed Aircraft Engine Installation. SAE Quarterly Transactions, Vol. 88, August 1980.

11. Corsiglia, V. R.; Katz, J.; and Kroeger, R. A.: Full-Scale Wind Tunnel Study of Nacelle Shape on Cooling Drag. AIAA Paper 79-1820, August 1979.

12. Rubert, K. F.; and Knopf, G. S.: A Method for the Design of Cooling Systems for Aircraft Power-Plant Installations. NACA WR L-491, 1942.

13. Biermann, A. E.: The Design of Metal Fins for Air-Cooled Engines. SAE Journal (Transactions), Vol. 41, No. 3, 1937.

14. Goldstein, A. W.; and Ellerbrock, H. H., Jr.: Compressibility and Heating Effects on Pressure Loss and Cooling of a Baffled Cylinder Barrel. NACA Report No. 783, 1944.

15. Neustein, J.; and Schafer, L. J., Jr.: Comparison of Several Methods of Predicting the Pressure Loss of Altitude Across a Baffled Aircraft-Engine Cylinder. NACA Report No. 858, 1946.

16. Pinkel, B.; and Ellerbrock, H. H., Jr.: Correlation of Cooling Data from an Air-Cooled Cylinder and Several Multi-cylinder Engines. NACA Report No. 683, 1940.

17. Manganiello, E. J.: Valerino, M. F.; and Bell, B. B.: High-Altitude Flight Cooling Investigation of a Radial Air-Cooled Engine. NACA Report No. 873, 1947.

18. Kuchemann, D.; and Weber, J.: Aerodynamics of Propulsion. McGraw-Hill Book Co., Inc., New York, 1953.

19. Stockman, N. O.; and Button S. L.: Computer Programs for Calculation Potential Flow in Propulsion System Inlets. NASA TM X-68278, 1973.

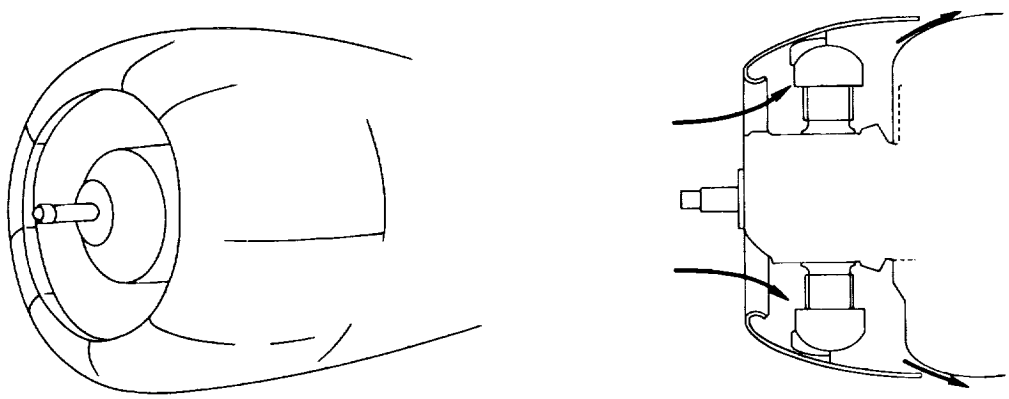

(a) radial

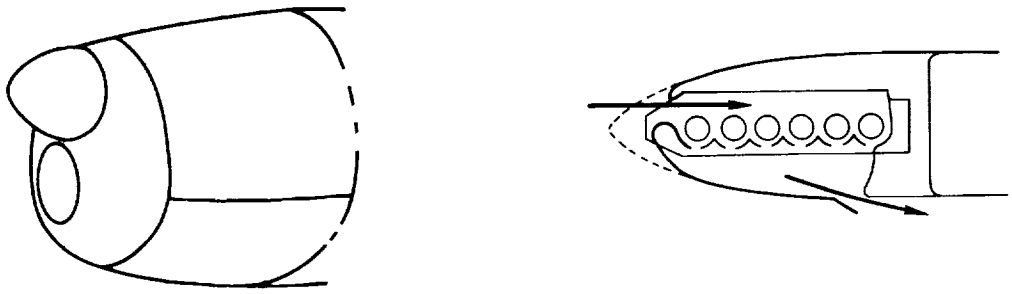

(b) in-line

Figure 1. - Aircraft engine cooling installations.

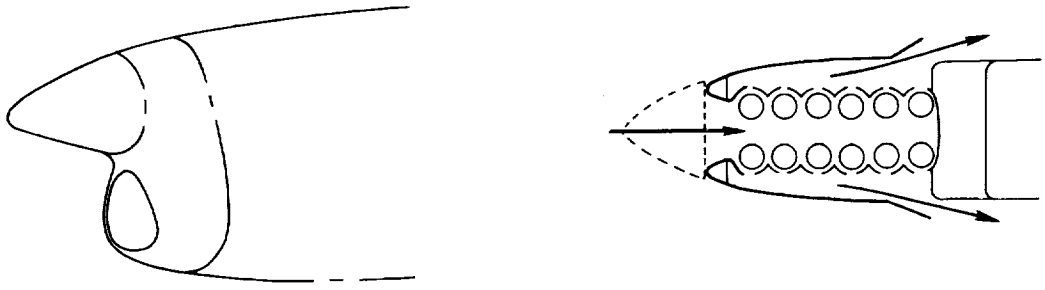

(c) vee

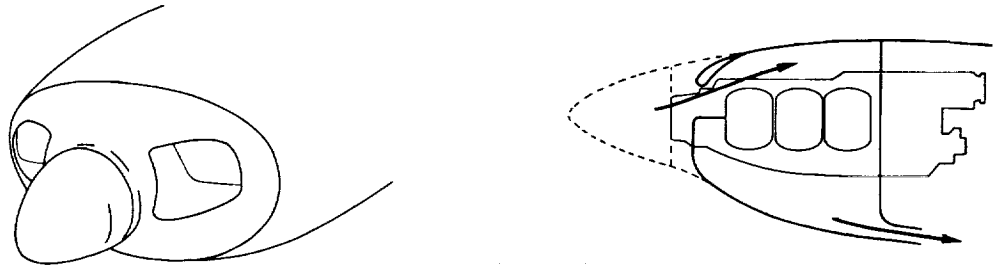

(d) horizontally-opposed

Figure 1. - Concluded.

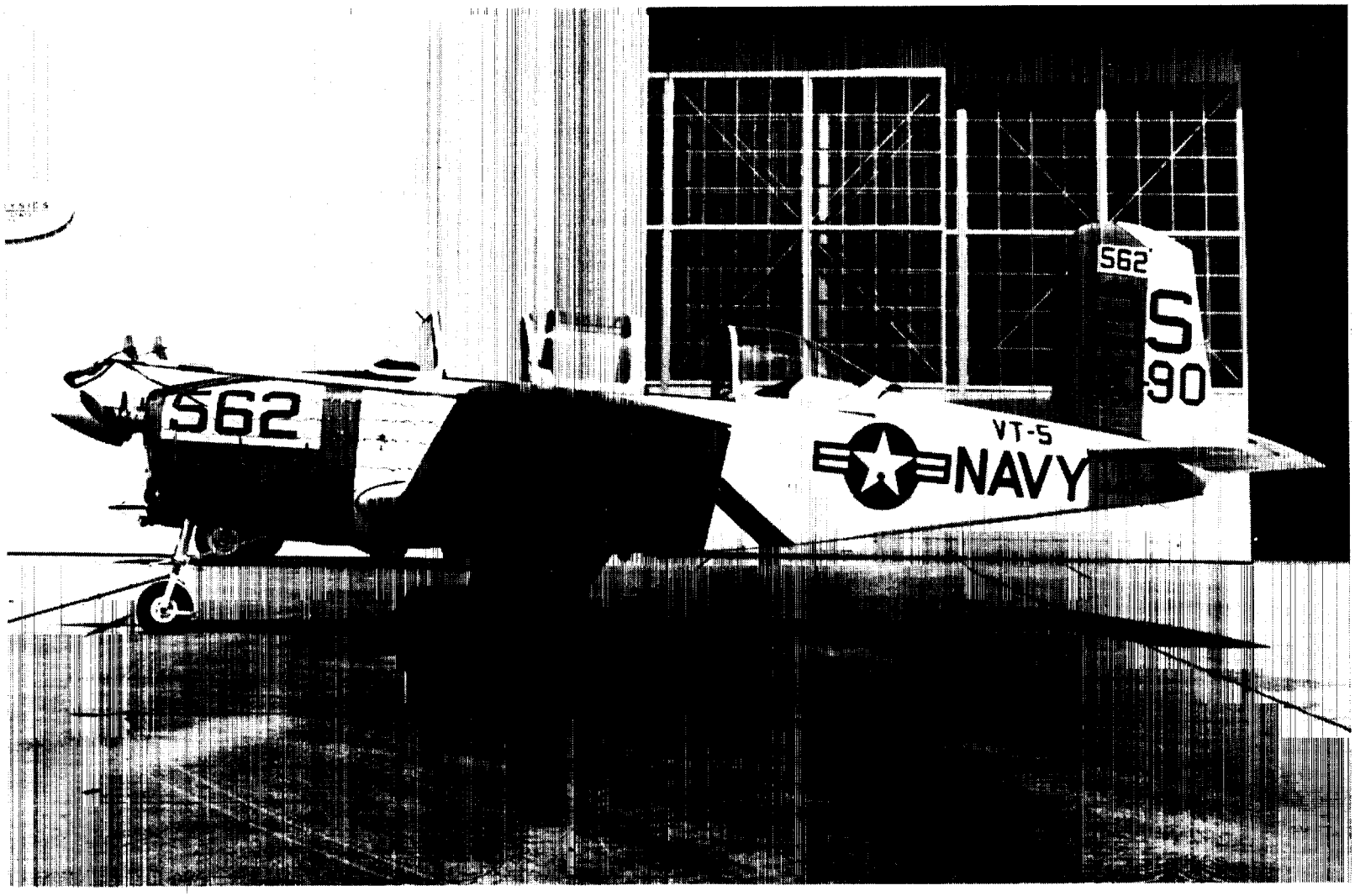

Figure 2. - Beech T34-B aircraft used in cooling drag measurement tests.

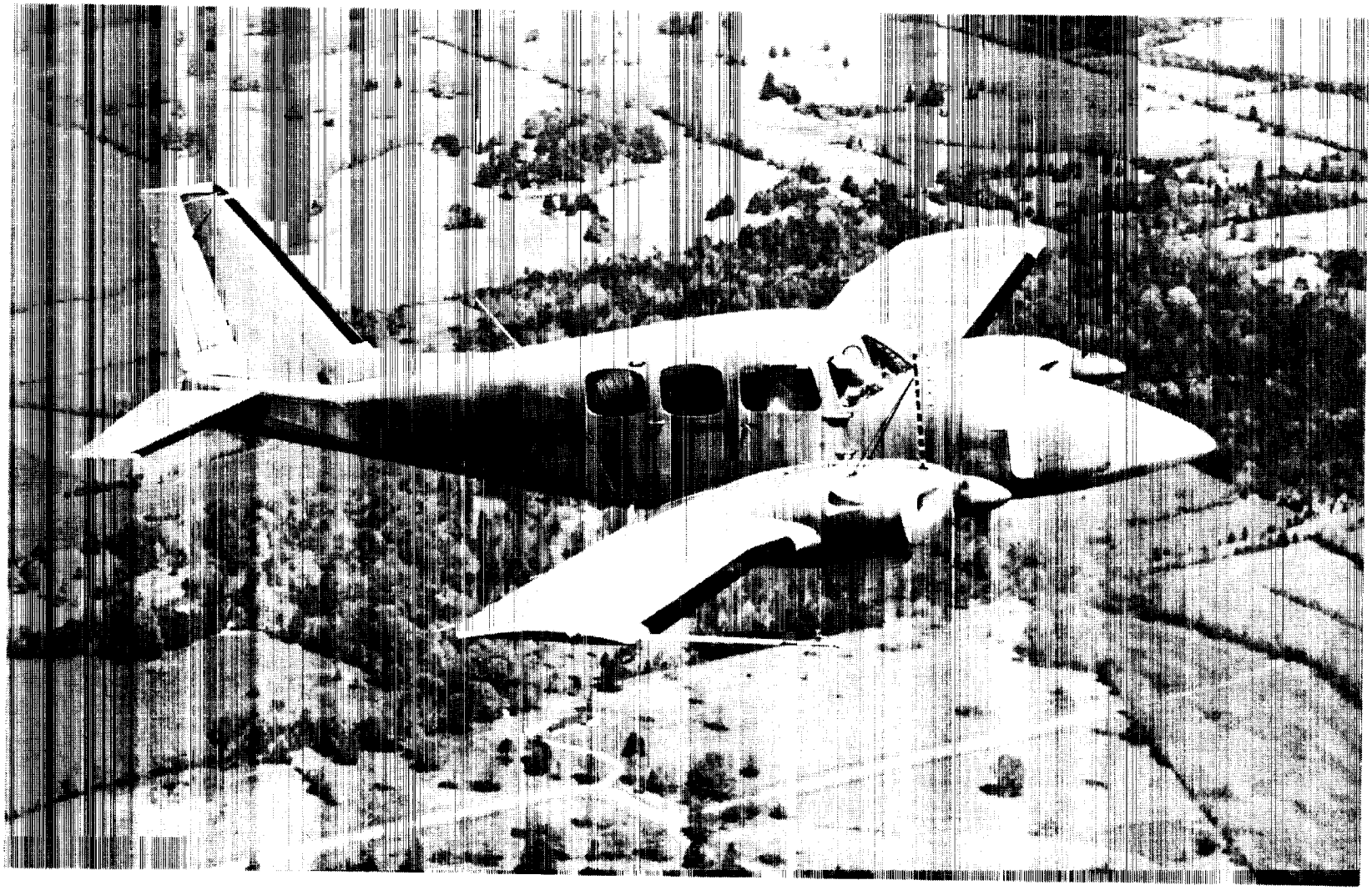

Figure 3. - Piper PA-41P Aztec test aircraft.

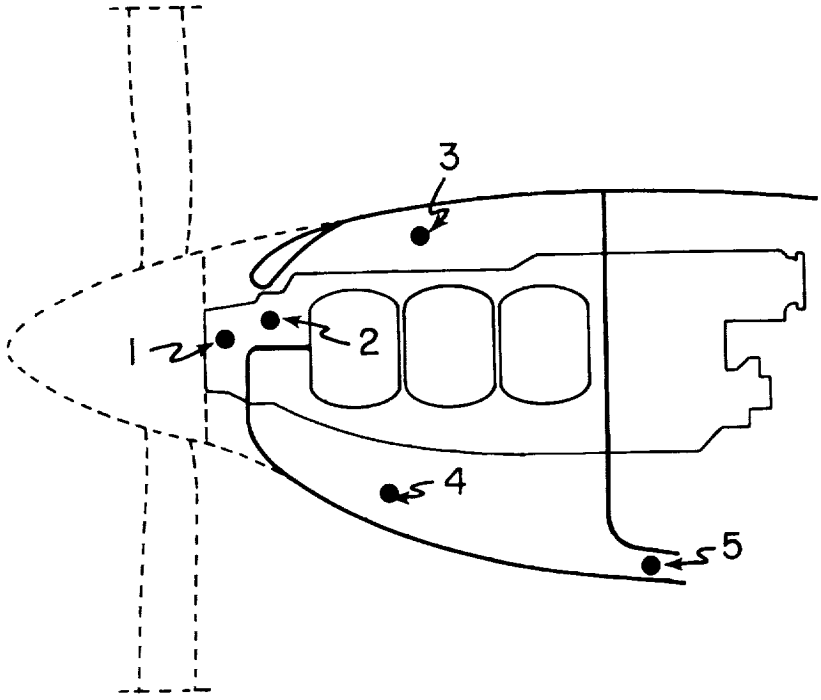

Figure 4. - PA-41P test aircraft cooling installation.

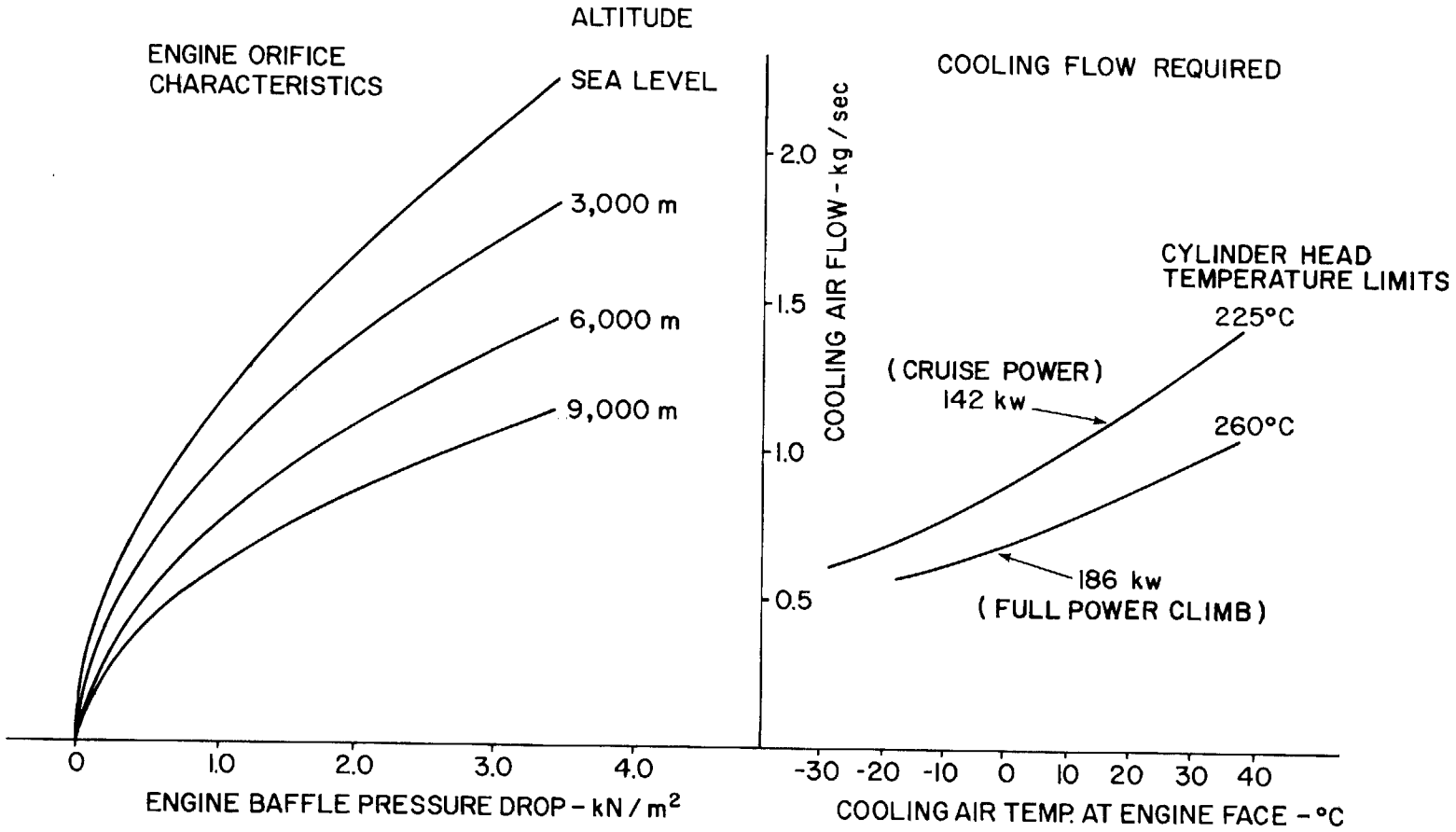

Figure 5. - Engine cooling requirements supplied by manufacturer.

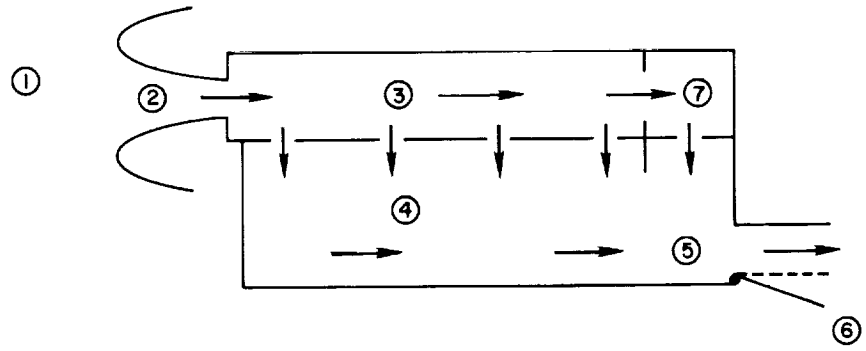

Figure 6. - Cooling installation model schematic.

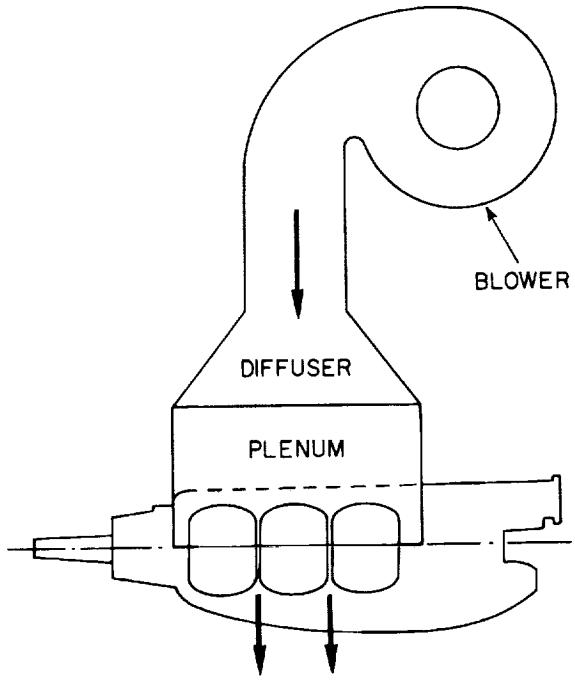

Figure 7. - Engine orifice characteristics and cooling requirements determination test set-up.

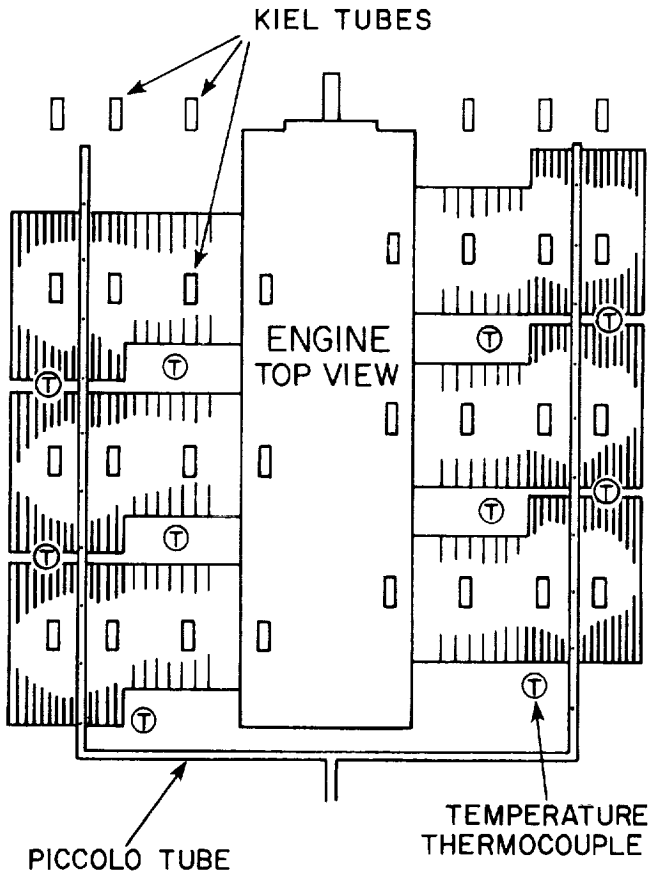

Figure 8. - Location of Kiel total pressure probes and temperature probes in the high pressure plenum.

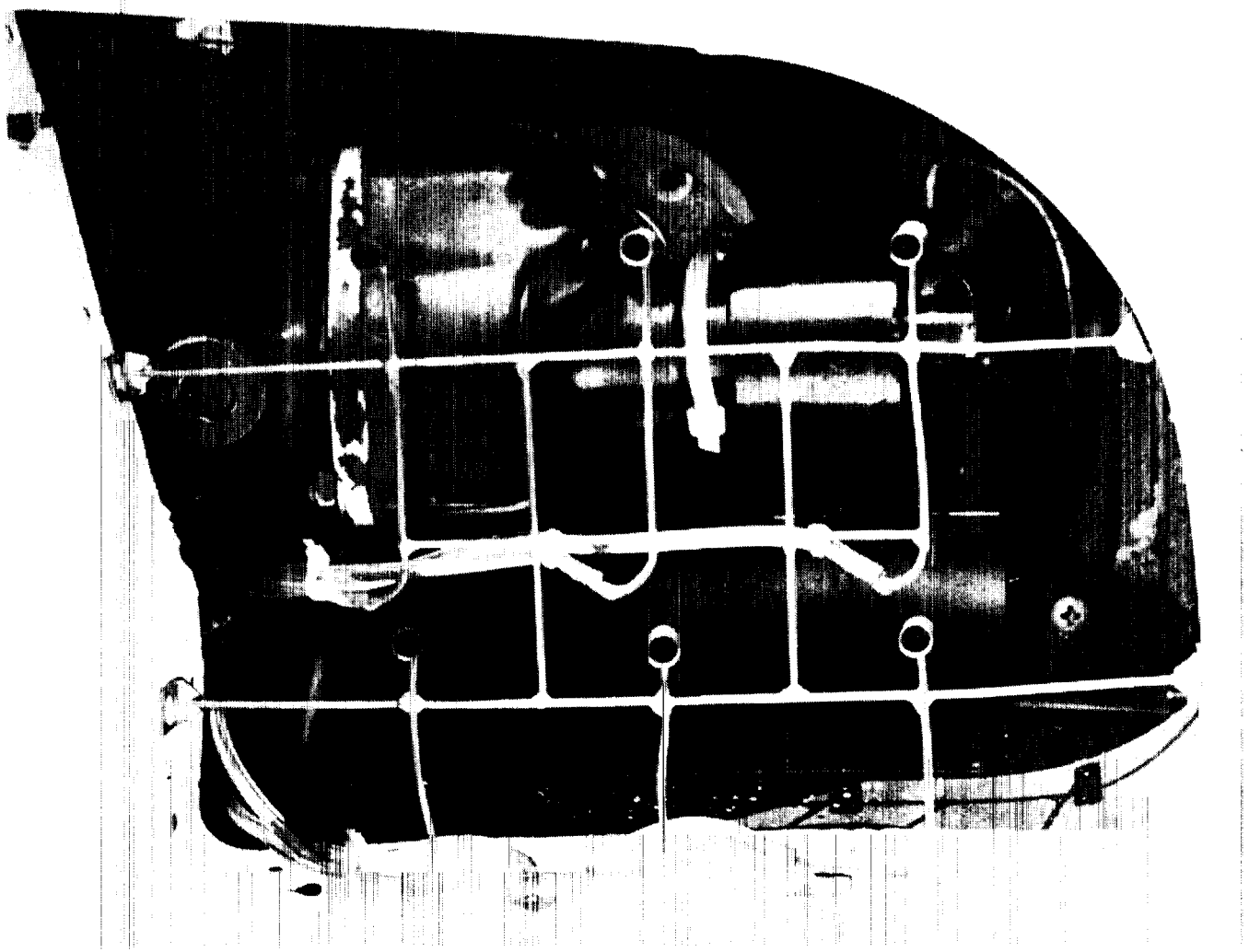

Figure 9. - Kiel total pressure probes located in the inlet.

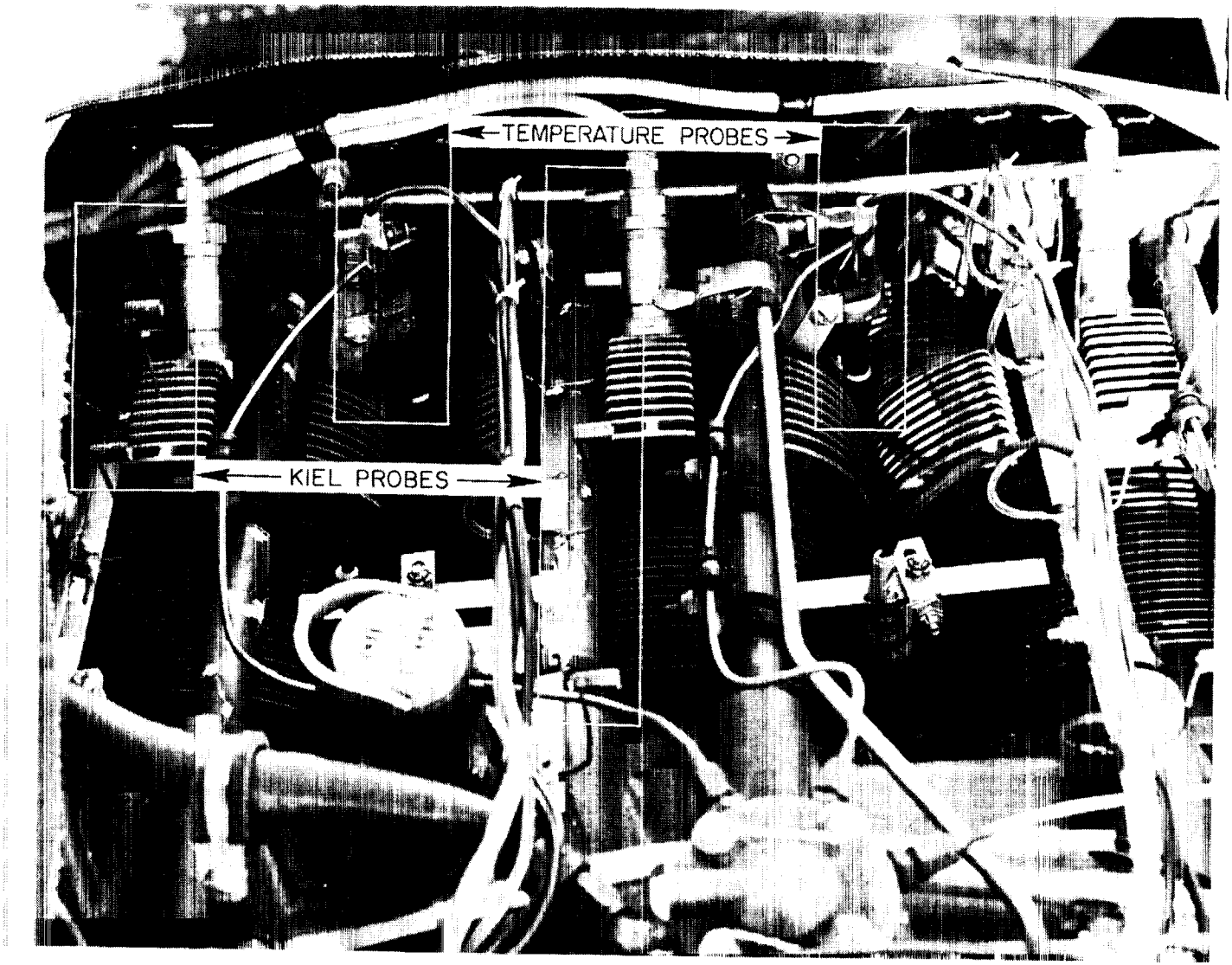

Figure 10. - Installation of the total pressure and temperature probes in the high pressure plenum.

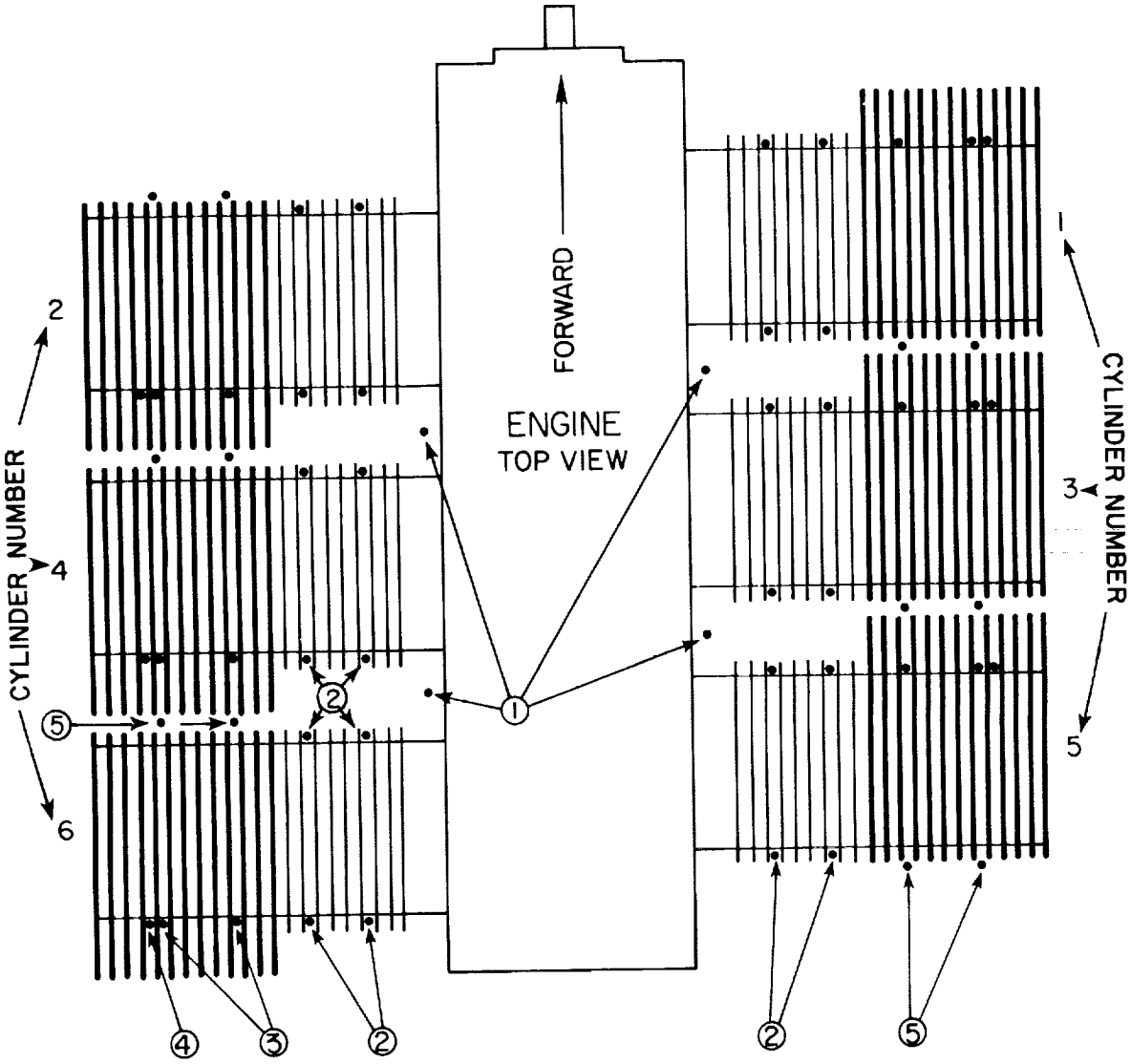

(a) probe locations

Figure 11. - Internal flow pressure probes, locations, and cylinder numbers. Circled numbers denote probe type; dots denote locations.

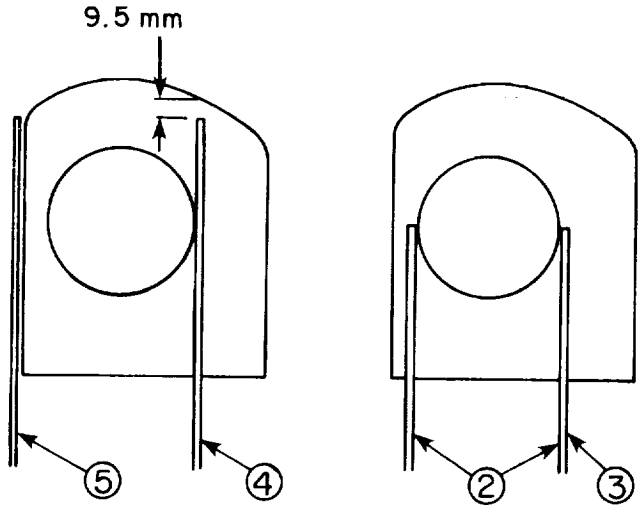

(b) probe vertical positions

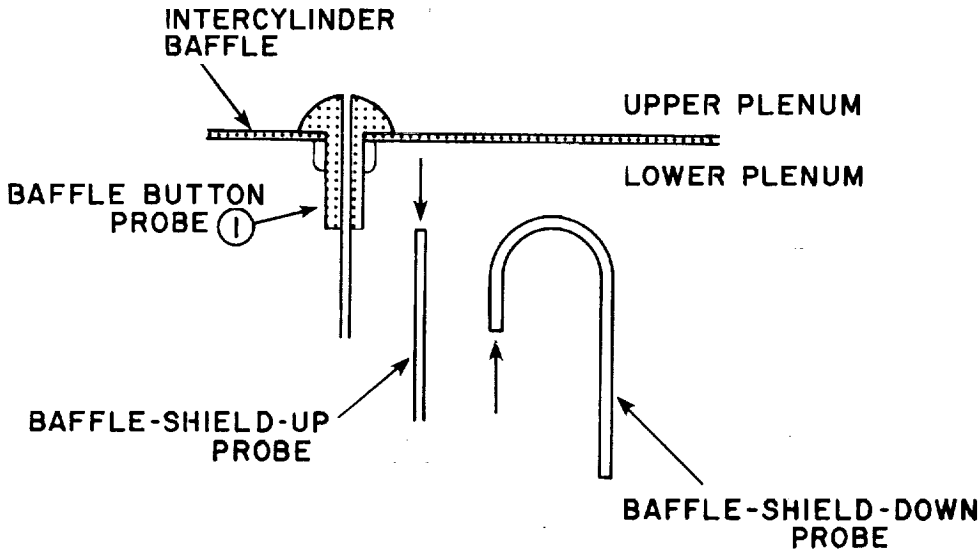

(c) baffle button and lower plenum static probes

Figure 11. - Continued.

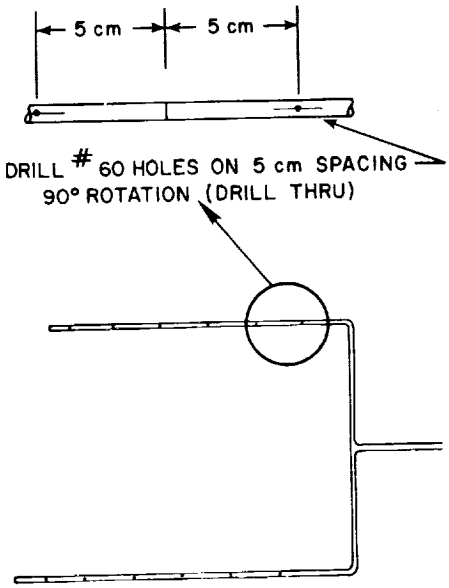

(d) piccolo tube detail

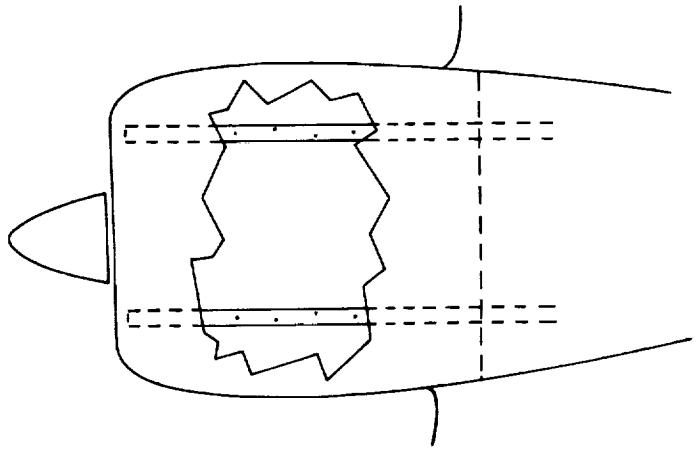

(e) static pressure belt location

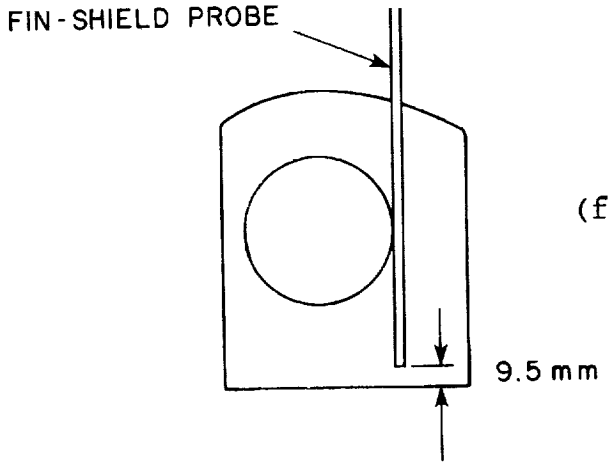

(f) fin-shield probe installation

Figure 11. - Concluded.

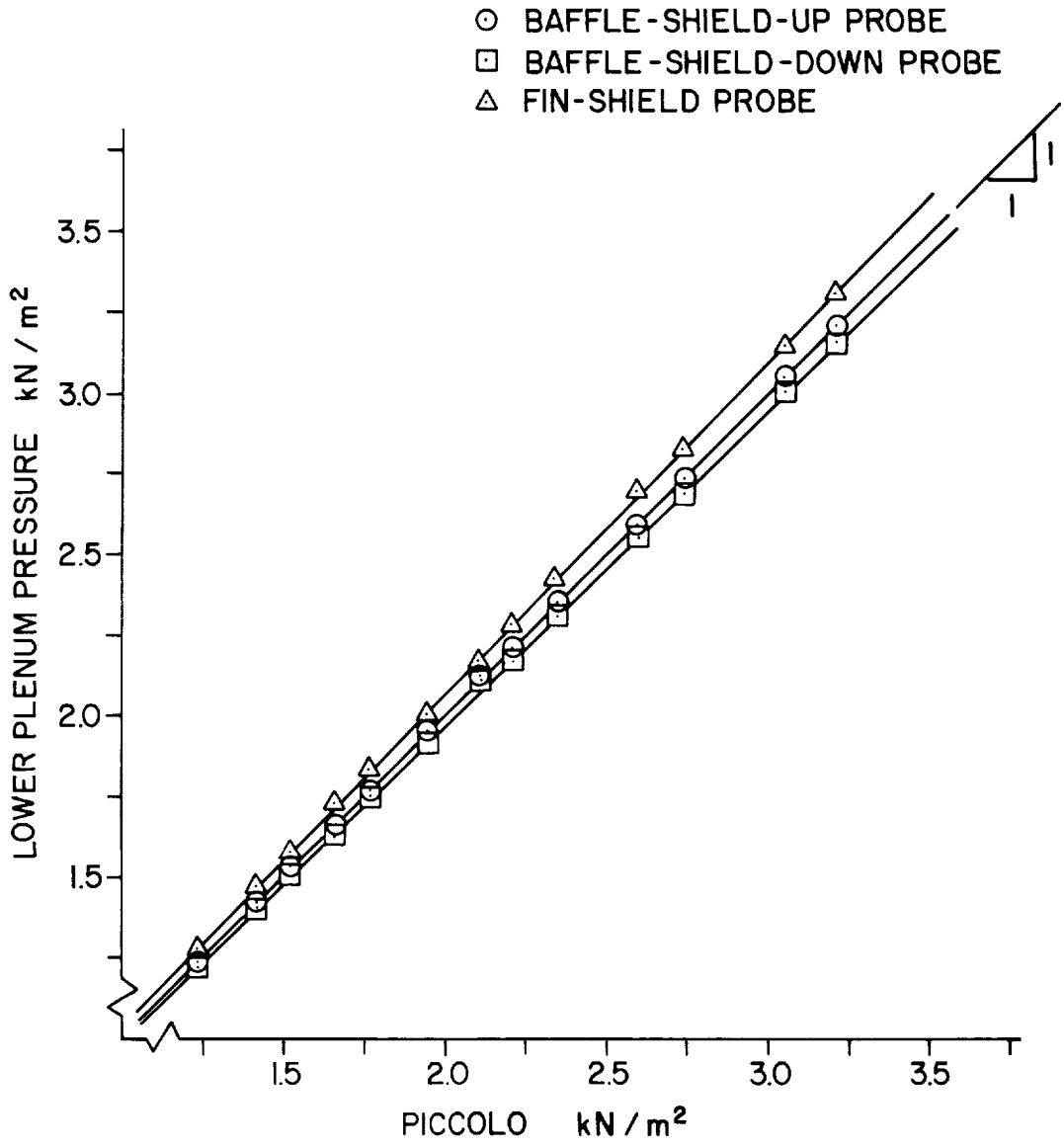

Figure 12. - Comparison of different lower plenum pressure measurements.

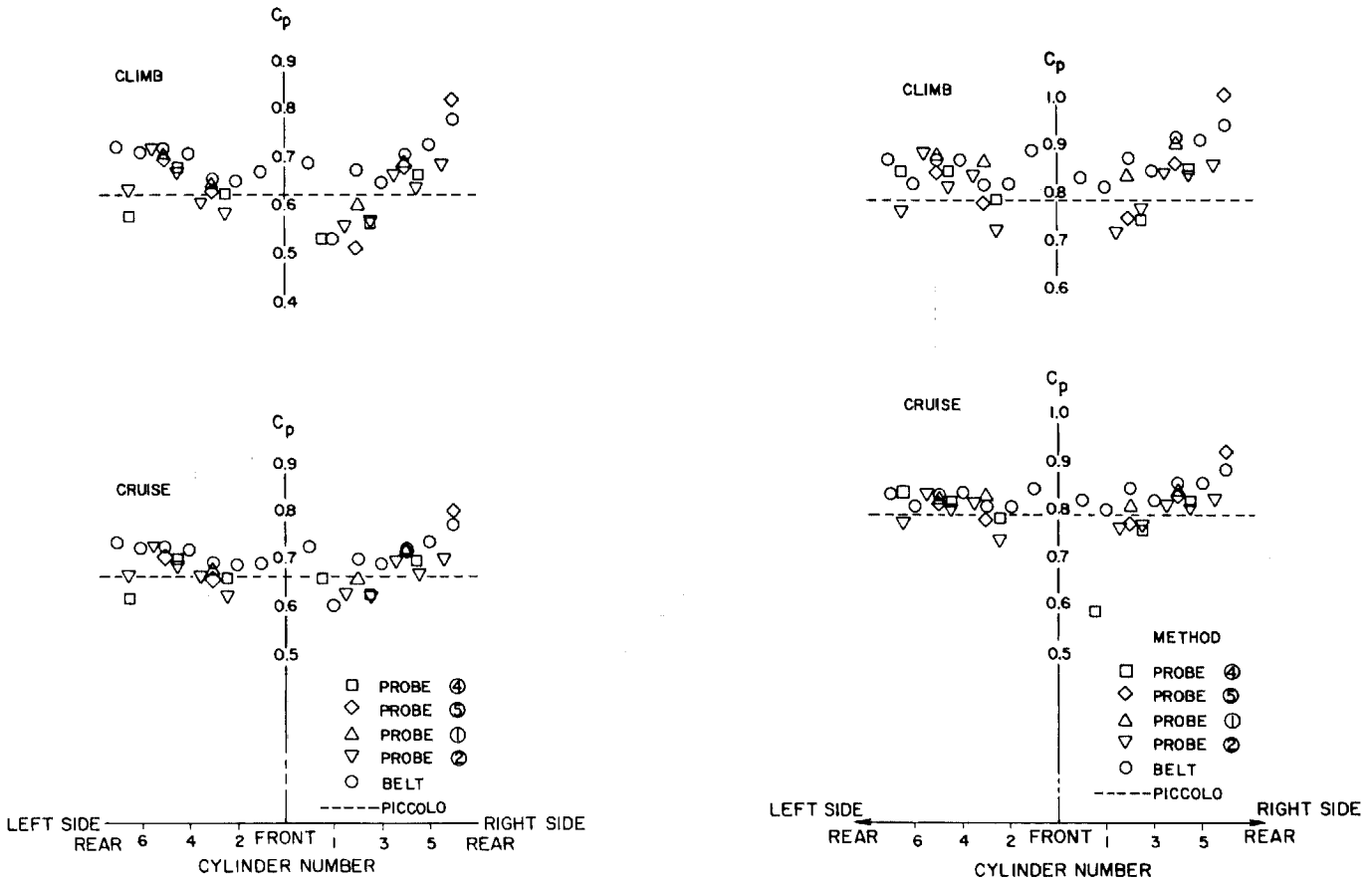

(a) original PA-41P inlet "STD"

(b) modified test inlet "0.3F"

Figure 13. - Engine face and upper plenum pressure results.

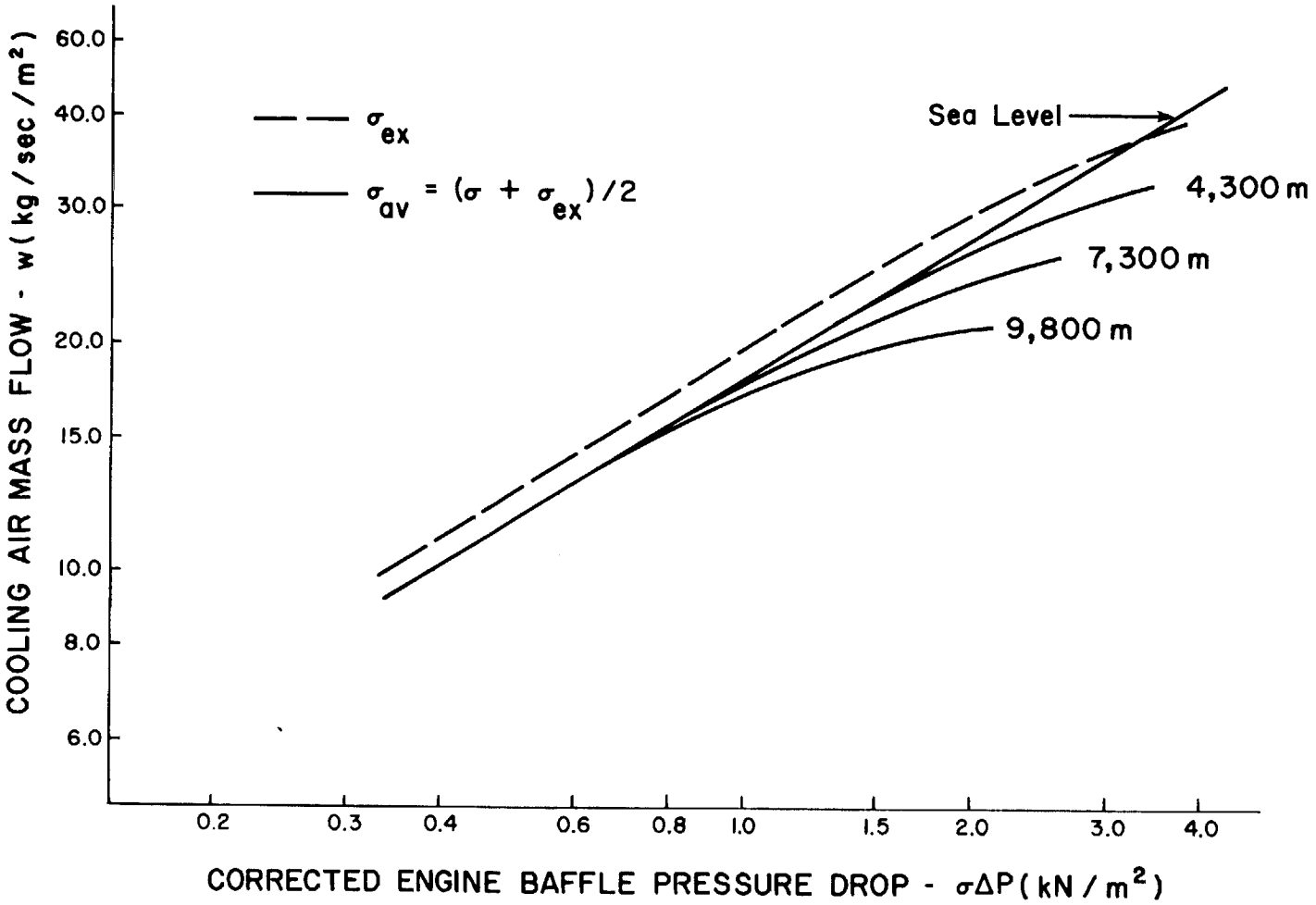

Figure 14. - Effect of density ratio term in orifice characteristics power law extrapolation. Data from reference 14.

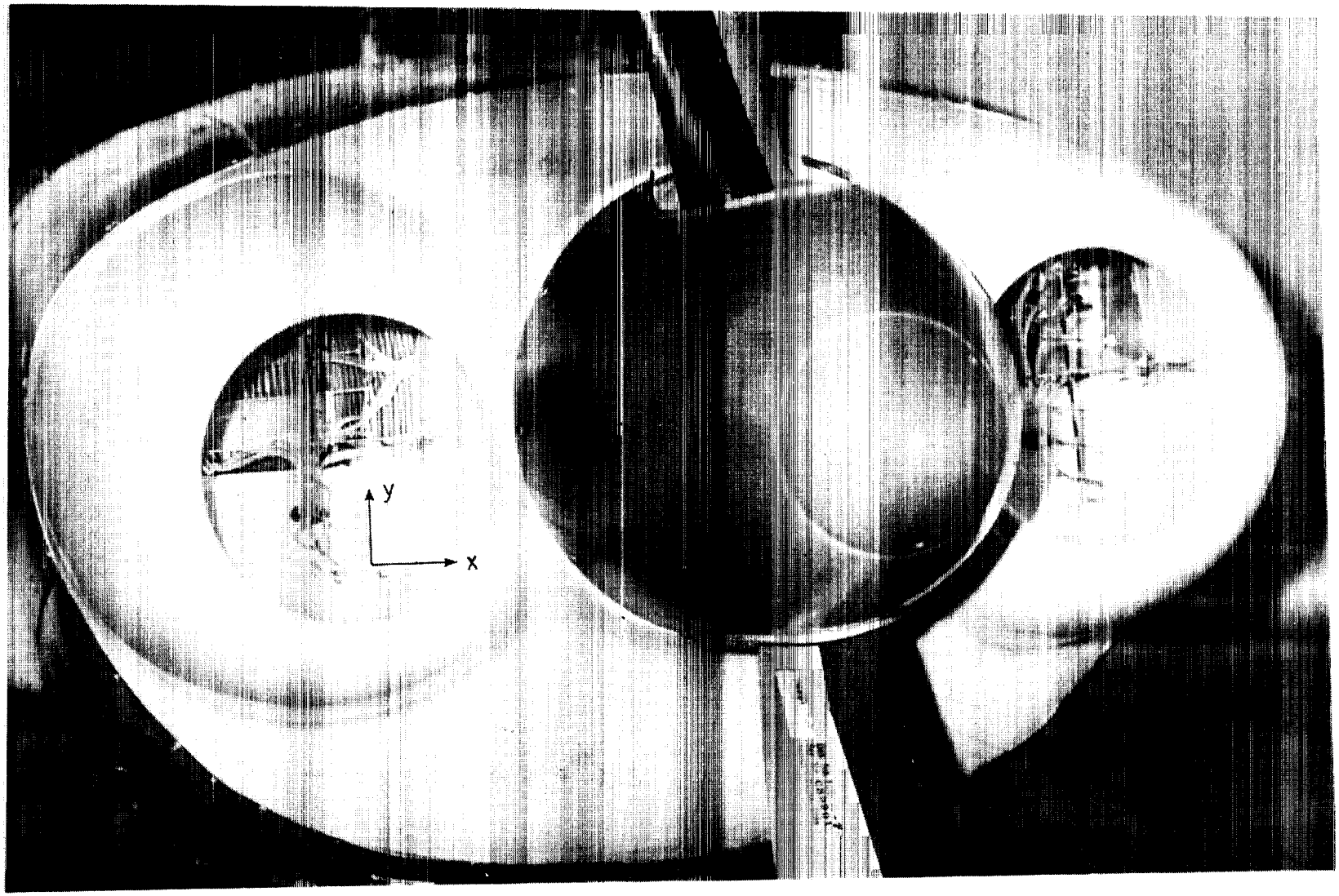

Figure 15. - Cooling air mass flow measurement system.
Coordinate system used for mass flow determination.

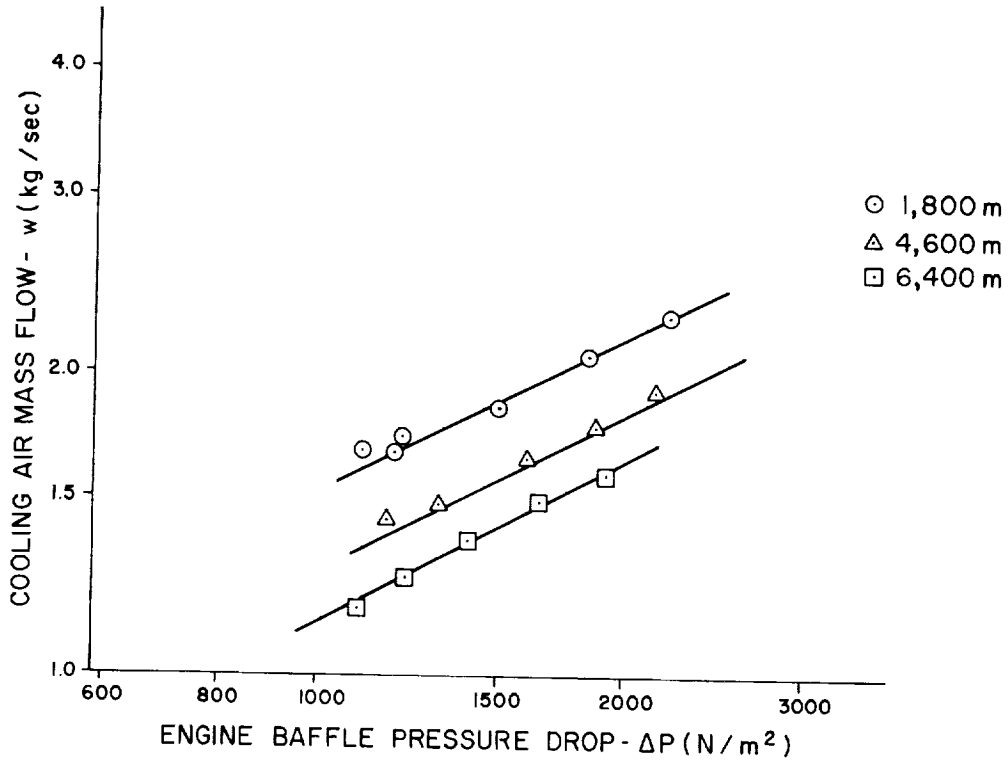

Figure 16. - Engine orifice characteristics in terms of uncorrected baffle pressure drop.

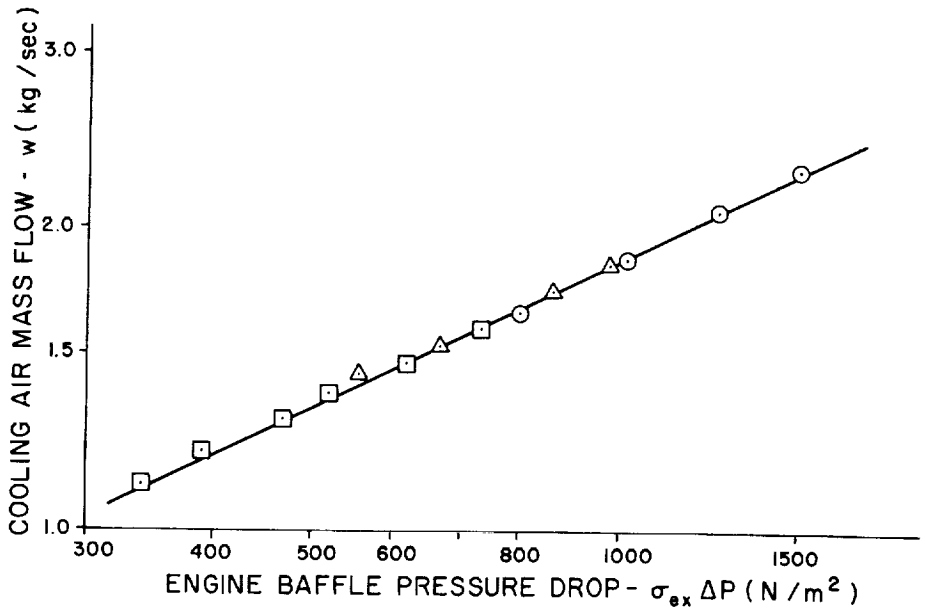

Figure 17. - Engine orifice characteristics in terms of corrected baffle pressure drop.

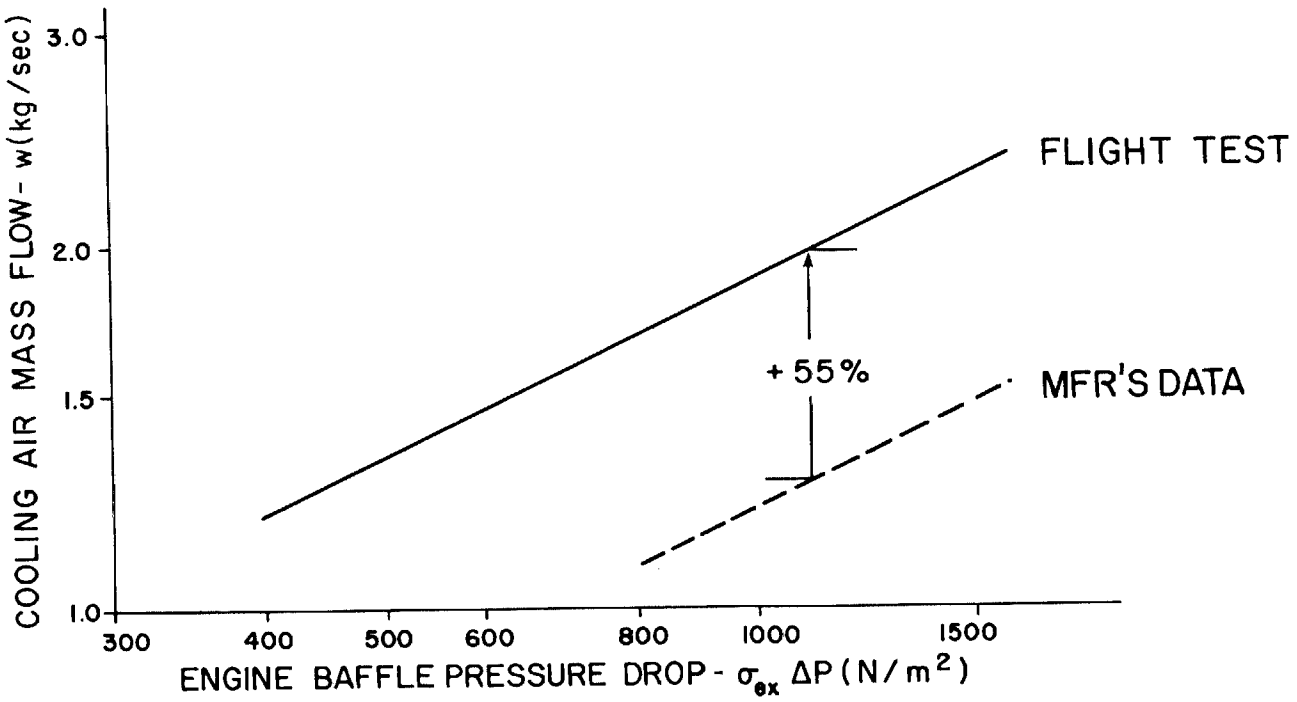

Figure 18. - Comparison of engine orifice characteristics data between flight test and engine manufacturer's data.

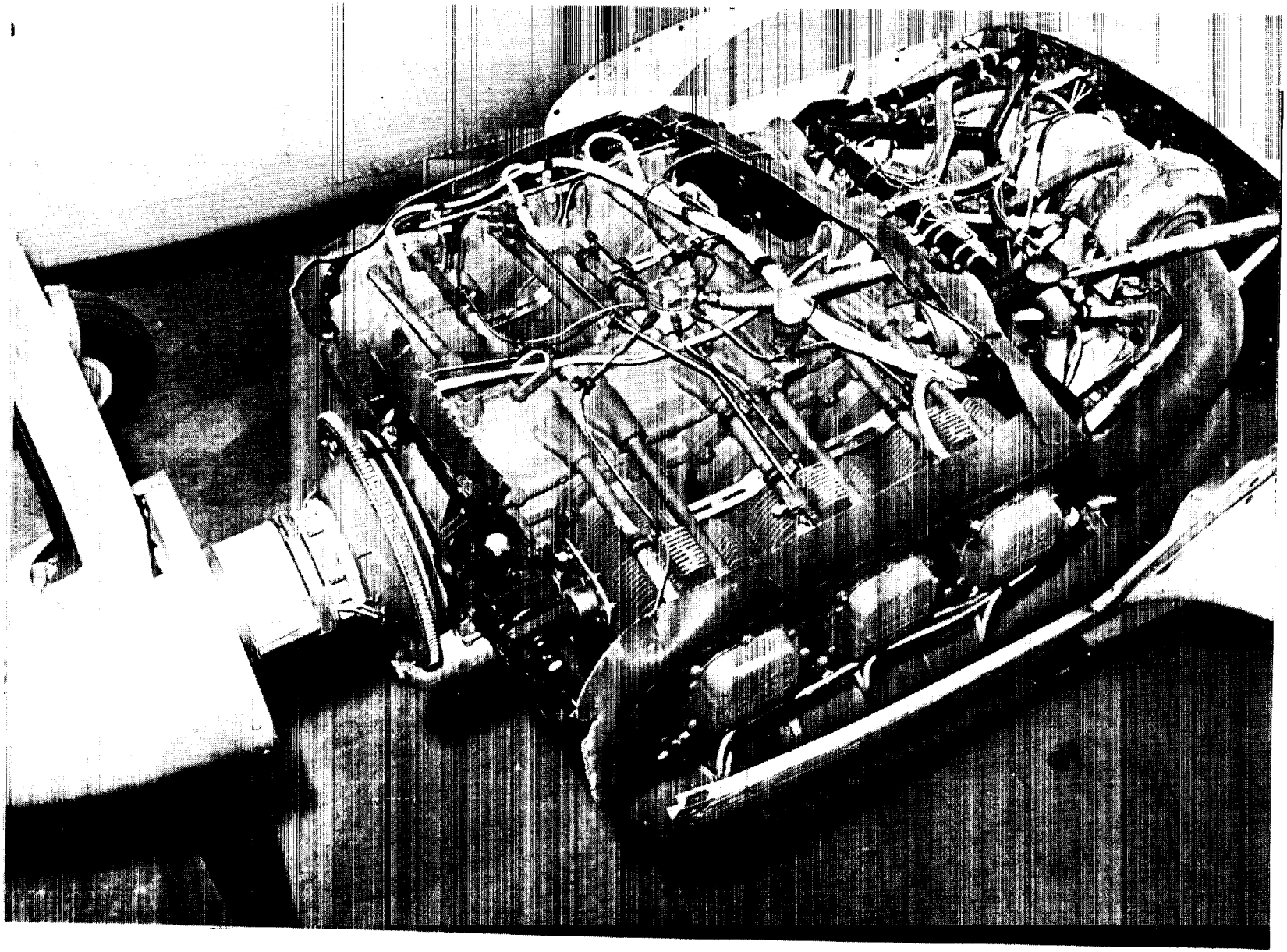

Figure 19. - PA-41P engine external baffle system.

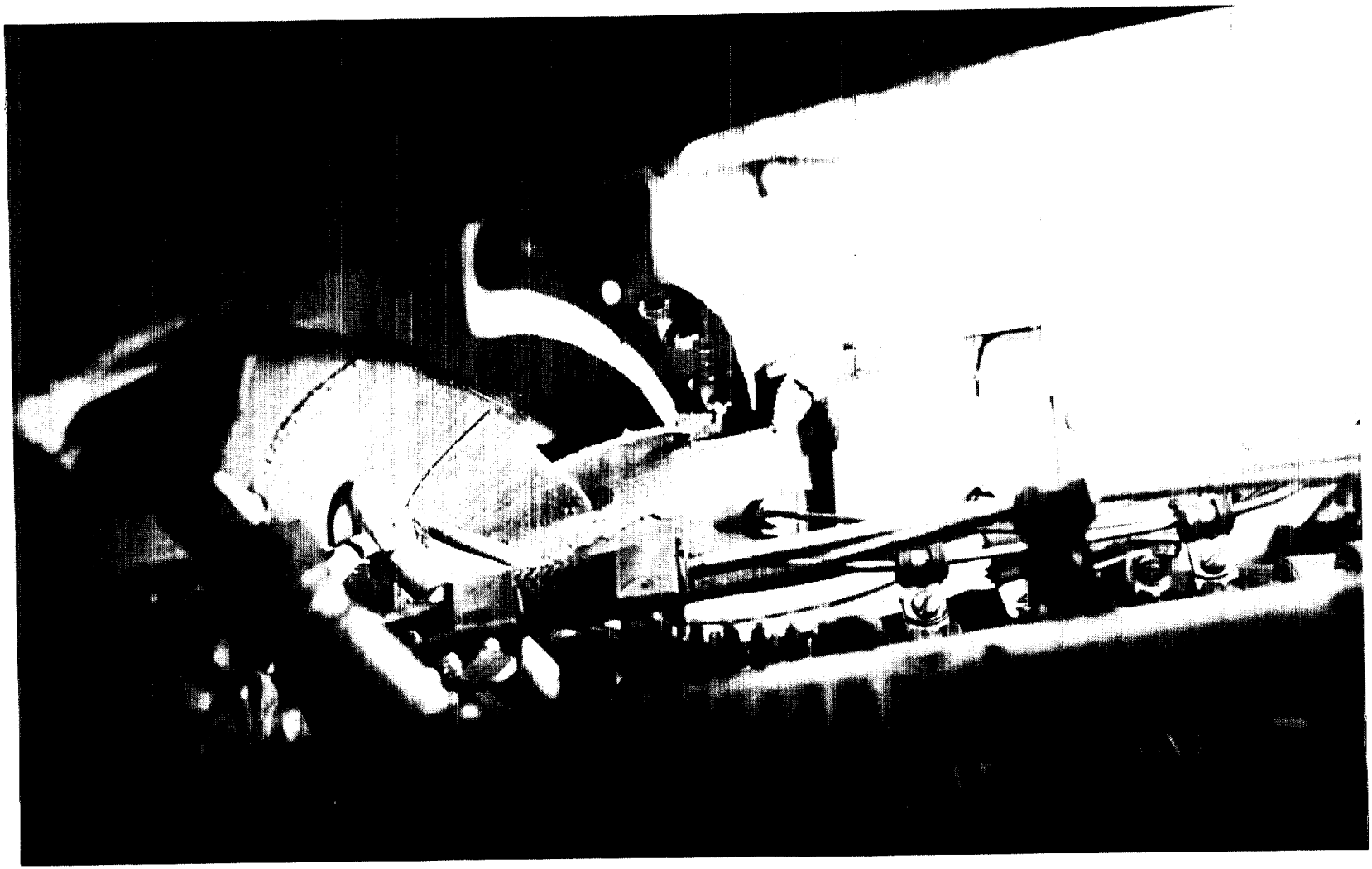

Figure 20. - External baffle system mechanism of pressure sealing.

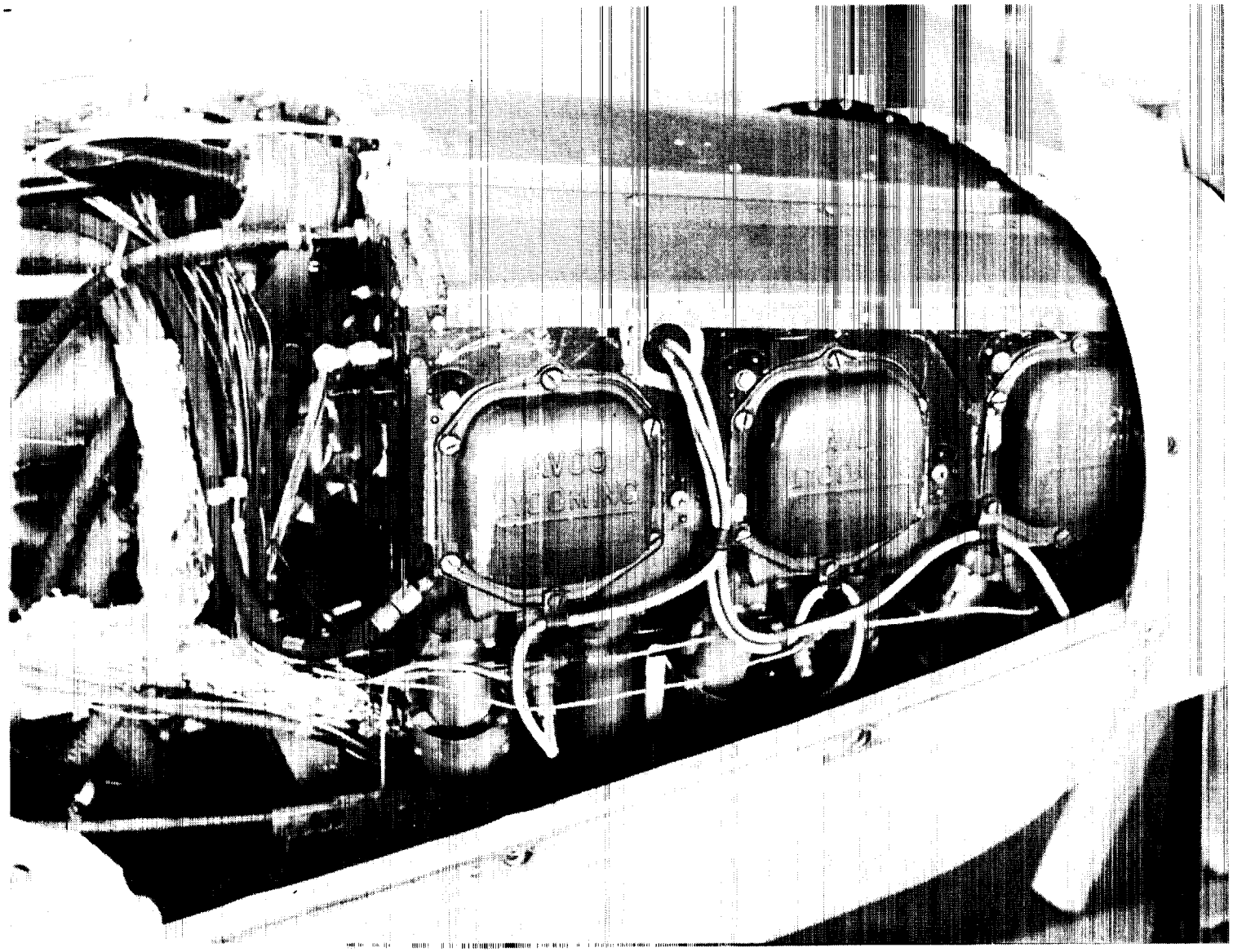

Figure 21. - Dog house external baffle system.

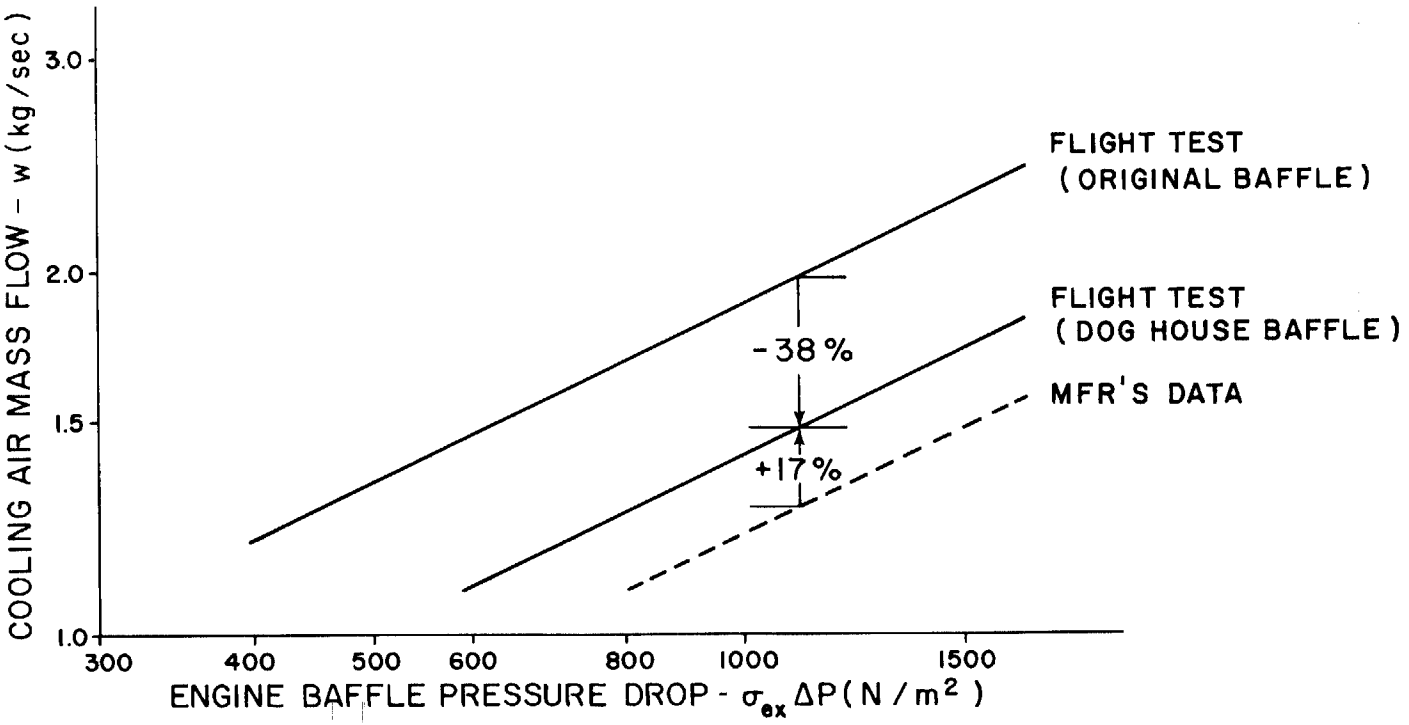

Figure 22. - Comparison of engine orifice characteristics with dog house baffle system.

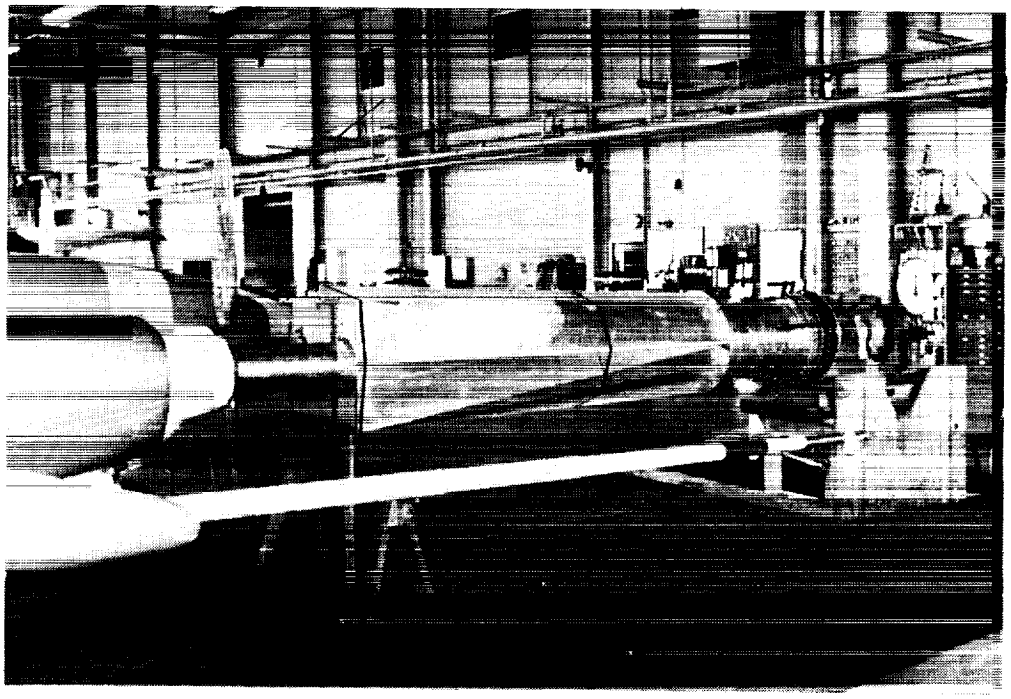

Figure 23. - Ground test system.

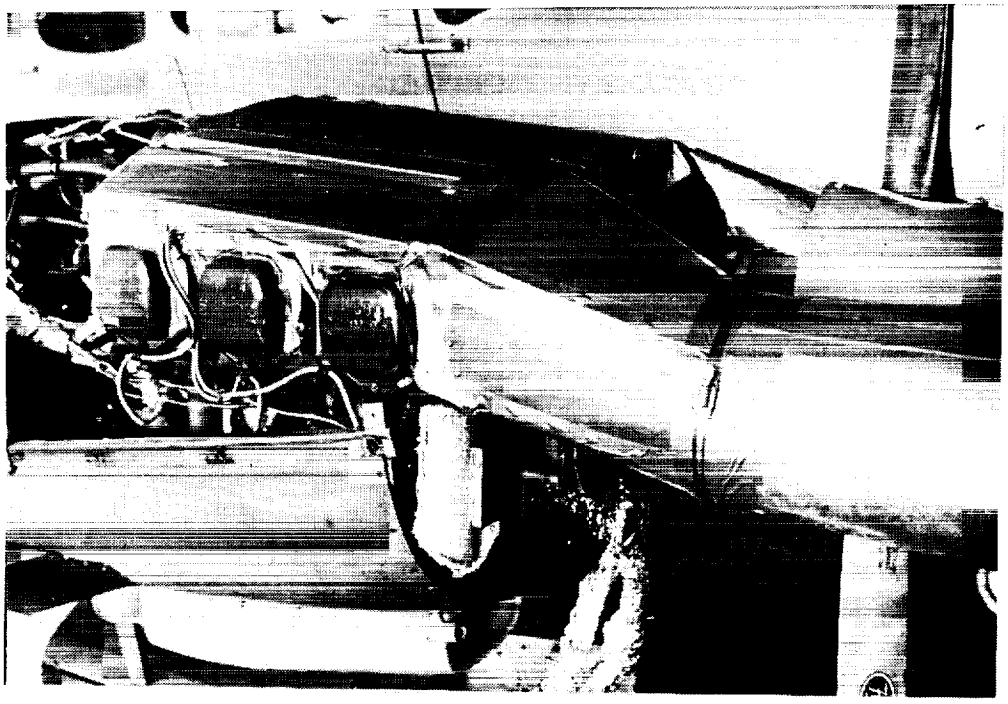

Figure 24. - Maximum seal flight configuration test.

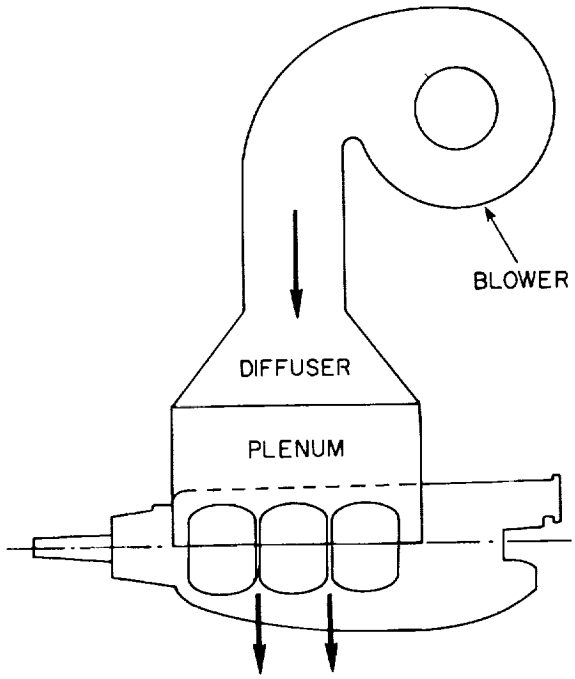

(a) ground test cell configuration

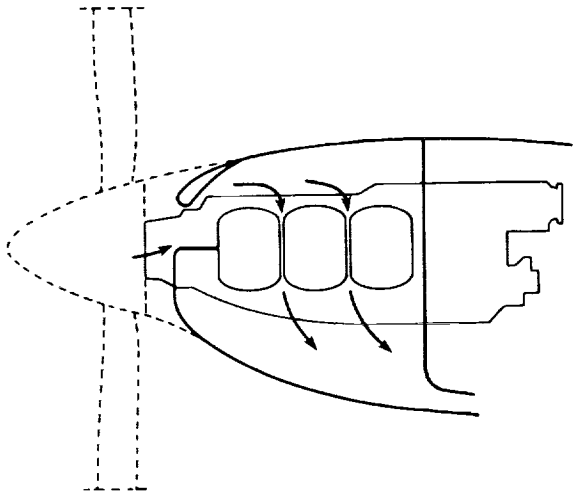

(b) aircraft flight configuration

Figure 25. - Comparison of cooling installations.

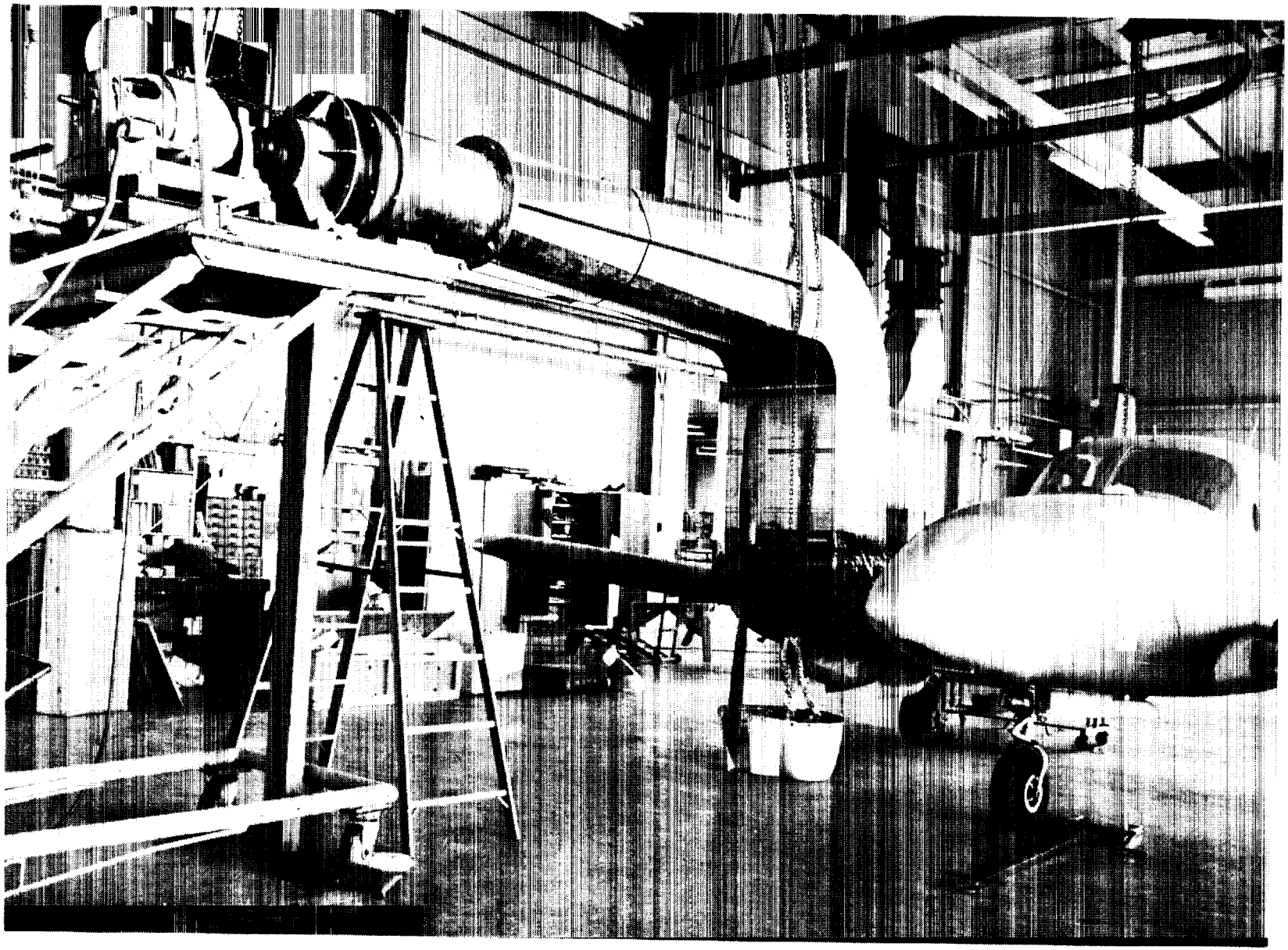

Figure 26. - Ground test cell configuration.

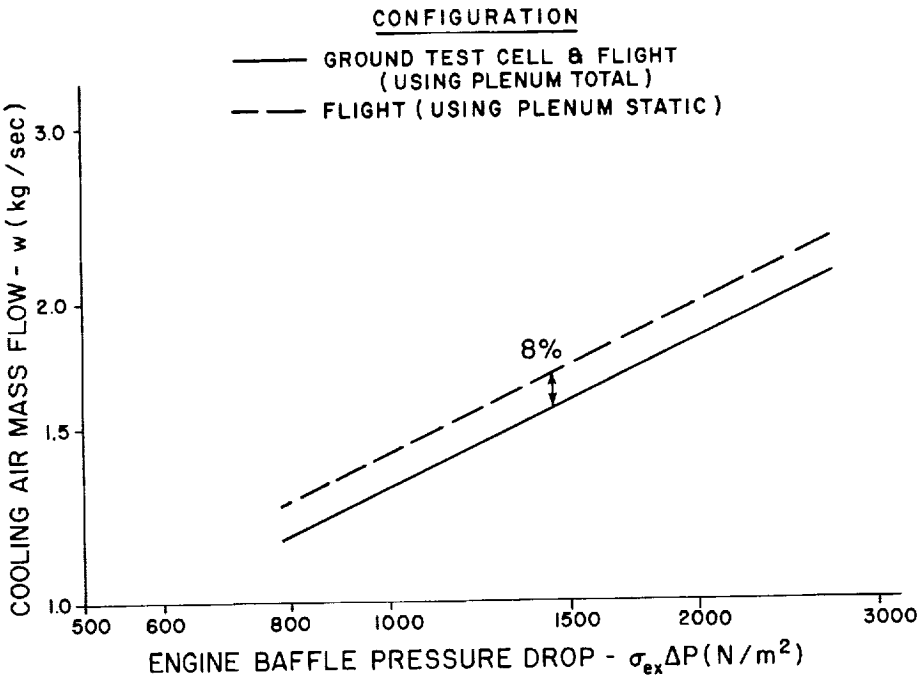

Figure 27. - Comparison of ground test measured engine orifice characteristic between the aircraft flight configuration and the ground test cell configuration shown in Figure 25.

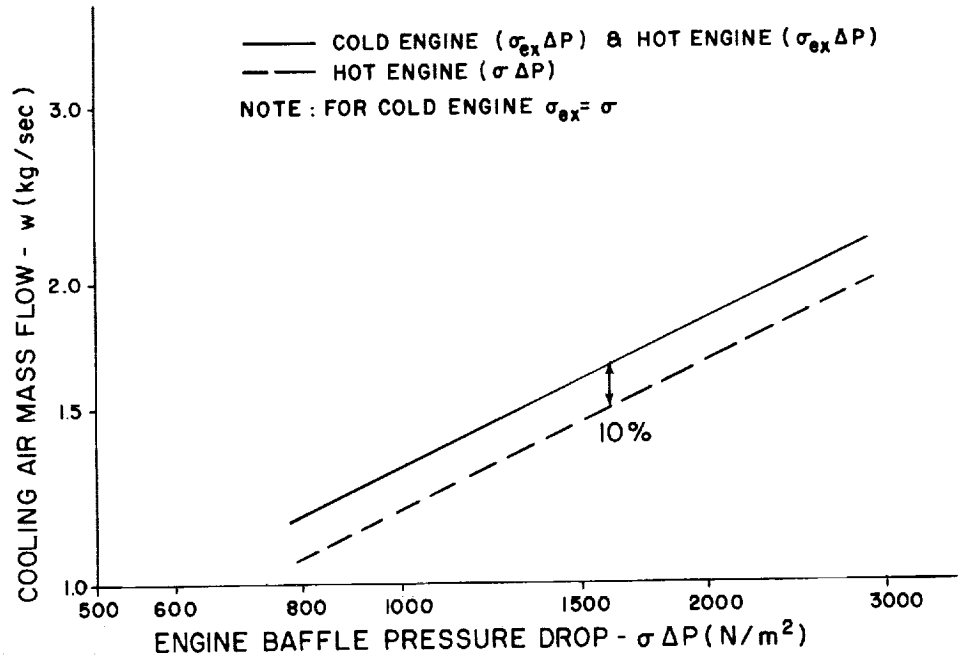

Figure 28. - Comparison of engine orifice characteristics between "hot" engine and "cold" engine, showing effect of different correction parameters.

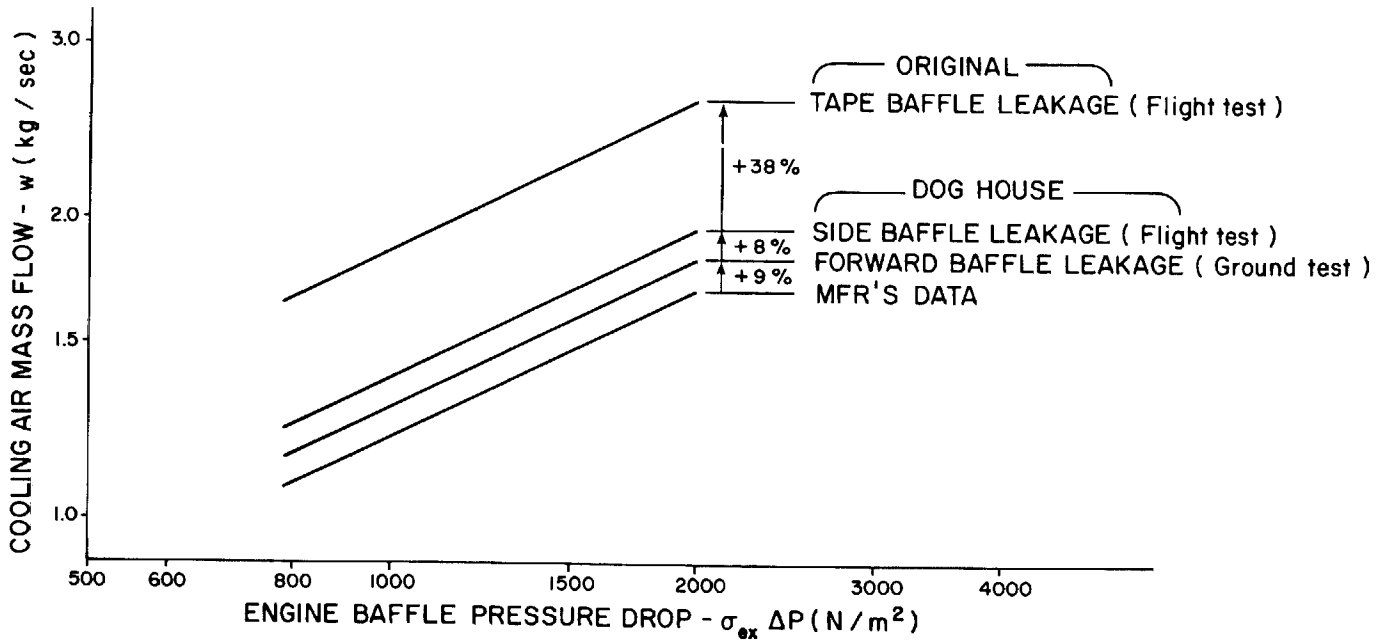

Figure 29. - Summary of engine orifice characteristics tests.

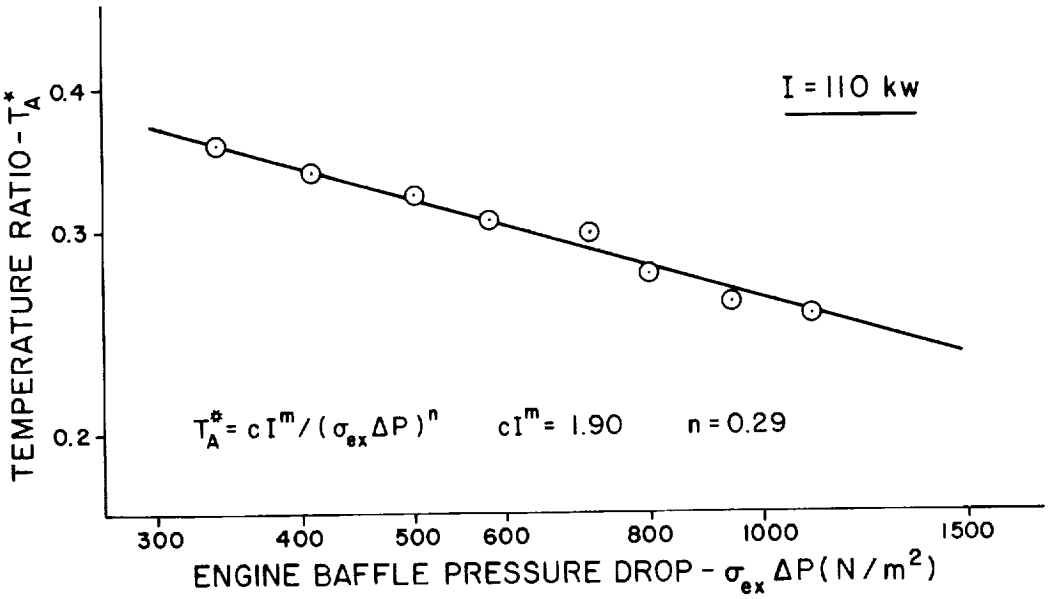

(a) constant engine power I = 110 kw, solution for "n" and "cI^m".

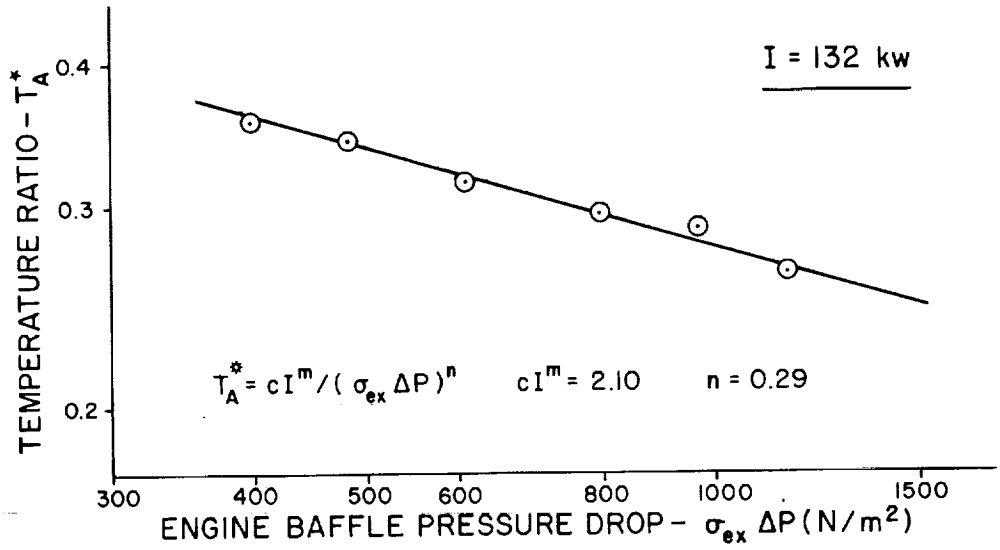

(b) constant engine power I = 132 kw, solution for "n" and "cI^m".

Figure 30. - Cooling correlation results. Solution for parameters "c","m", and "n".

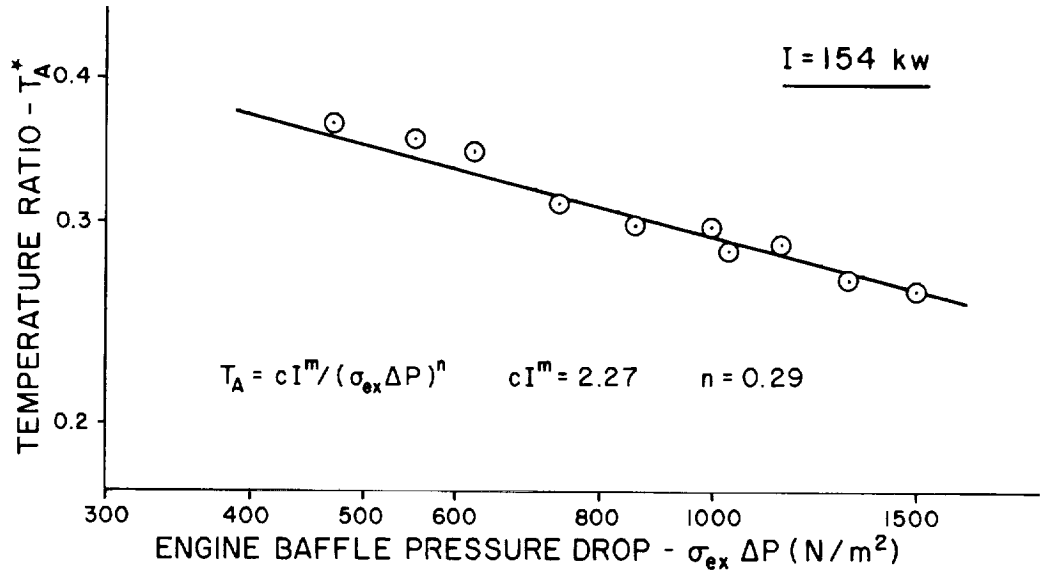

(c) constant engine power I = 154 kw, solution for "n" and "cI^m".

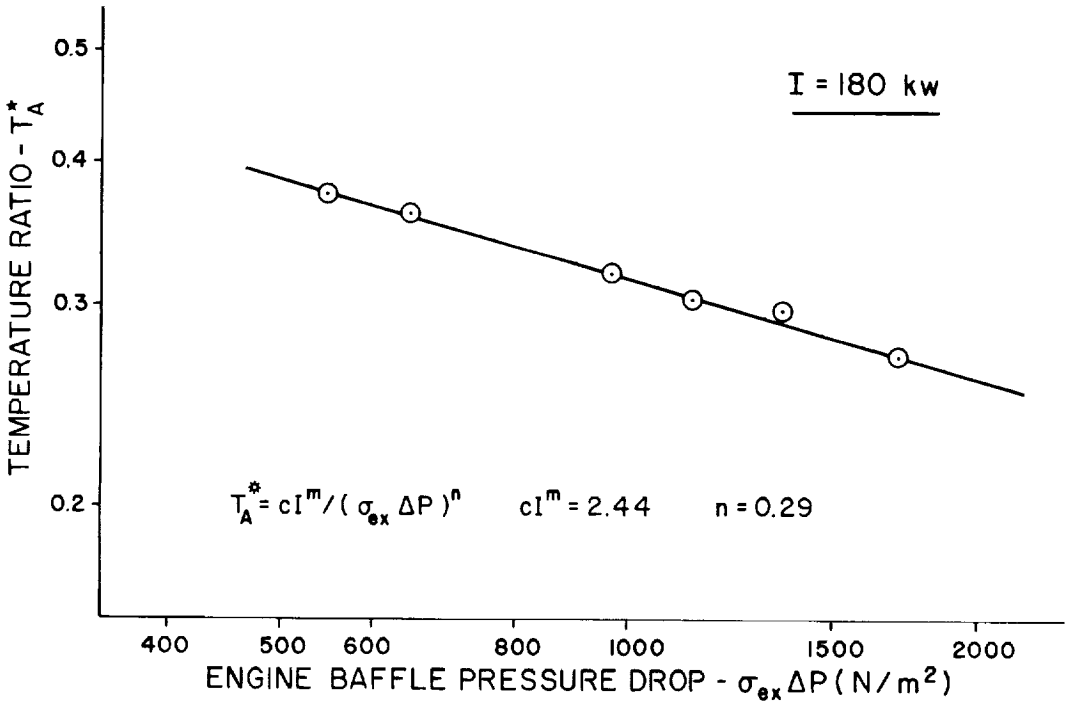

(d) constant engine power I = 180 kw, solution for "n" and "cI^m".

Figure 30. - Continued.

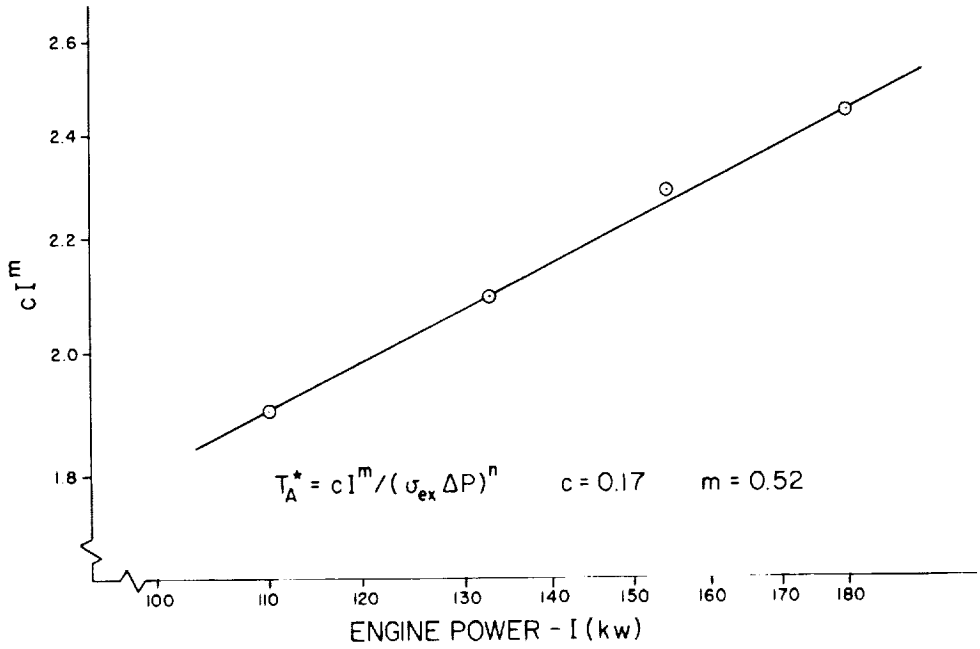

(e) solution for "e" and "m".

Figure 30. - Concluded.

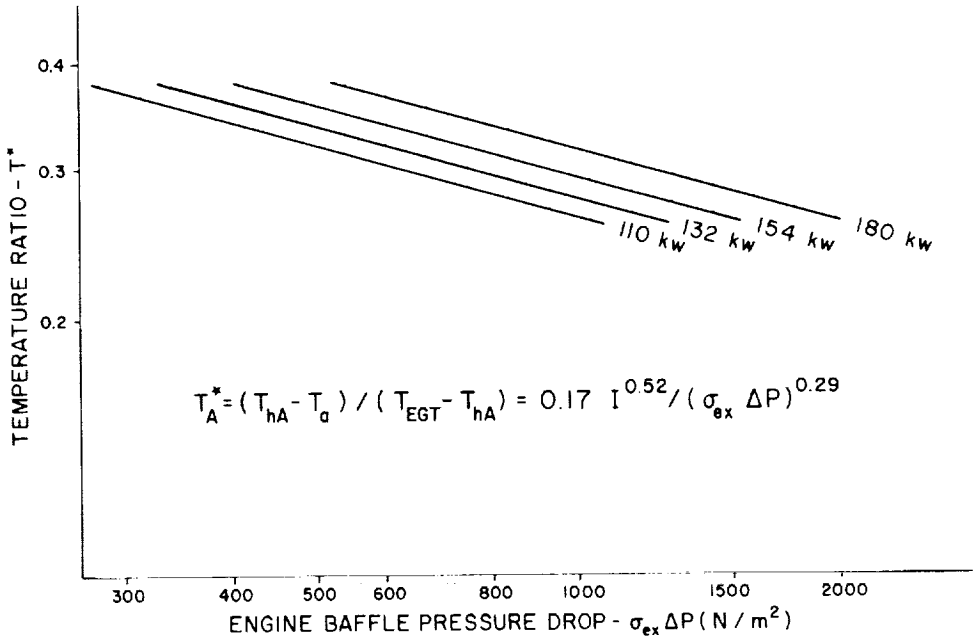

Figure 31. - Summary of cooling correlation results.

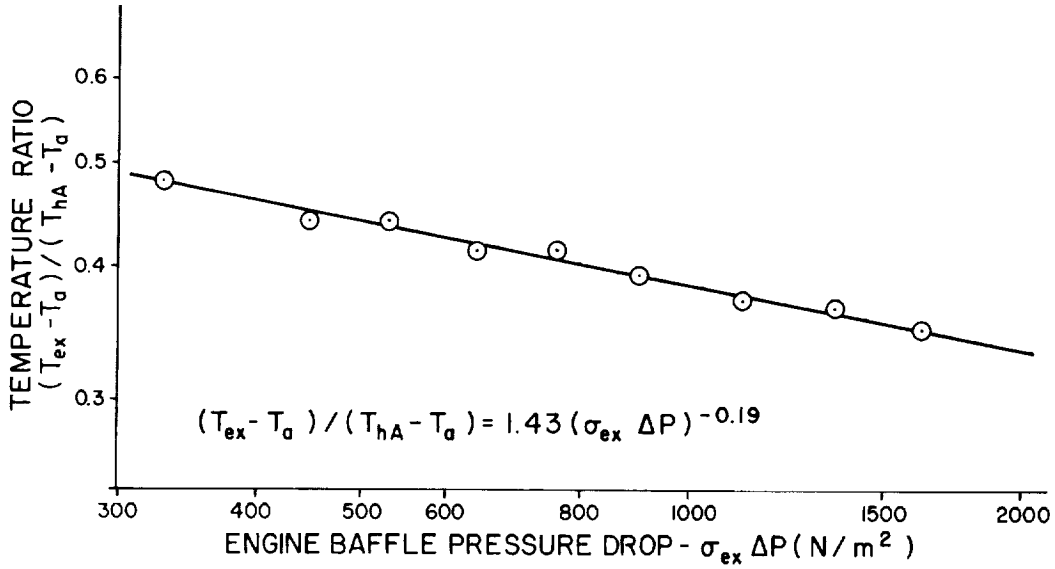

Figure 32. - Correlation for cooling flow temperature rise across the engine baffle.

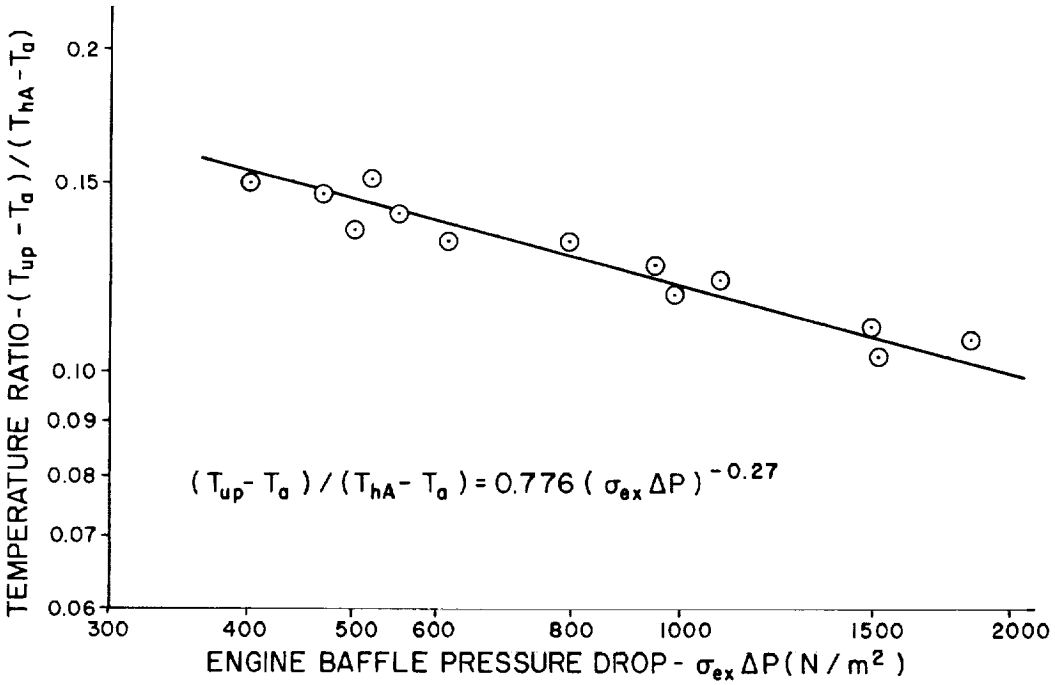

Figure 33. - Correlation for cooling flow temperature rise at rear engine baffle.

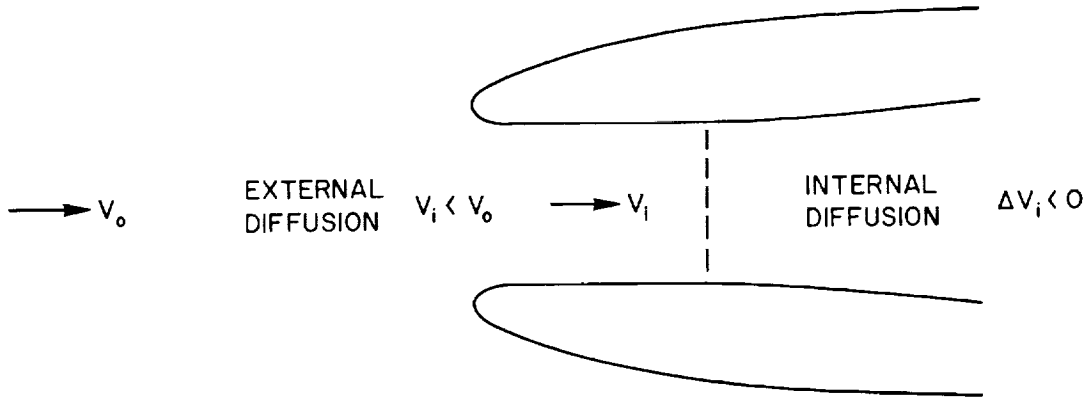

Figure 34. - Inlet geometry and operation.

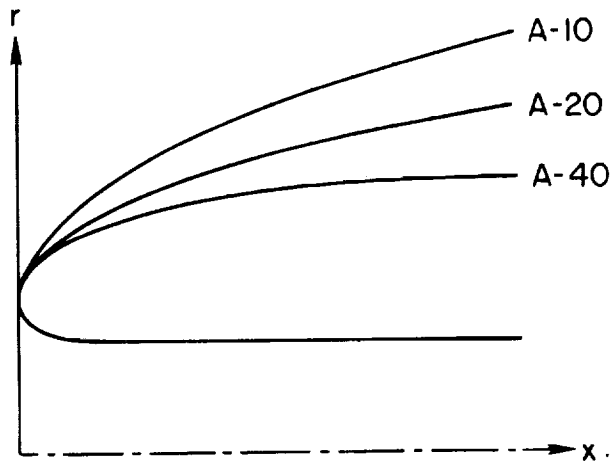

Figure 35. - Kuchemann A-series axisymmetric inlet contours.

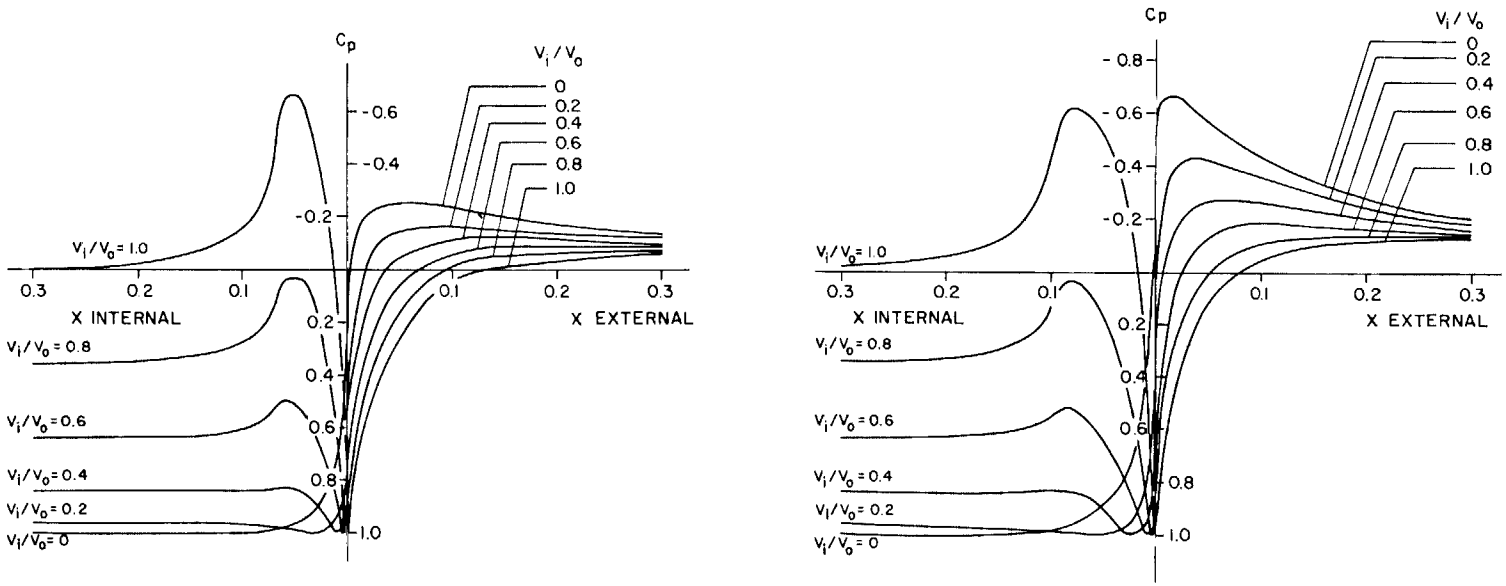

(a) A-10, variation in inlet velocity ratio

(b) A-20, variation in inlet velocity ratio

Figure 36. - Potential flow pressure distributions for Kuchemann A-series axisymmetric inlets.

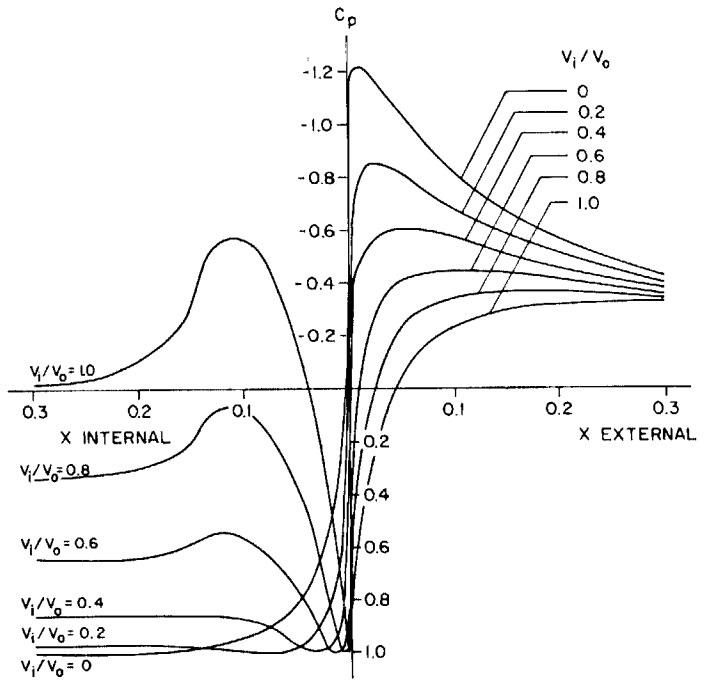

(c) A-40, variation in inlet velocity ratio

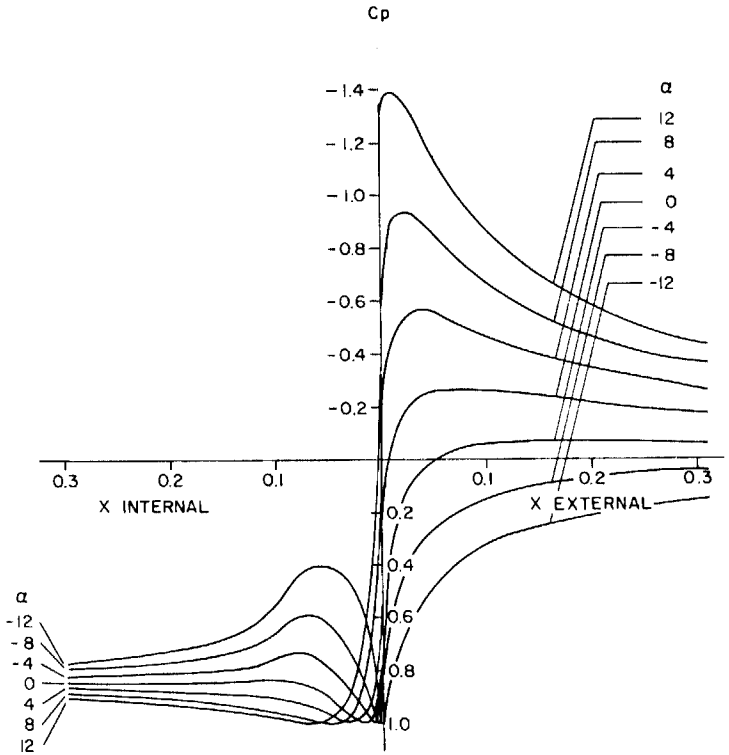

(d) A-20, variation in angle of attack for V_i/V_o = 0.4

Figure 36. - Concluded.

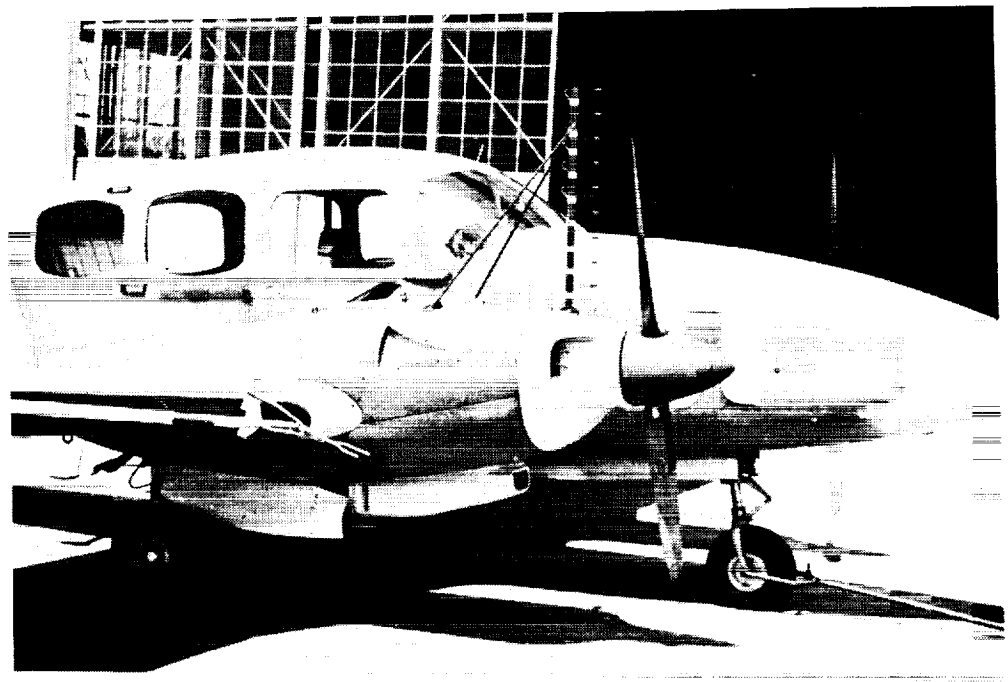

(a) side view

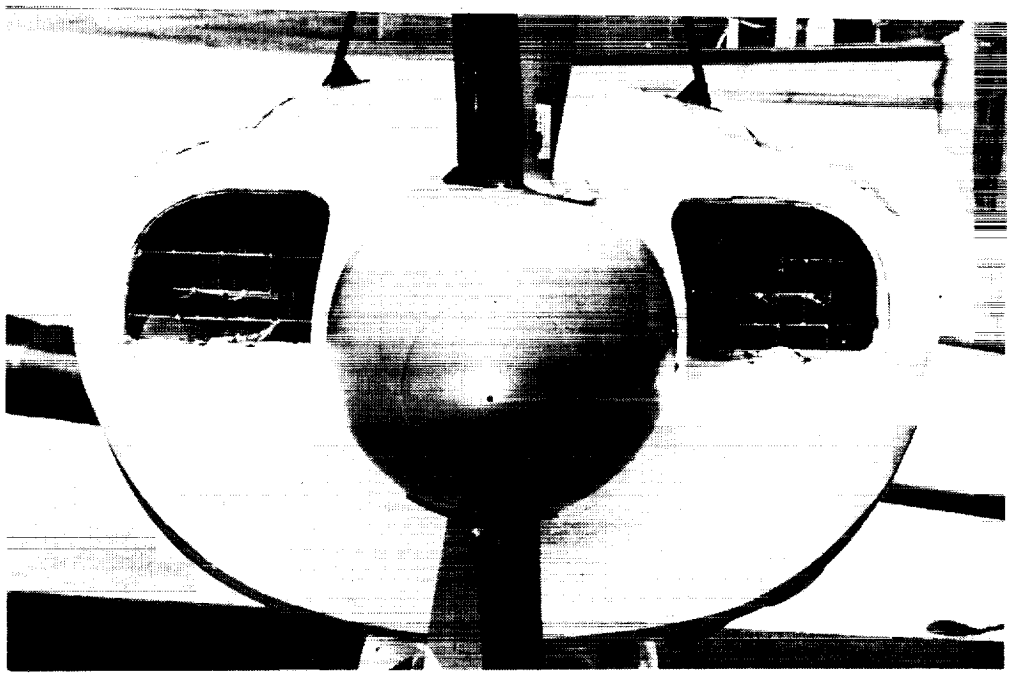

(b) front view

Figure 37. - Original PA-41P inlet, designation "STD."

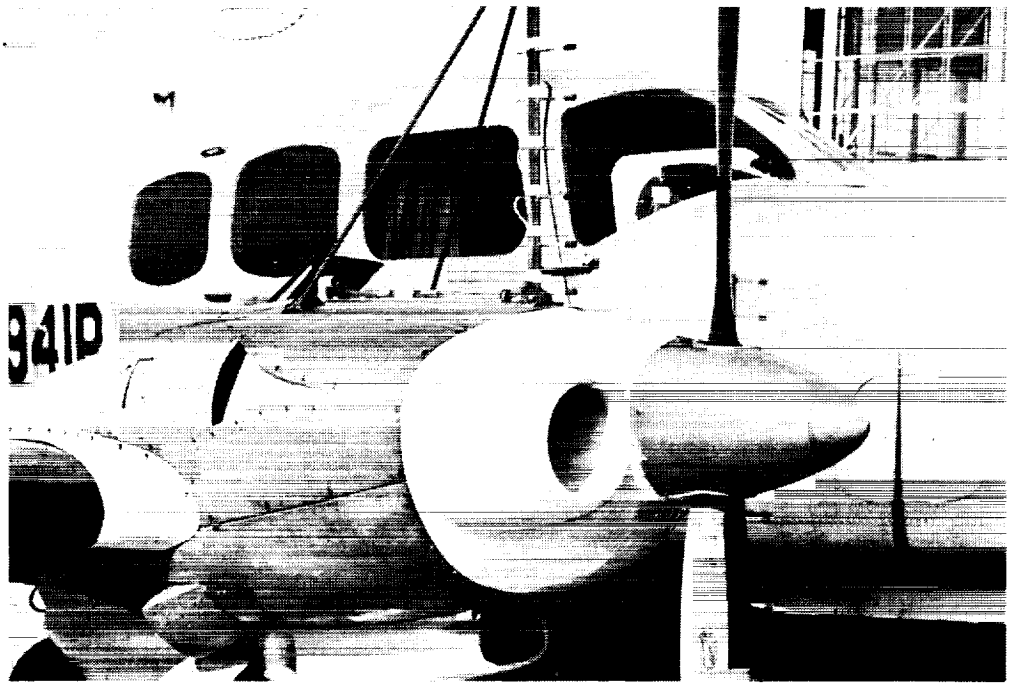

(a) side view

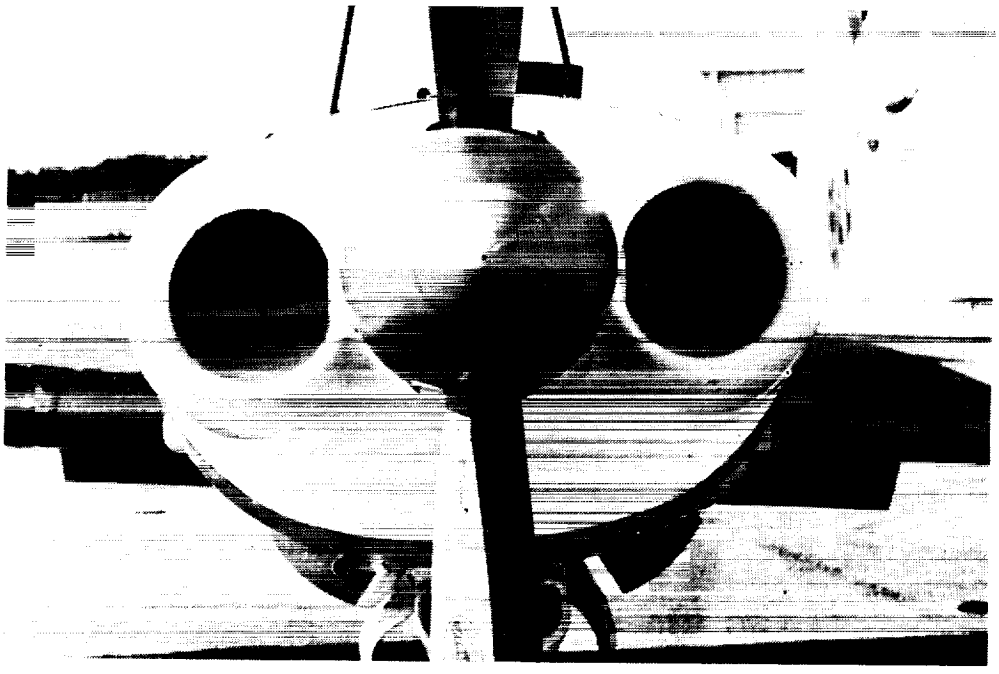

(b) front view

Figure 38. - Axisymmetric inlet, forward location, design velocity ratio V_i/V_o = 0.3, designation "0.3F."

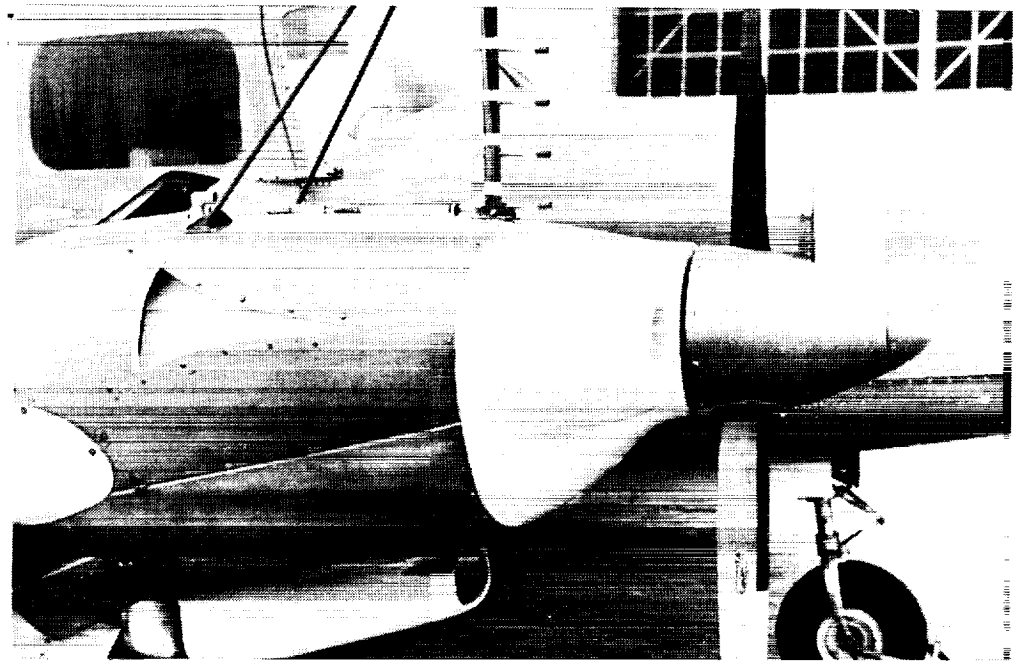

(a) side view

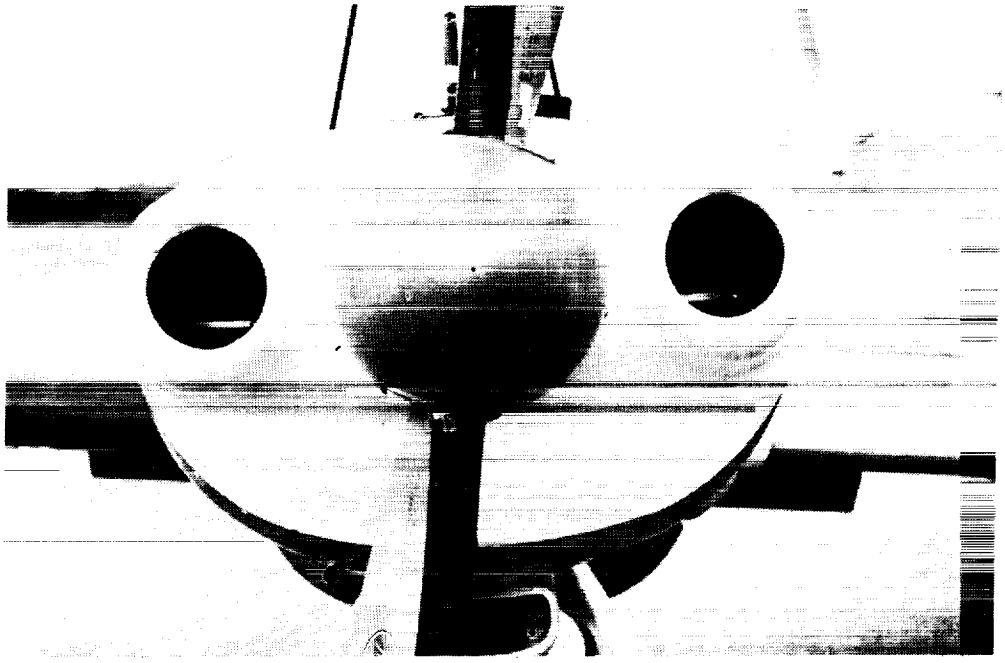

(b) front view

Figure 39. - Axisymmetric inlet, forward location, design velocity ratio, V_i/V_o = 0.6, designation "0.6F."

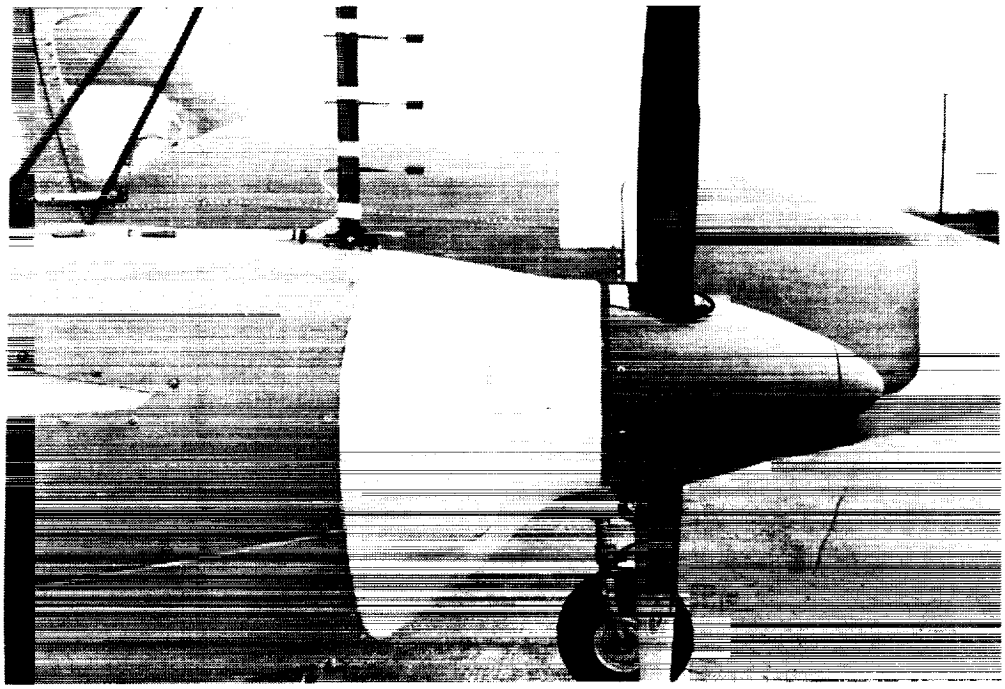

(a) side view

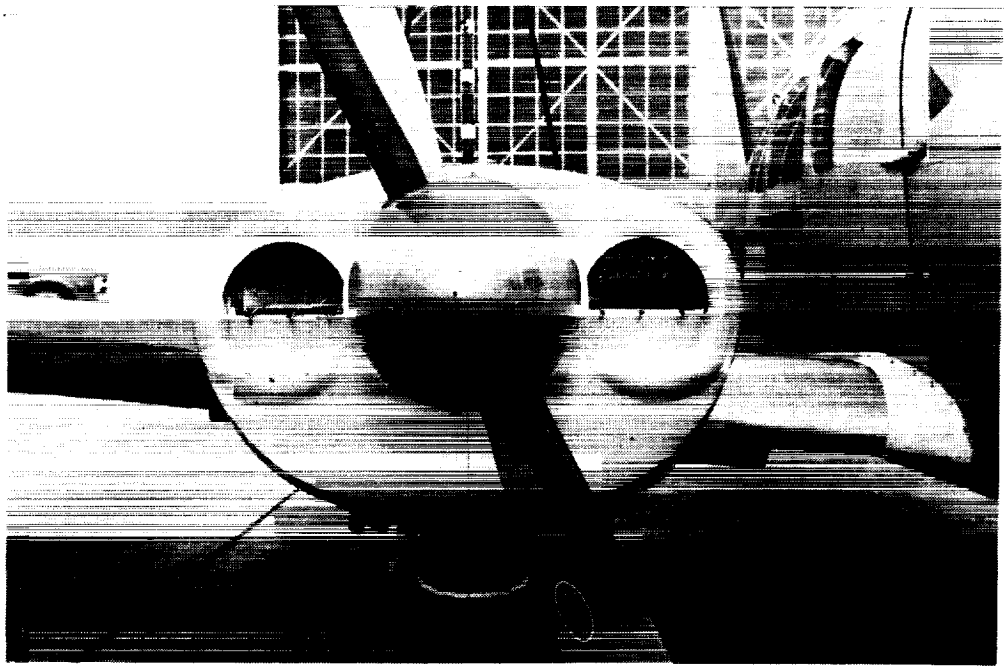

(b) front view

Figure 40. - Axisymmetric inlet, aft location, design velocity ratio V_i/V_o = 0.3, designation "0.3A."

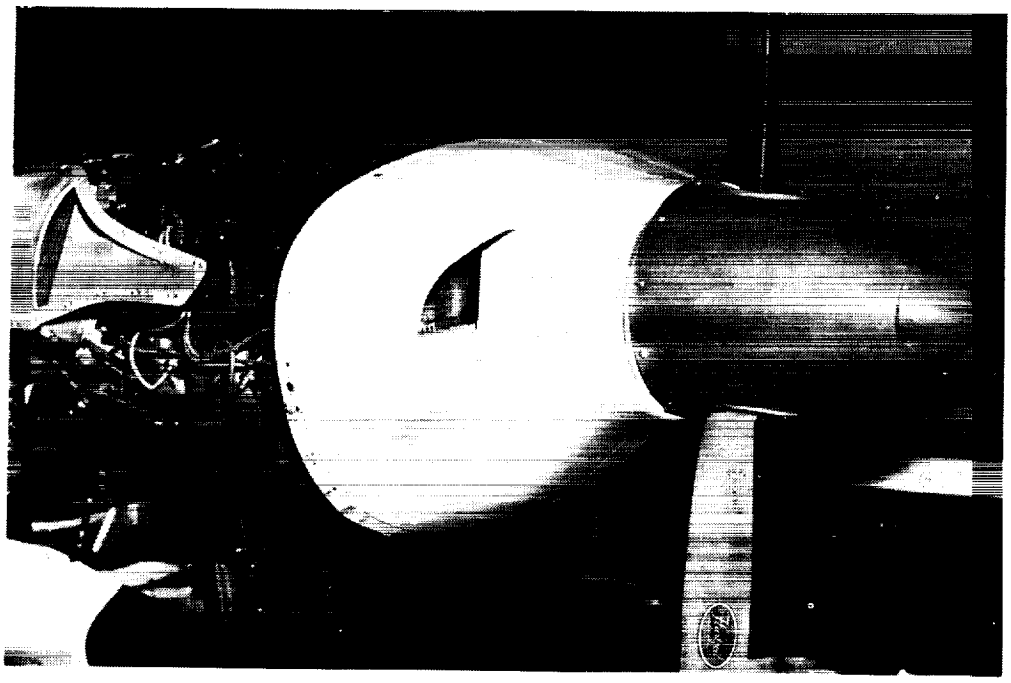

(a) side view

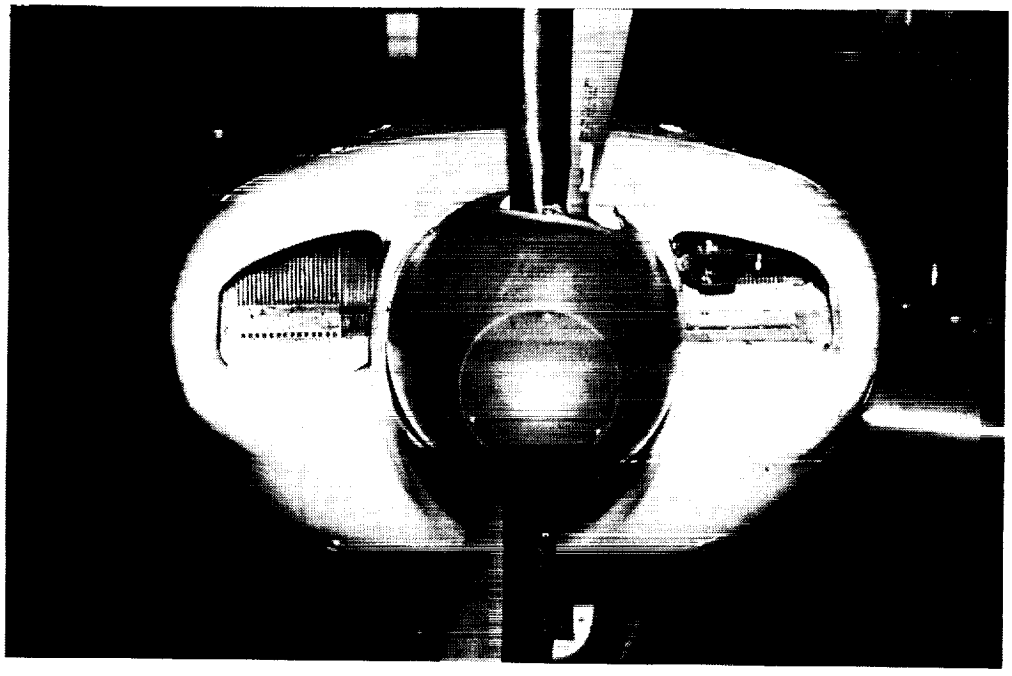

(b) front view

Figure 41. - General aviation conventional style inlet, design velocity ratio V_i/V_o = 0.3, designation "GAC."

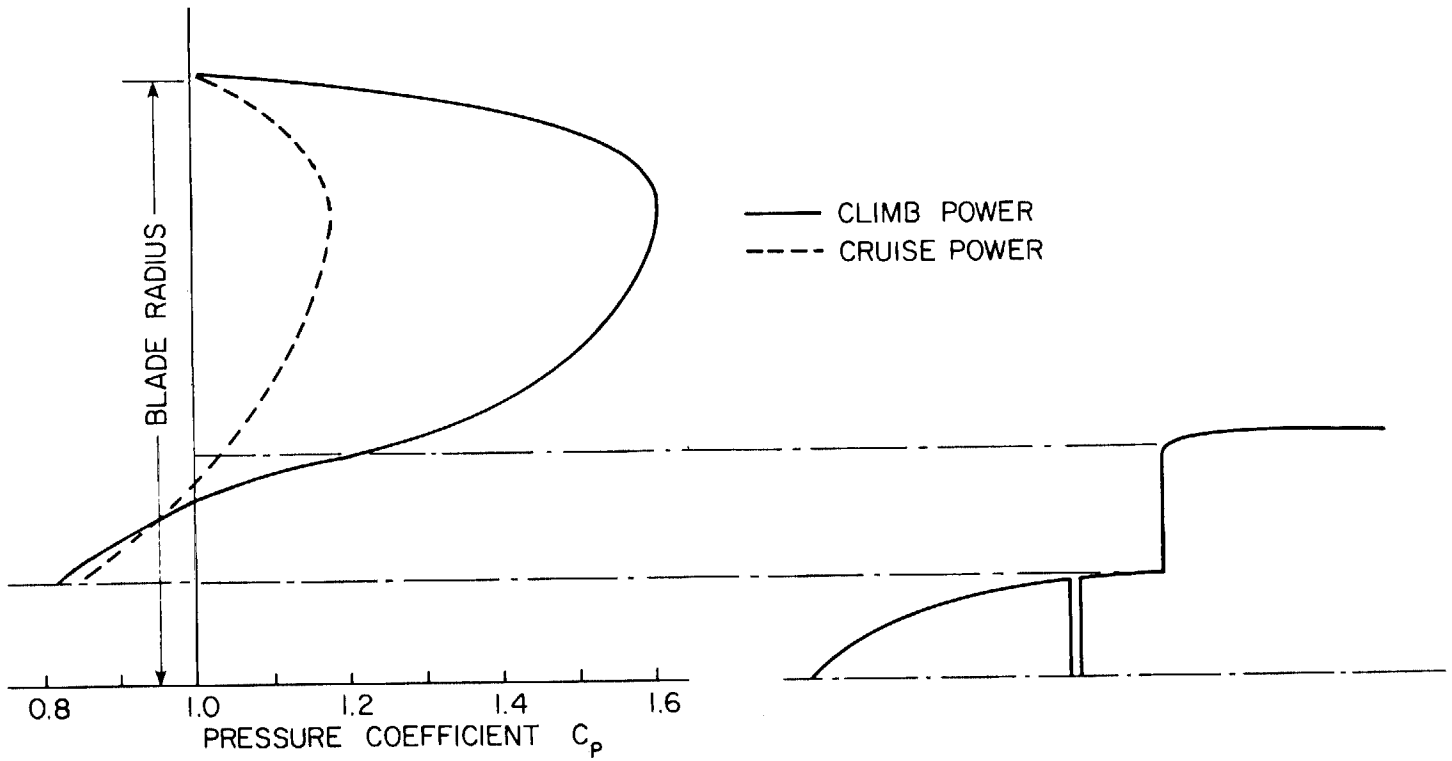

Figure 42. - Propeller slipstream total pressure variation.

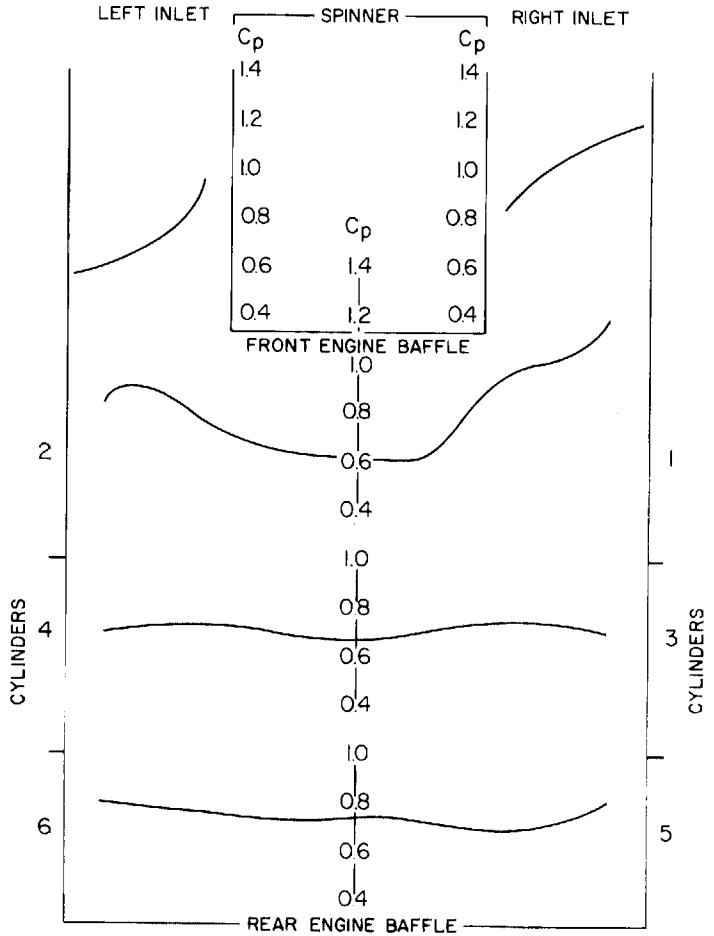

(a) climb condition

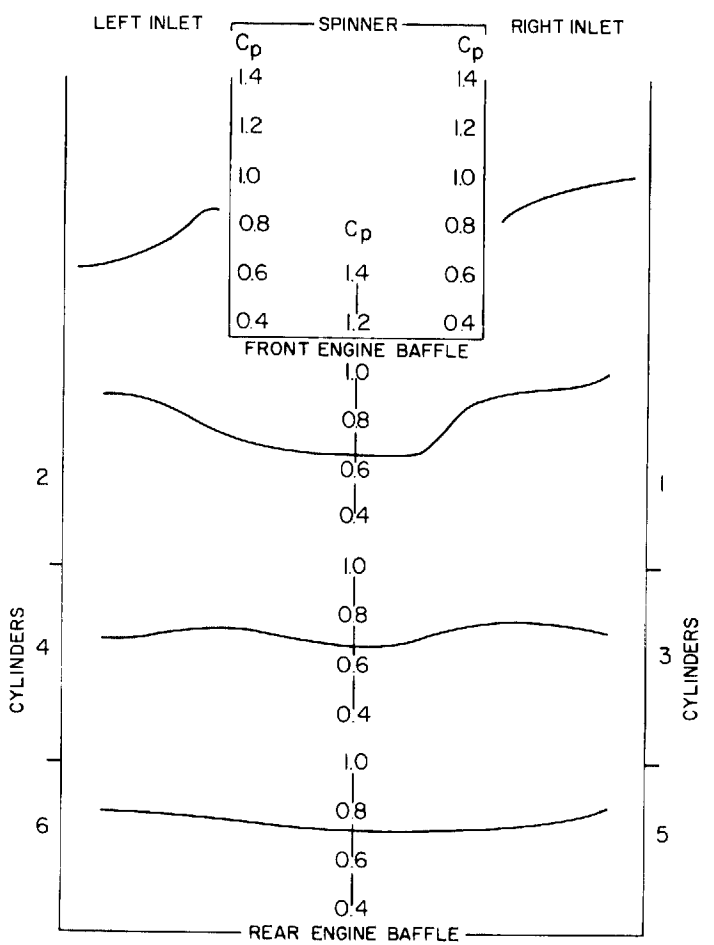

(b) cruise condition

Figure 43. - Upper plenum total pressure survey, STD inlet. Top view schematic of inlets and plenum.

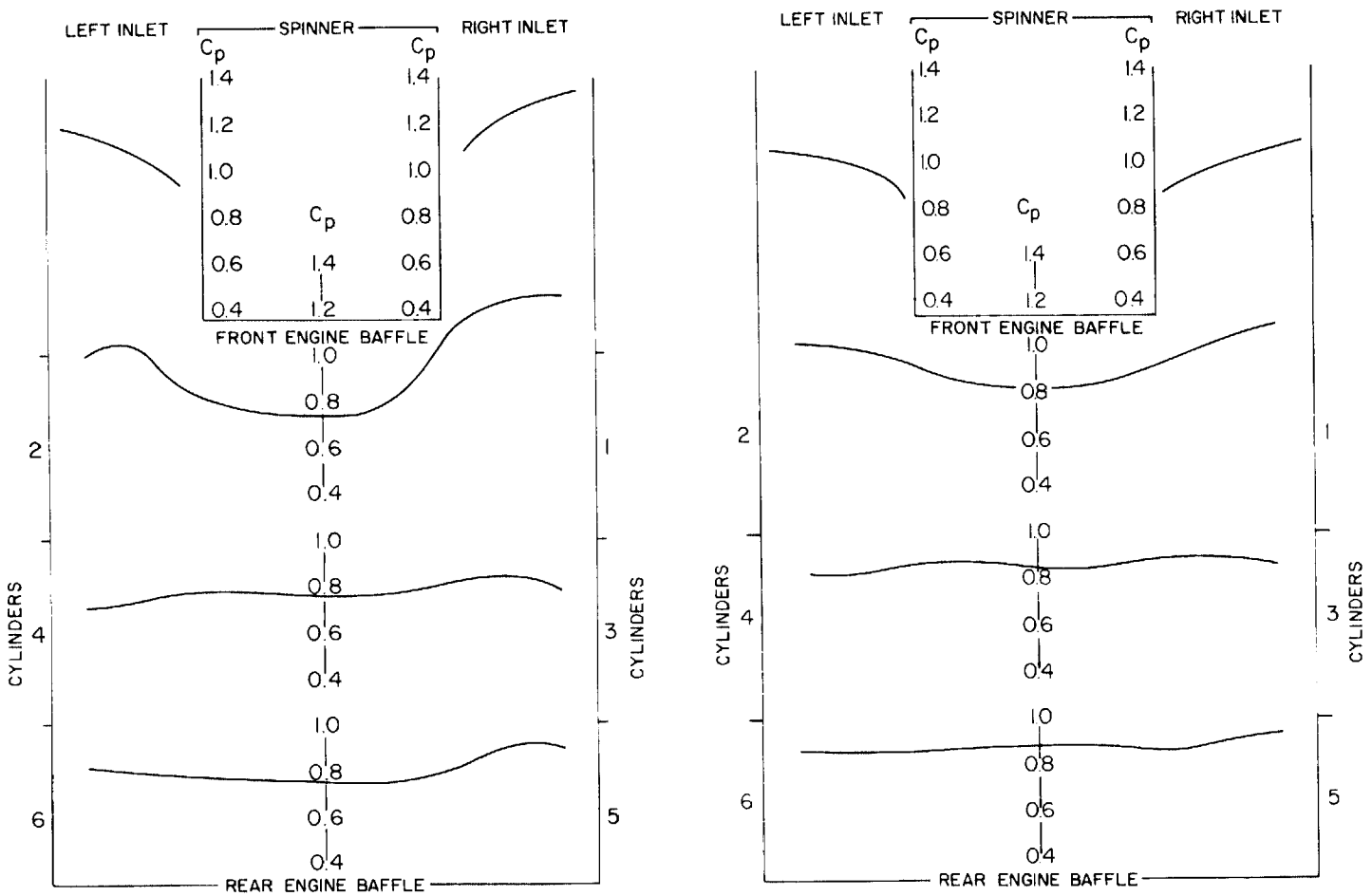

(a) climb condition

(b) cruise condition

Figure 44. - Upper plenum total pressure survey, 0.3F inlet. Top view schematic of inlets and plenum.

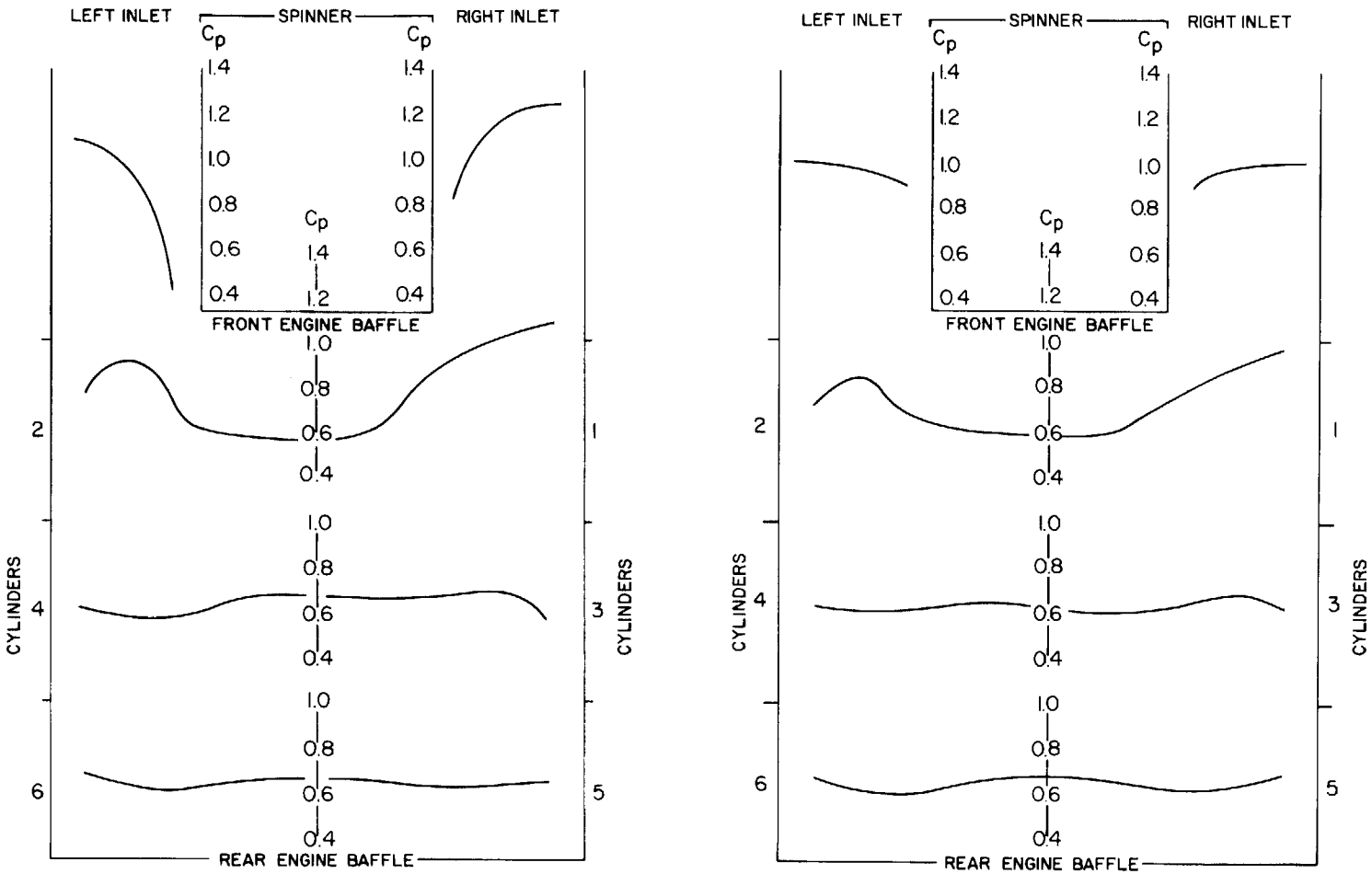

(a) climb condition

(b) cruise condition

Figure 45. - Upper plenum total pressure survey, 0.3A inlet. Top view schematic of inlets and plenum.

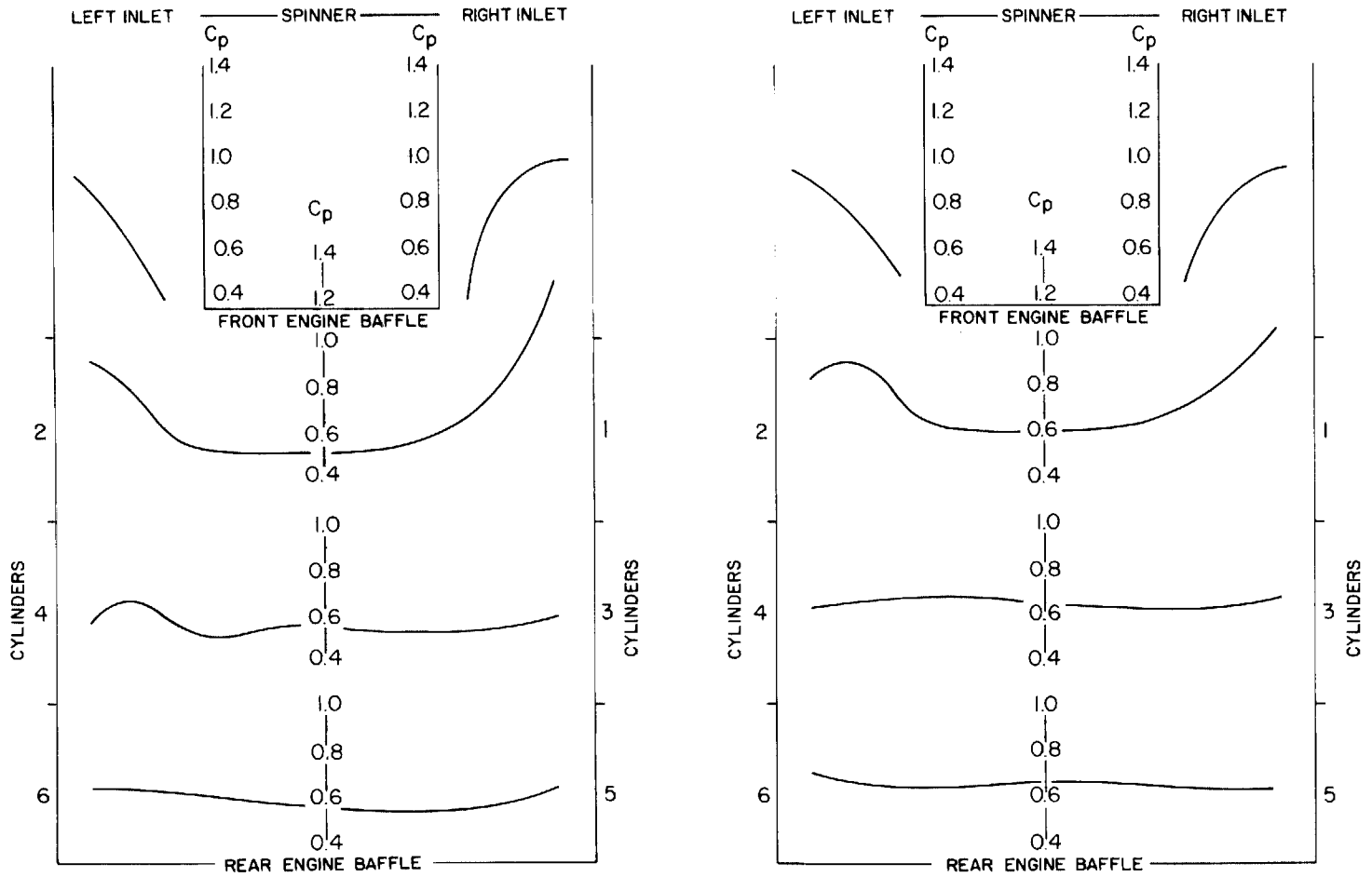

(a) climb condition

(b) cruise condition

Figure 46. - Upper plenum total pressure survey, 0.6F inlet. Top view schematic of inlets and plenum.

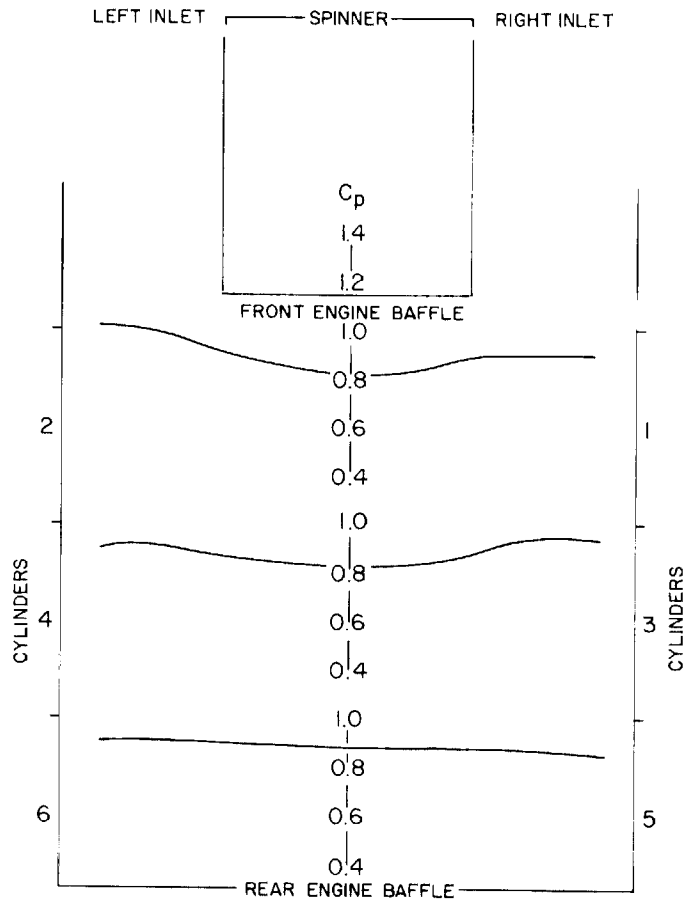

Figure 47. - Upper plenum total pressure survey, 0.3F inlet. Top view schematic of inlets and plenum.

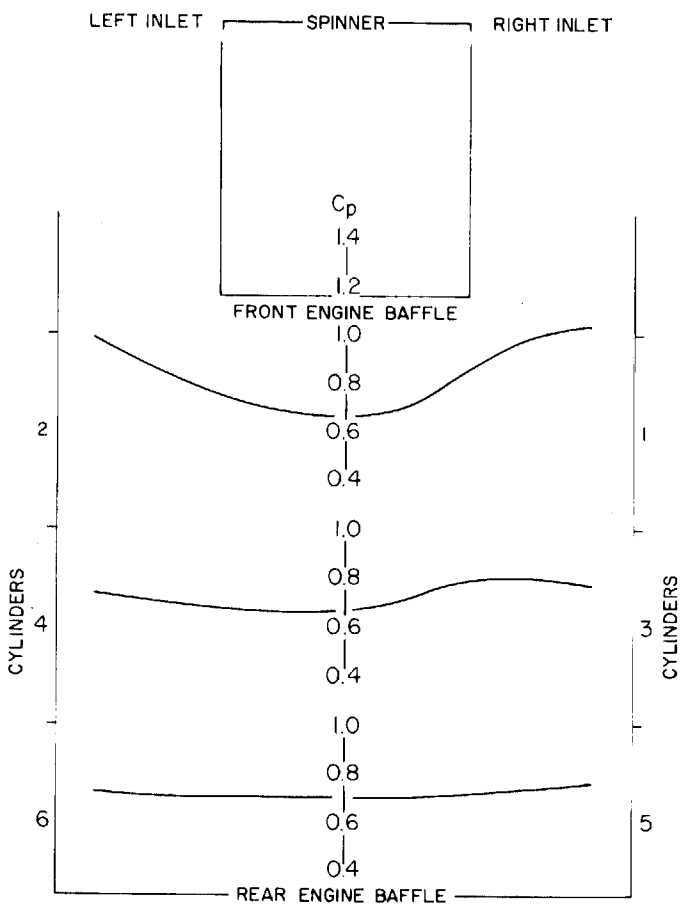

Figure 48. - Upper plenum total pressure survey, GAC inlet. Top view schematic of inlets and plenum.

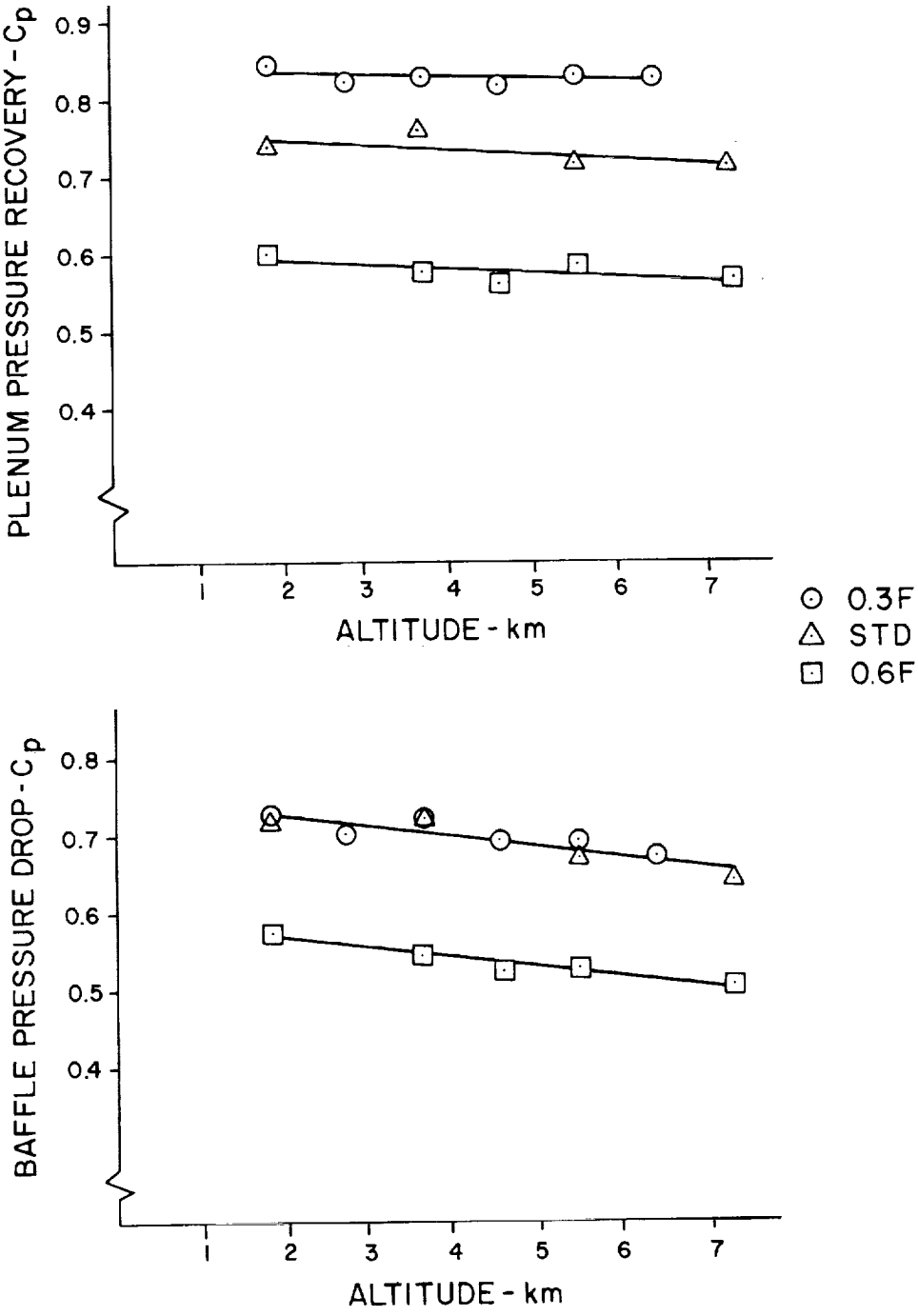

Figure 49. - Engine baffle pressure drop and upper plenum pressure recovery for climb condition, STD, 0.3F, 0.6F inlets.

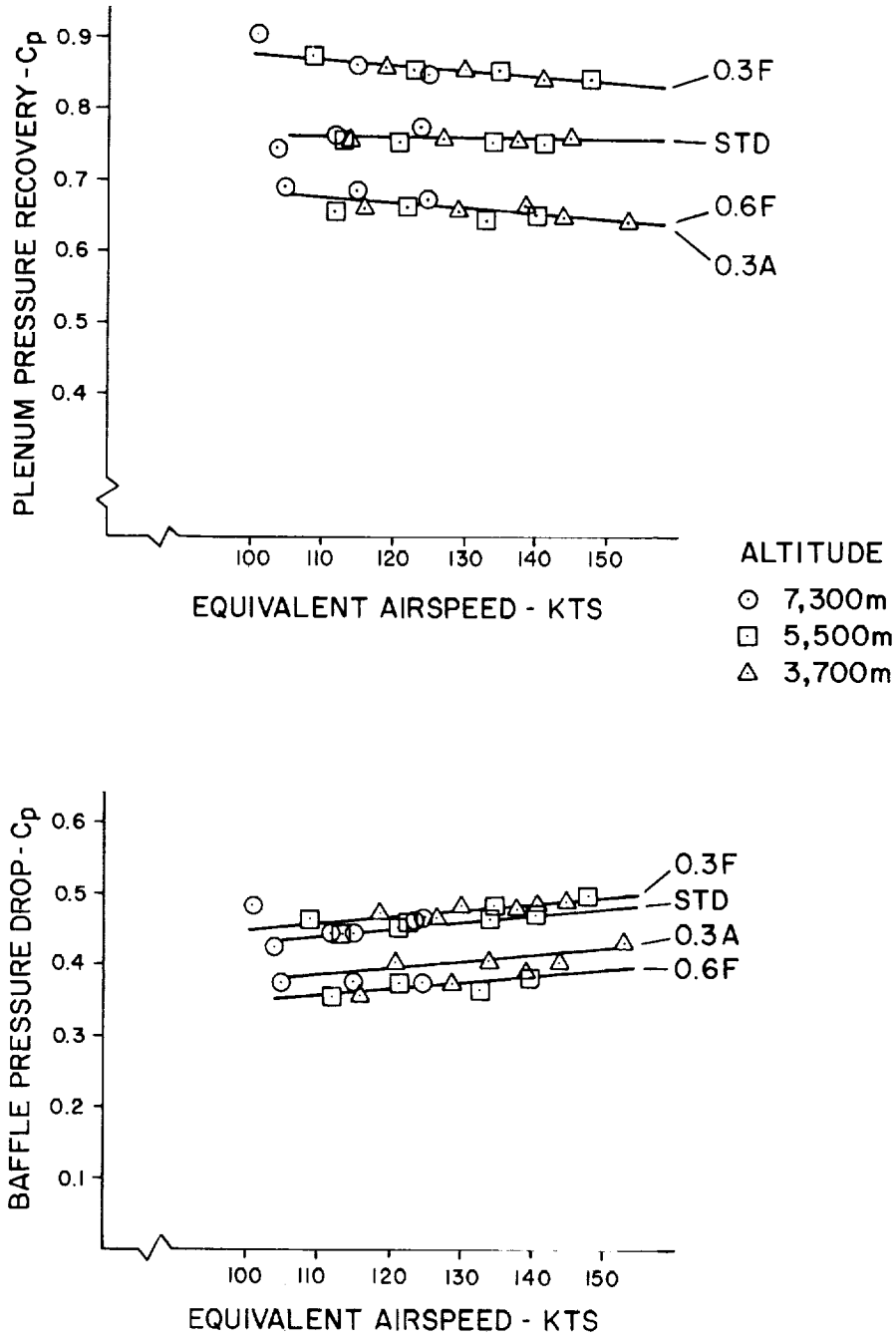

Figure 50. - Engine baffle pressure drop and upper plenum pressure recovery for climb condition, STD, 0.3F, 0.6F, 0.3A inlets.

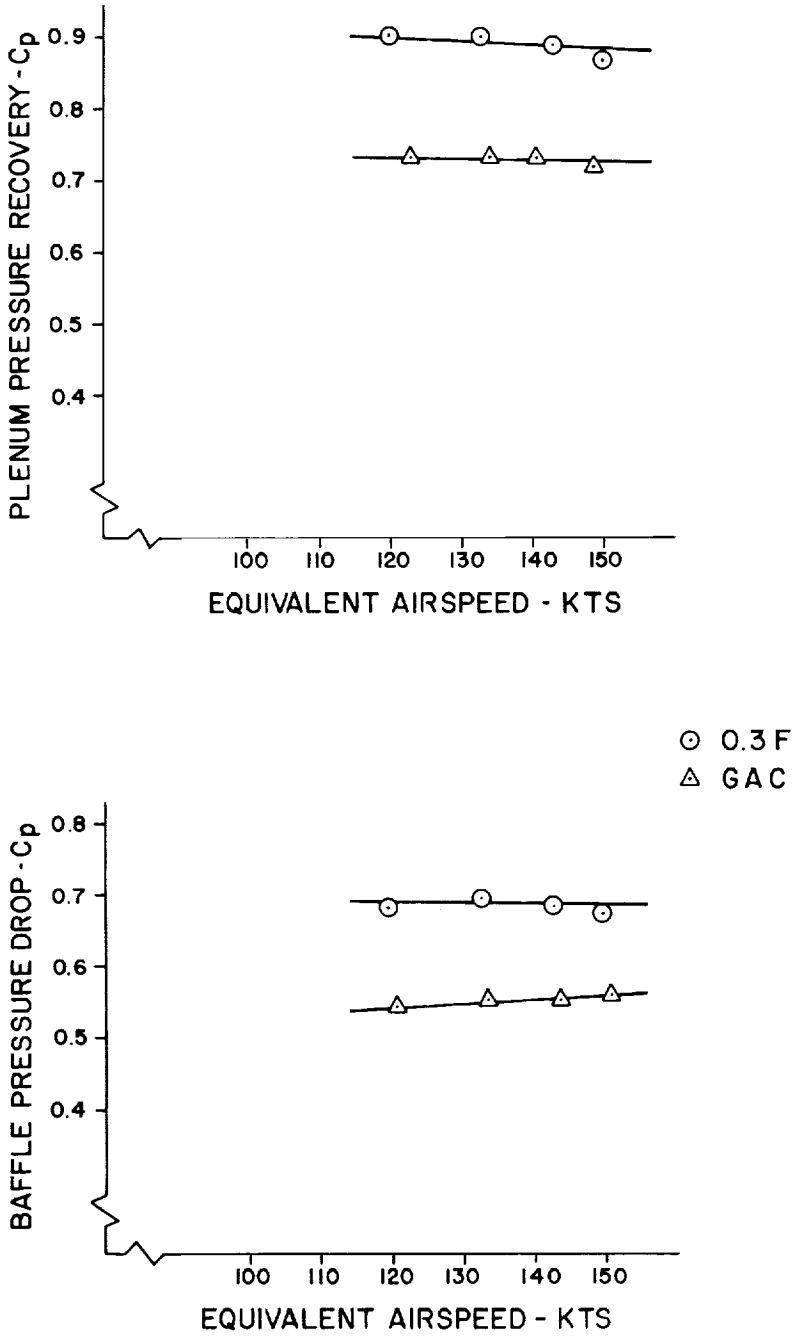

Figure 51. - Engine baffle pressure drop and upper plenum pressure recovery for climb condition, 0.3F, GAC inlets.

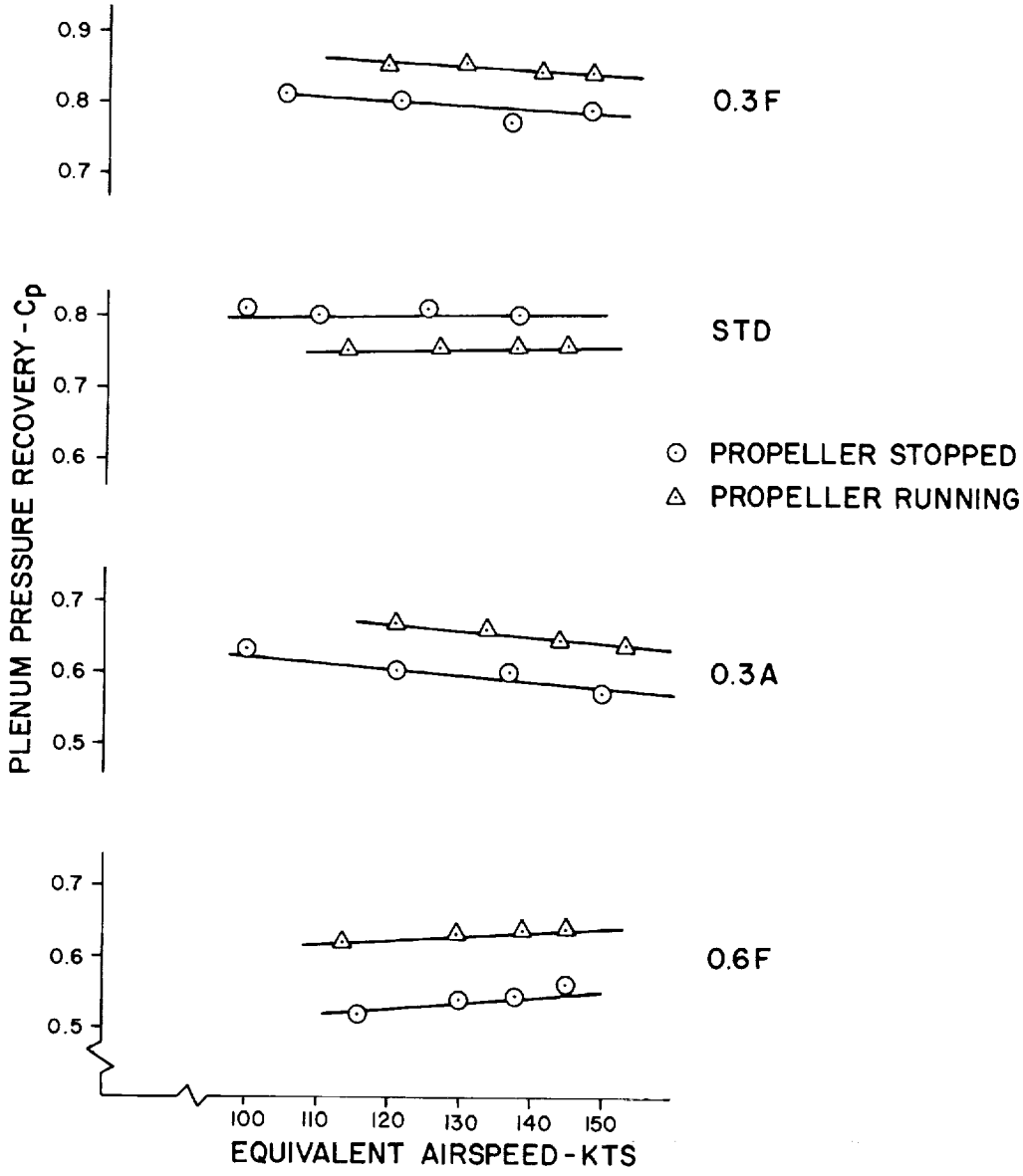

(a) upper plenum pressure recovery

Figure 52. - Propeller effects on engine baffle pressure drop and upper plenum pressure recovery for cruise condition.

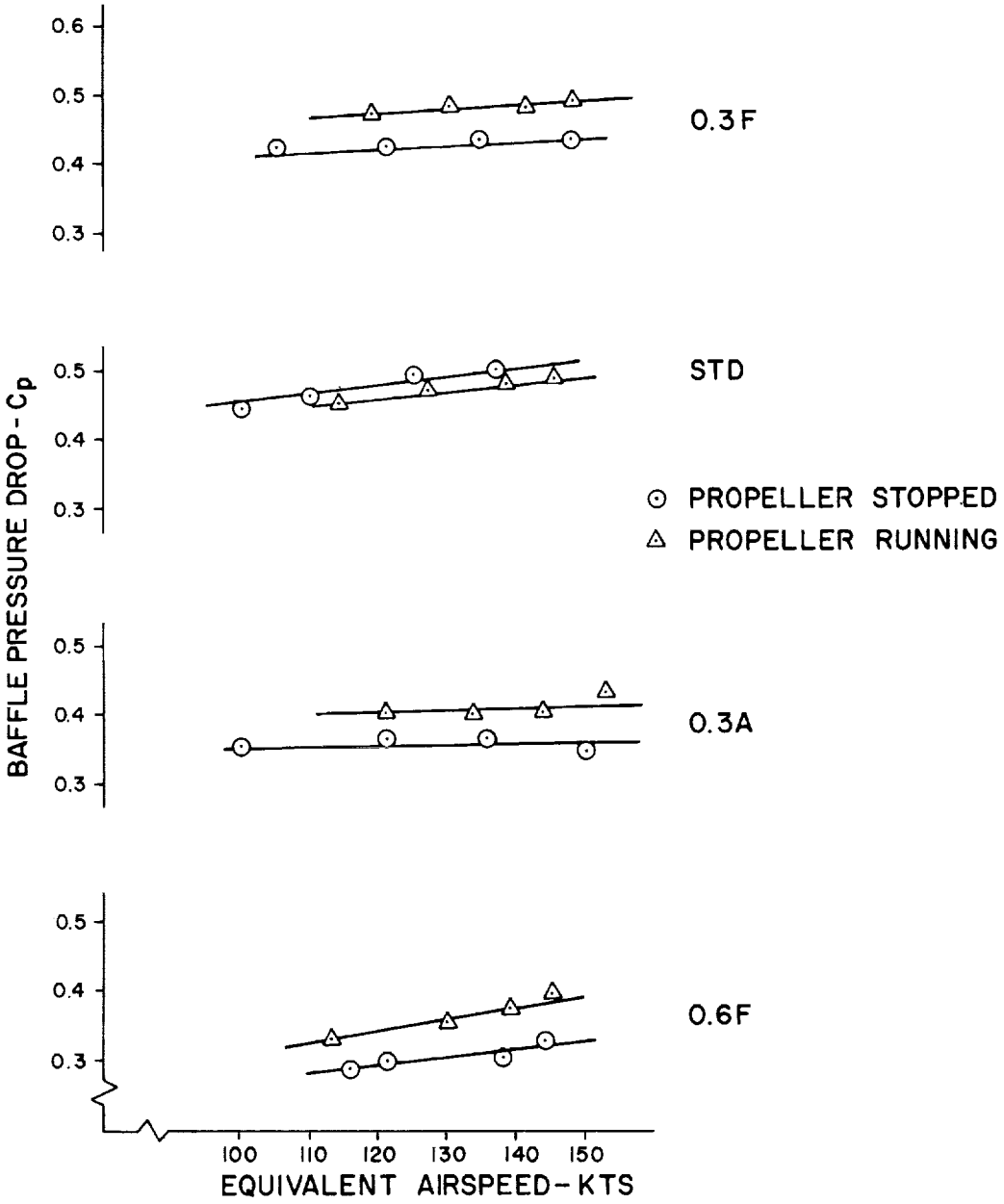

(b) engine baffle pressure drop

Figure 52. - Continued.

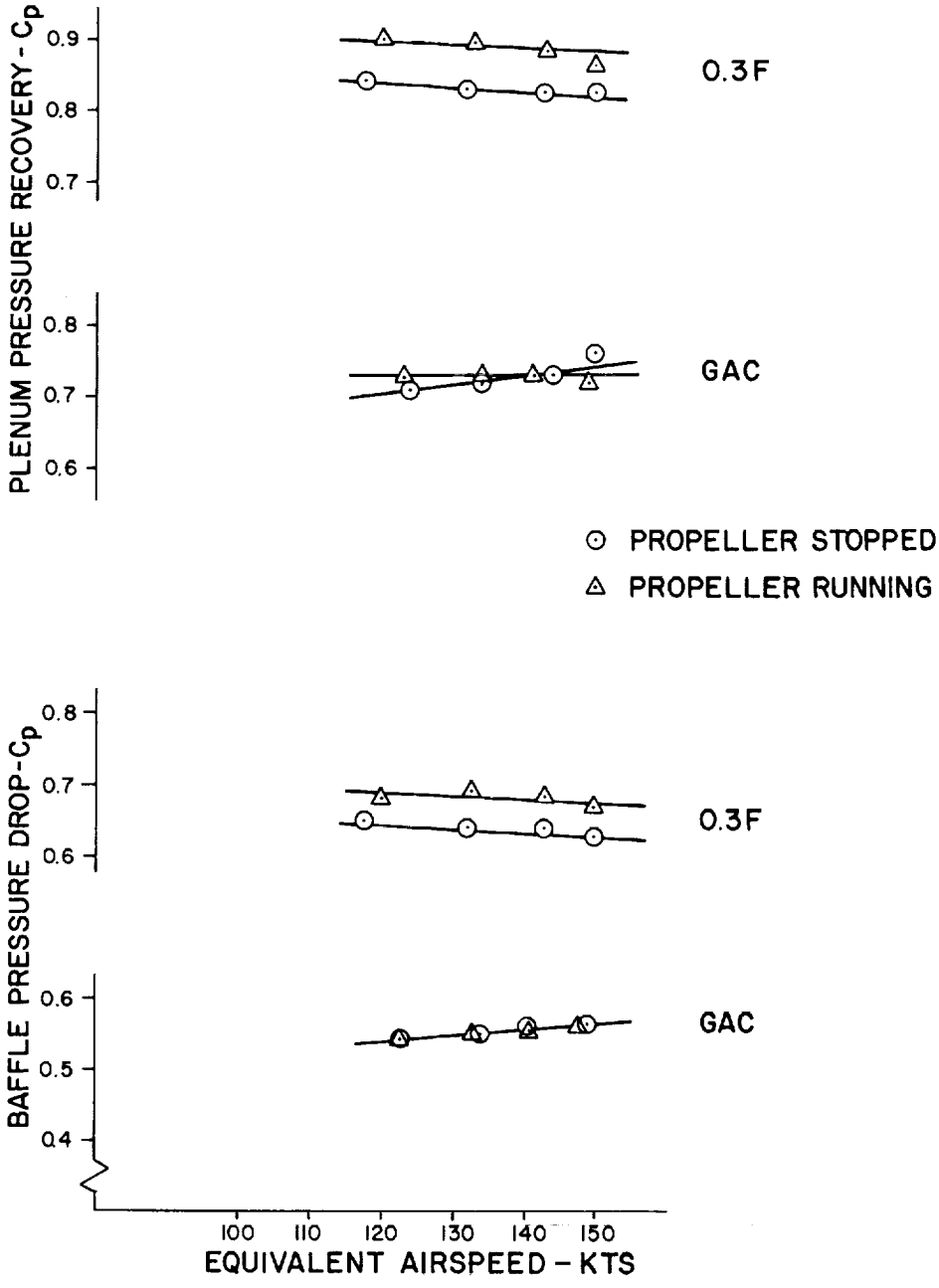

(c) separate results for 0.3F and GAC inlets

Figure 52. - Concluded.

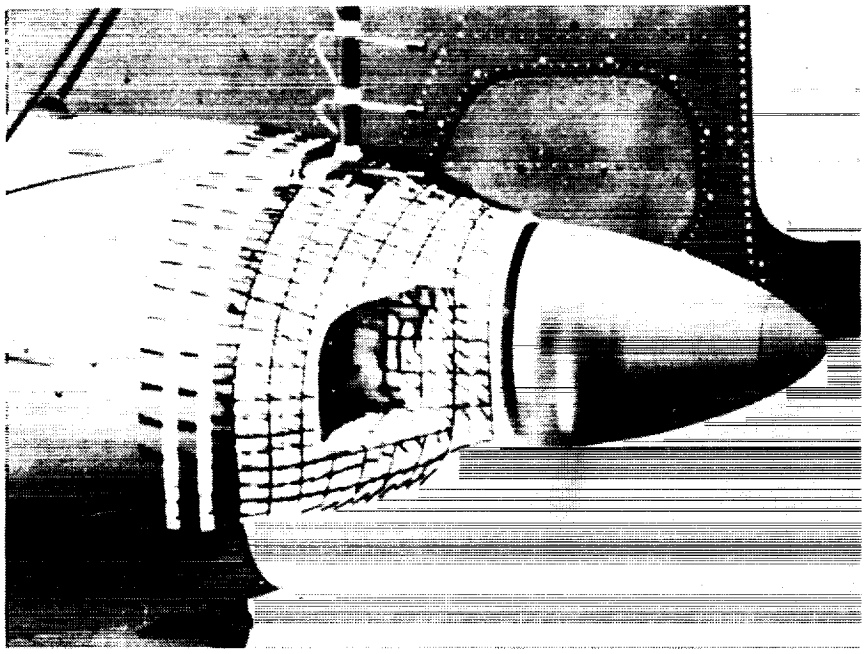

(a) outboard side, propeller running

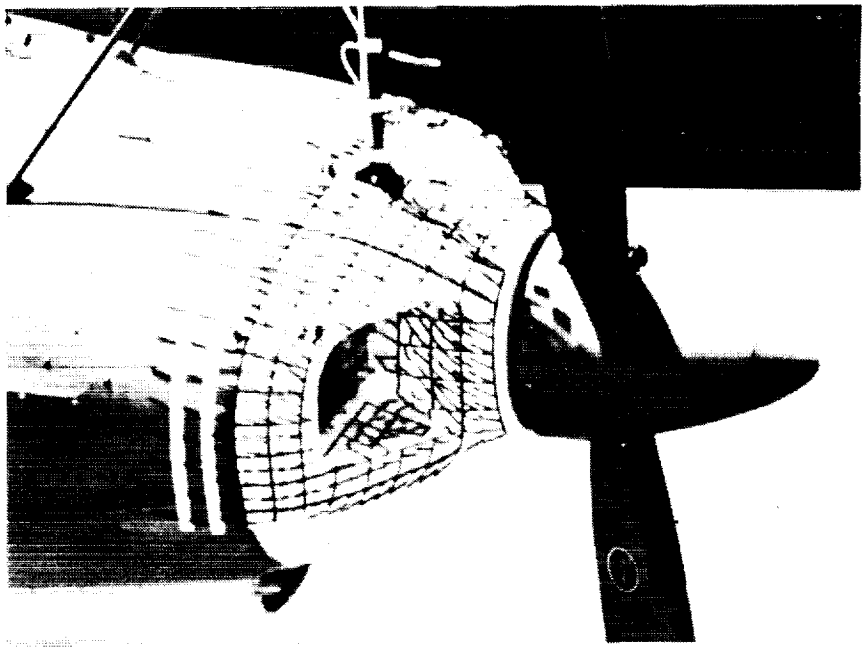

(b) outboard side, propeller stopped

Figure 53. - STD inlet.

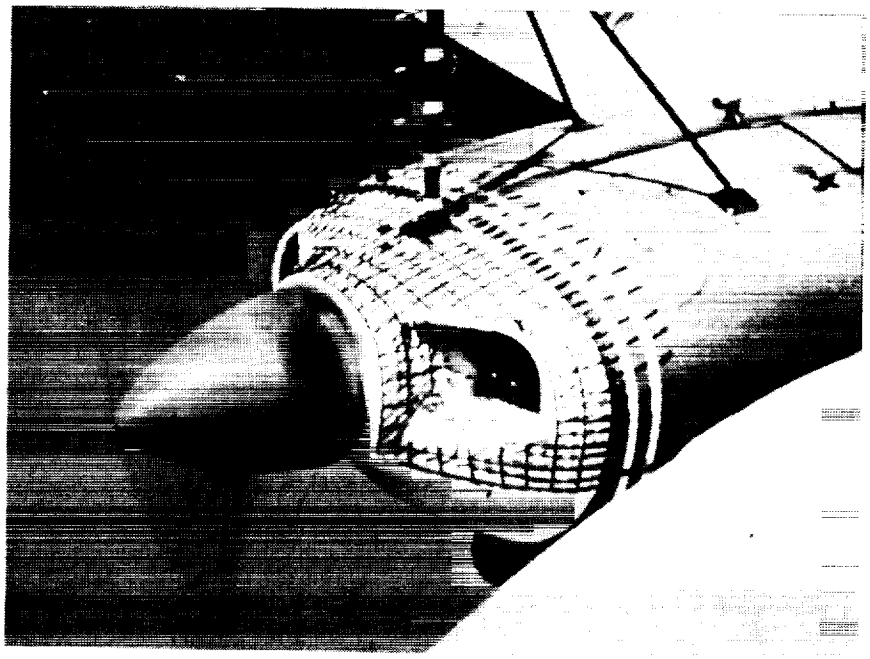

(c) inboard side, propeller running

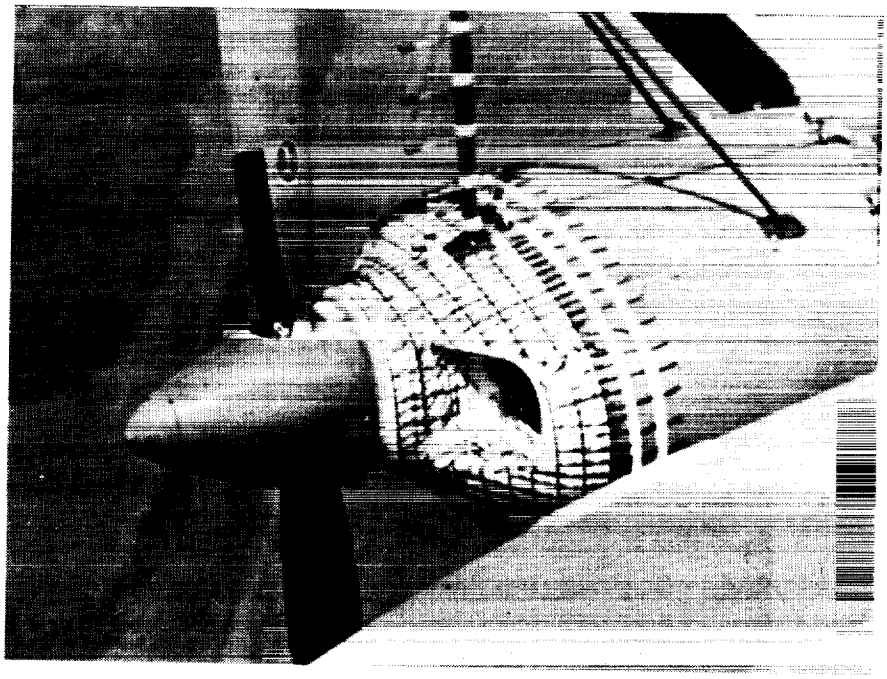

(d) inboard side, propeller stopped

Figure 53. - Continued.

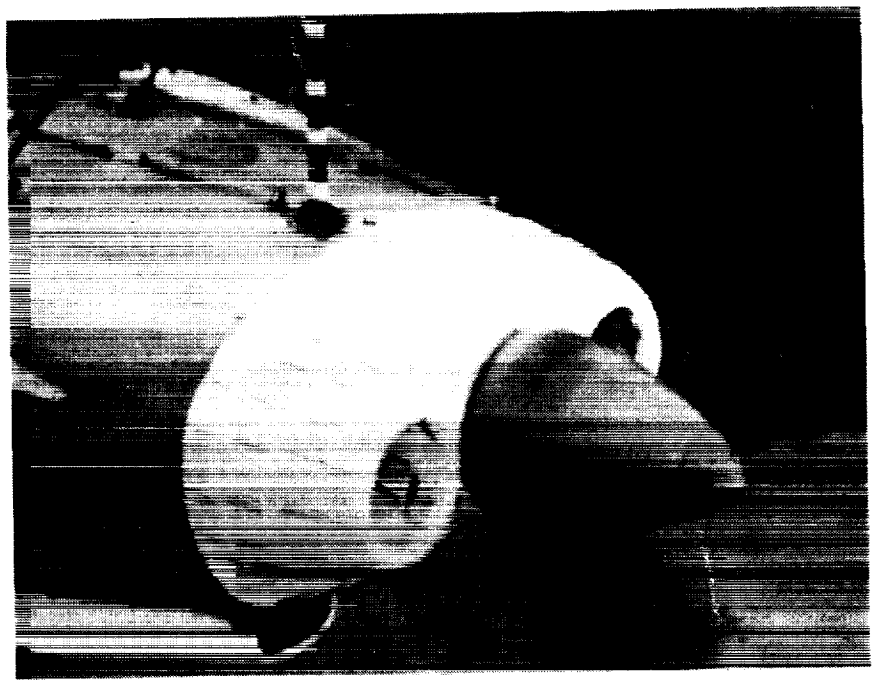

(a) outboard side

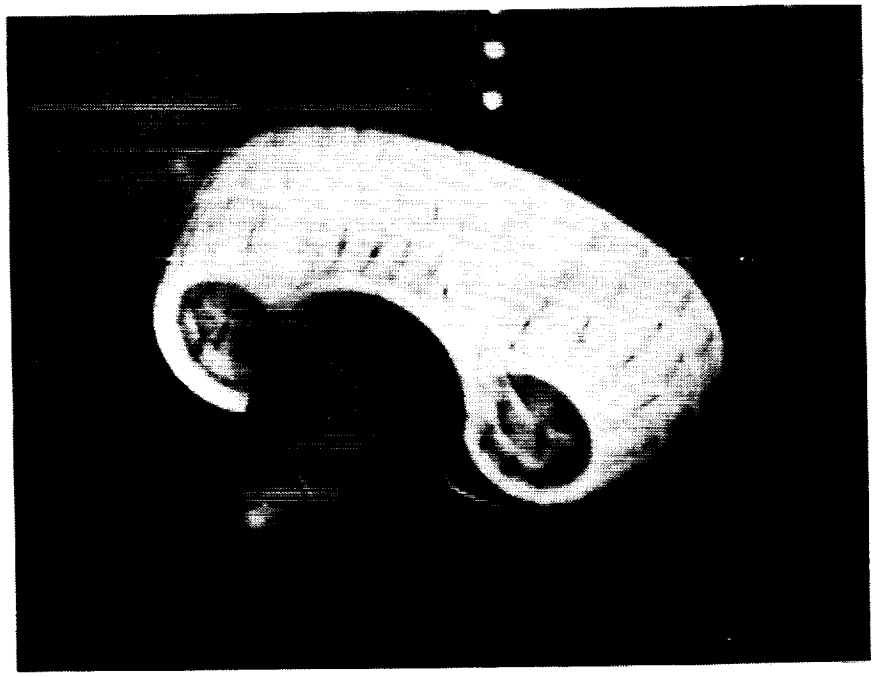

(b) inboard side

Figure 54. - 0.3F inlet.

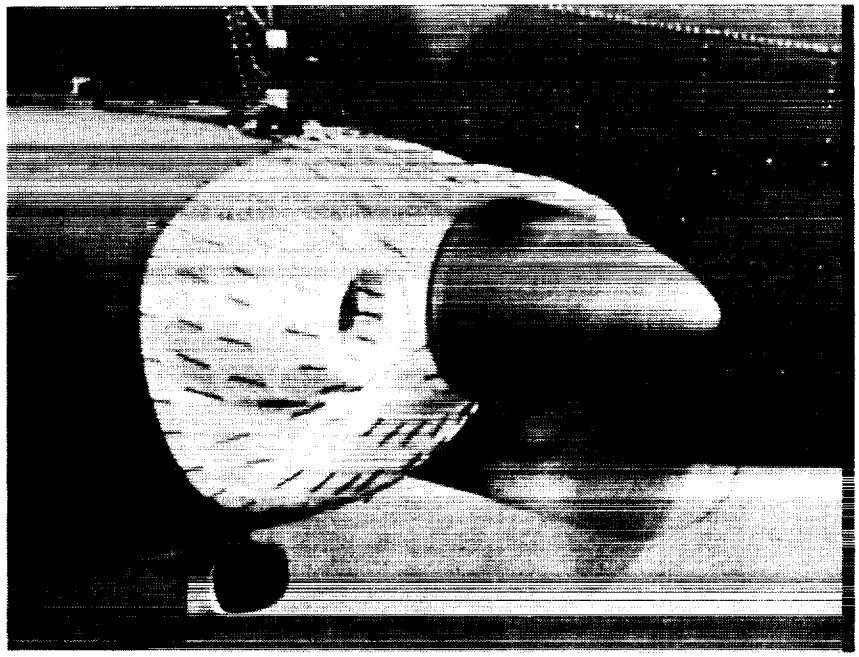

(a) outboard side

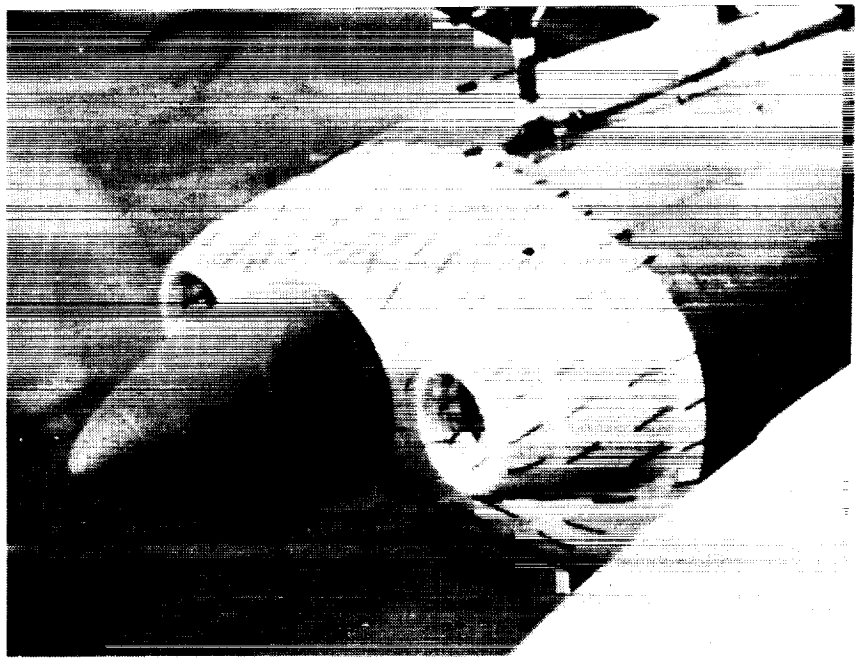

(b) inboard side

Figure 55. - 0.6F inlet.

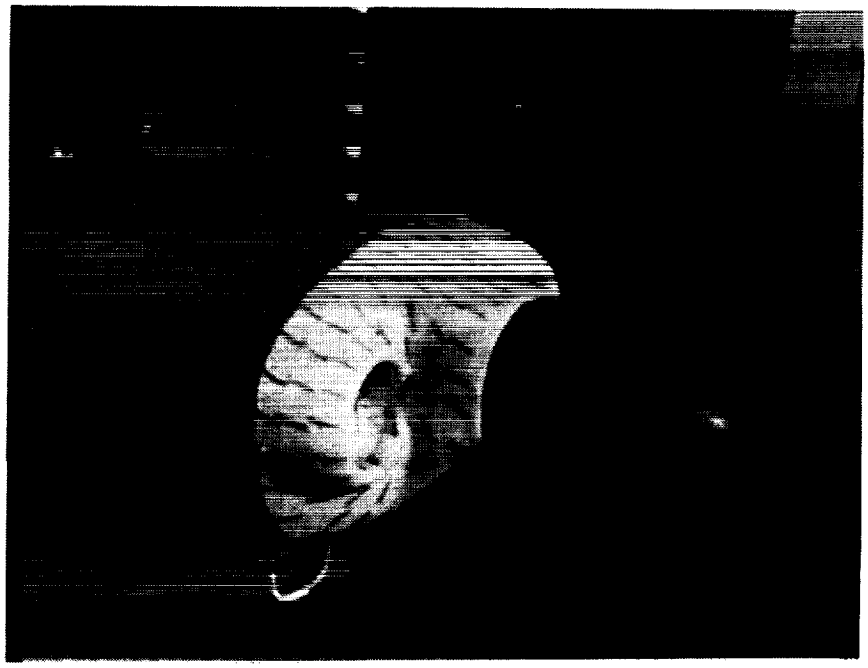

(a) outboard side

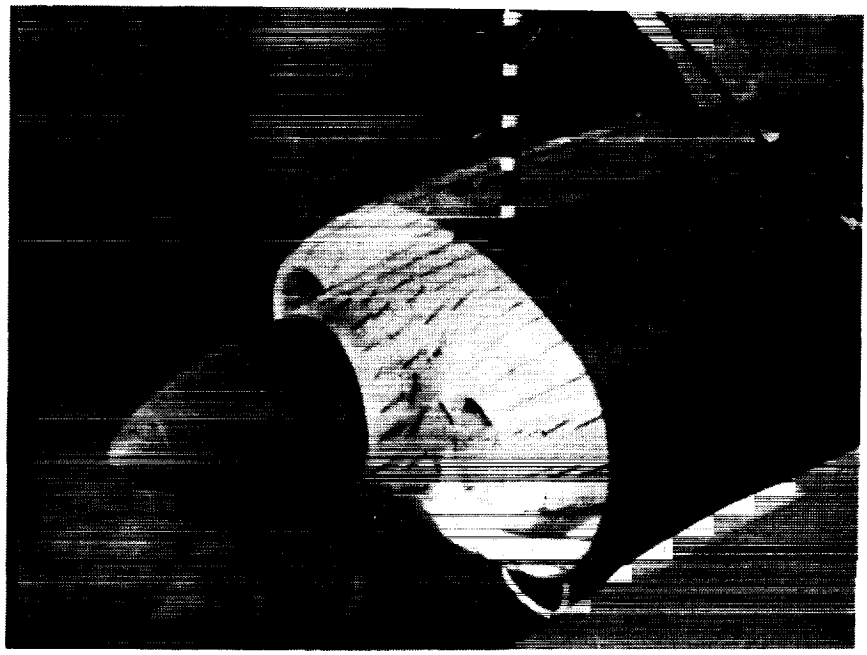

(b) inboard side

Figure 56. - 0.3A inlet.

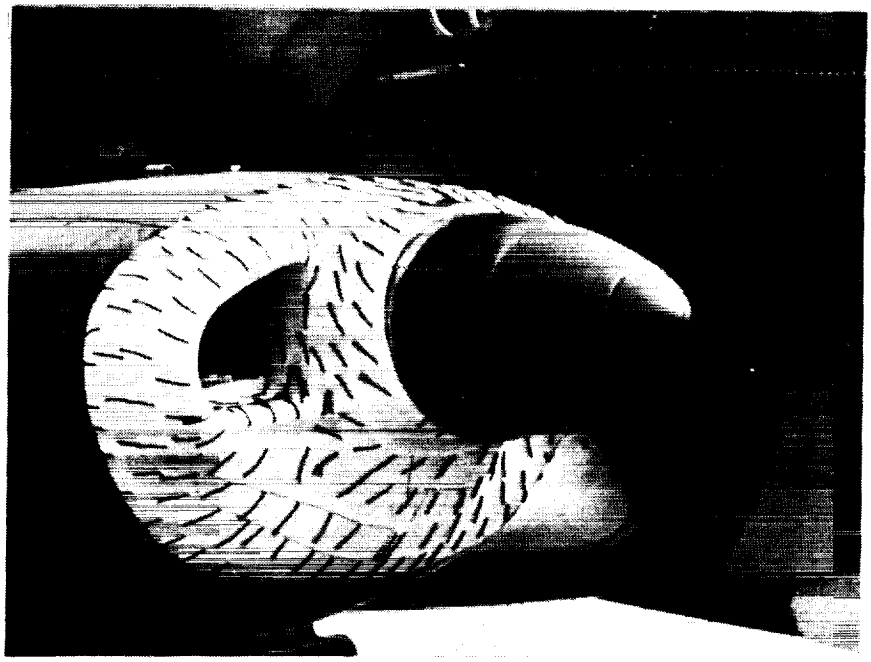

(a) outboard side

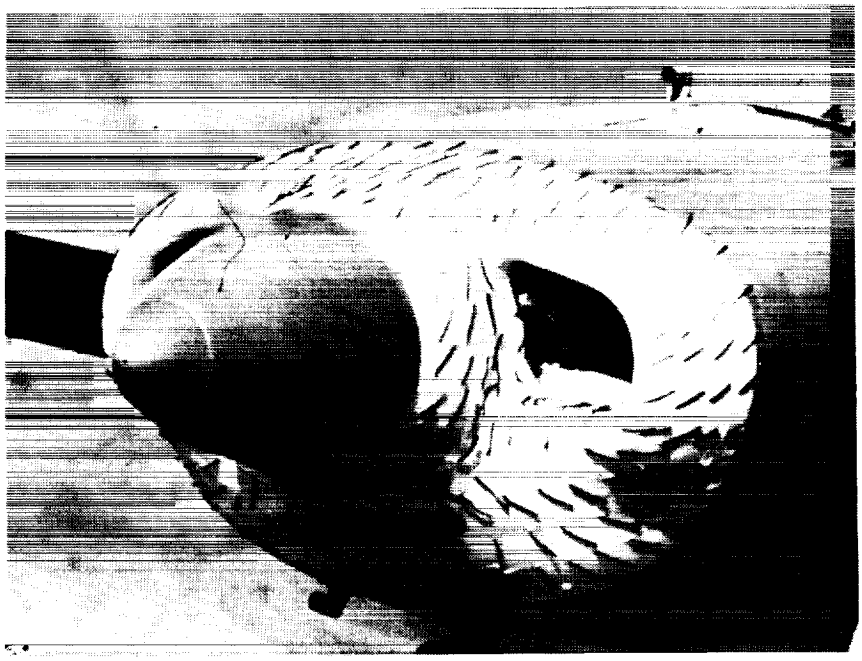

(b) inboard side

Figure 57. - GAC inlet.

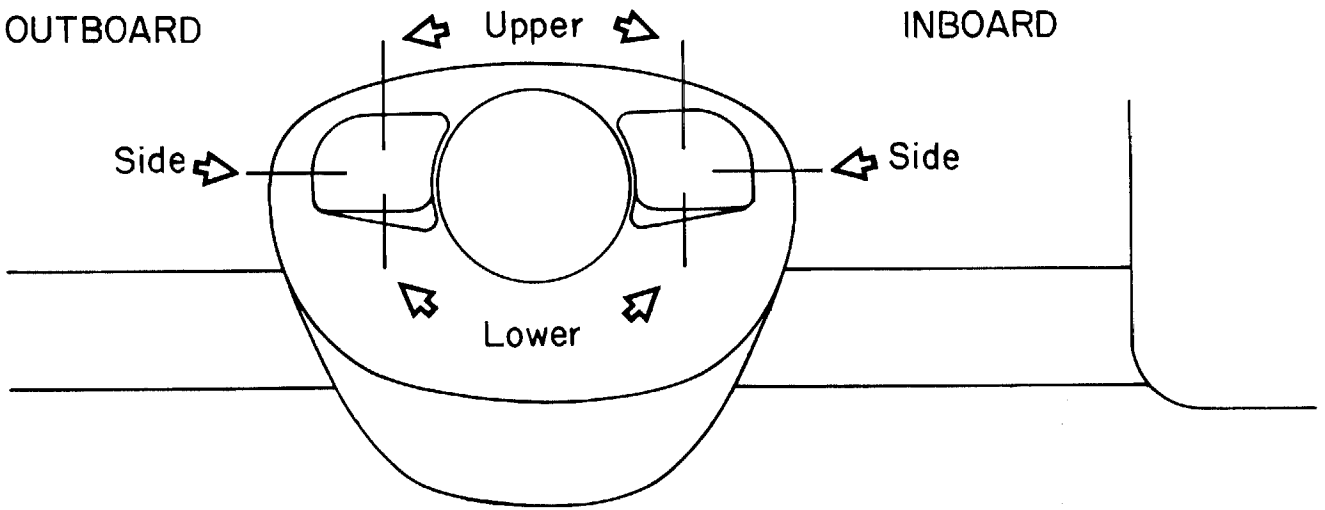

Figure 58. - Locations for inlet external pressure distribution measurements.

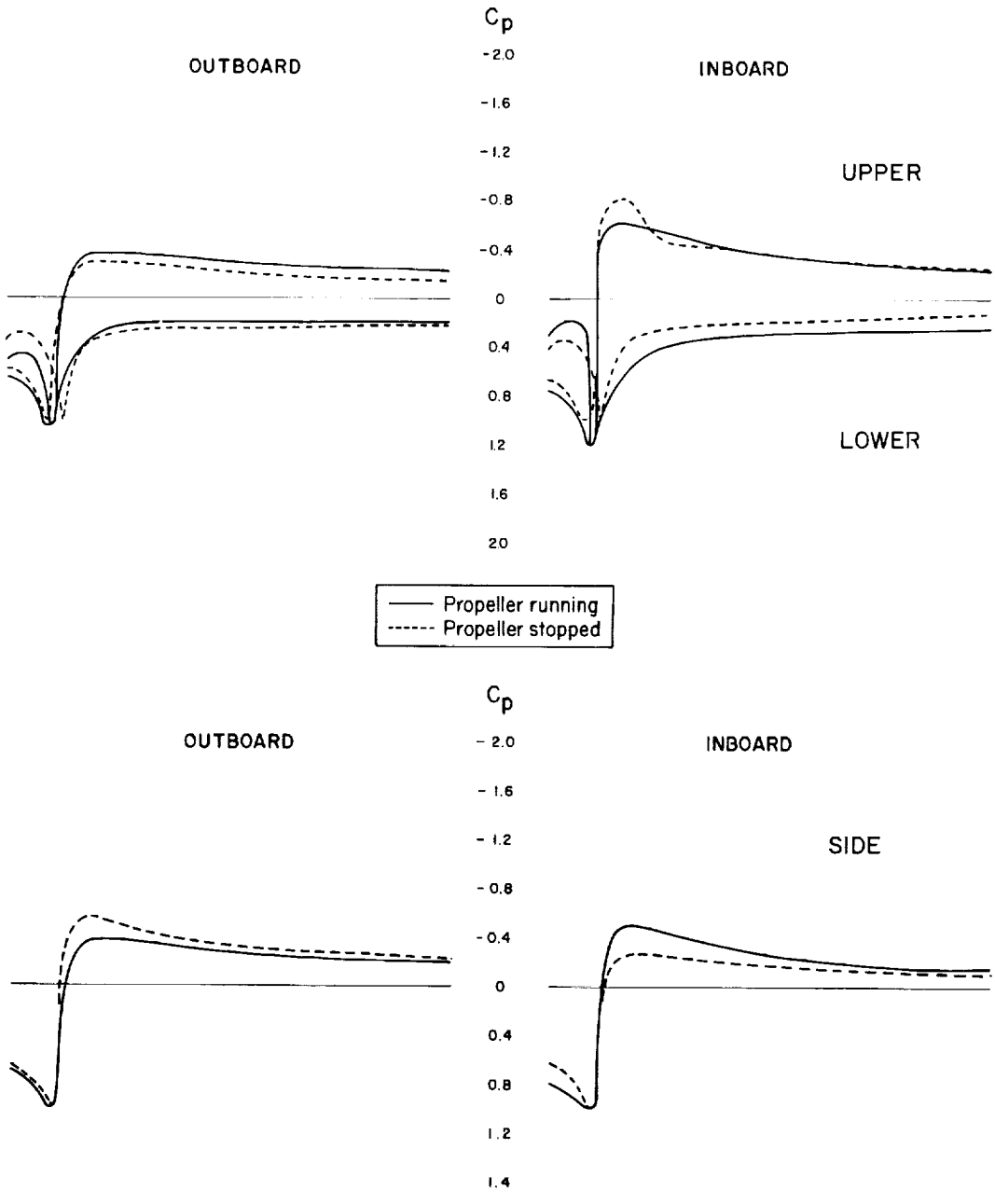

Figure 59. - External pressure distributions for 0.3F inlet.

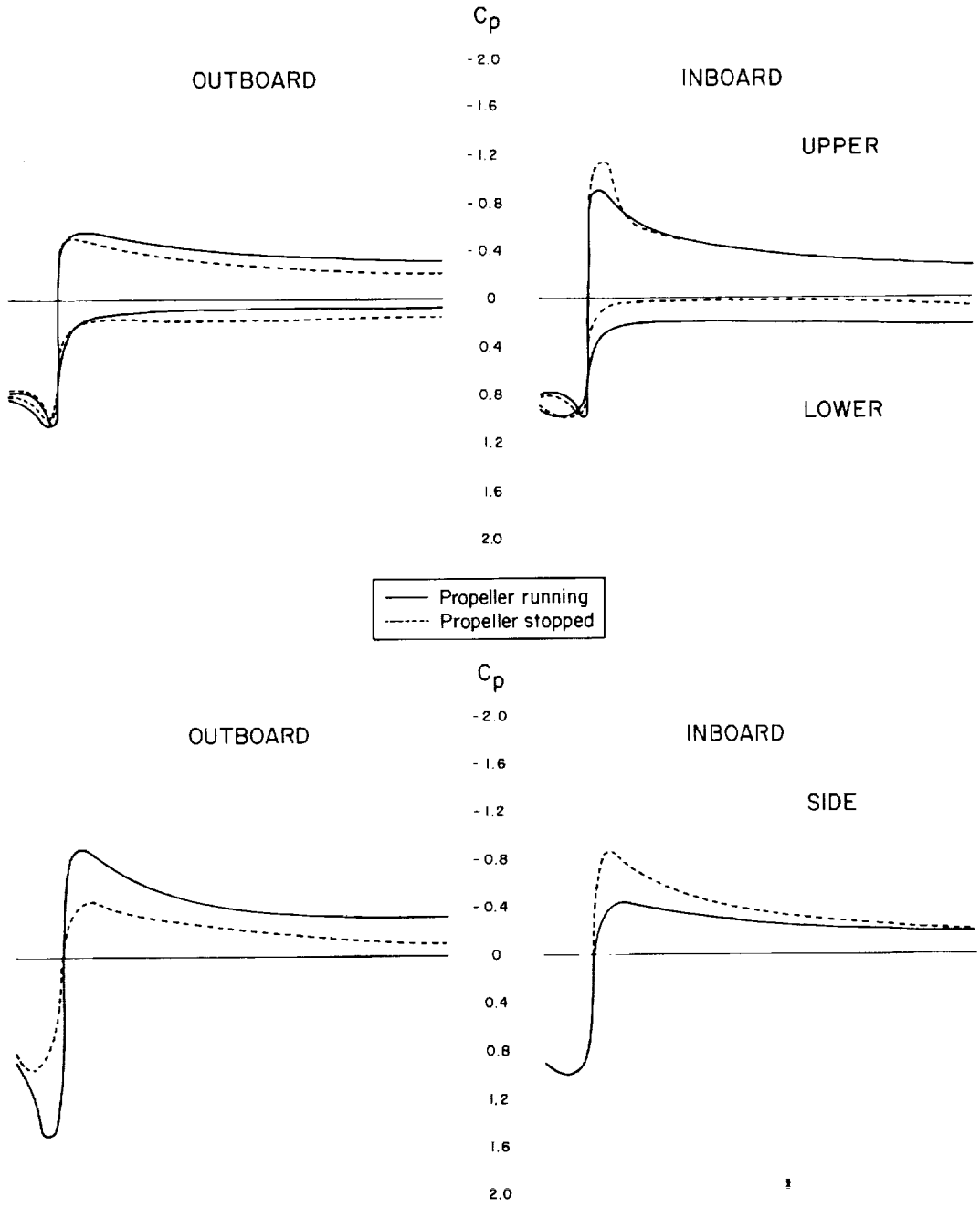

Figure 60. - External pressure distributions for 0.6F inlet.

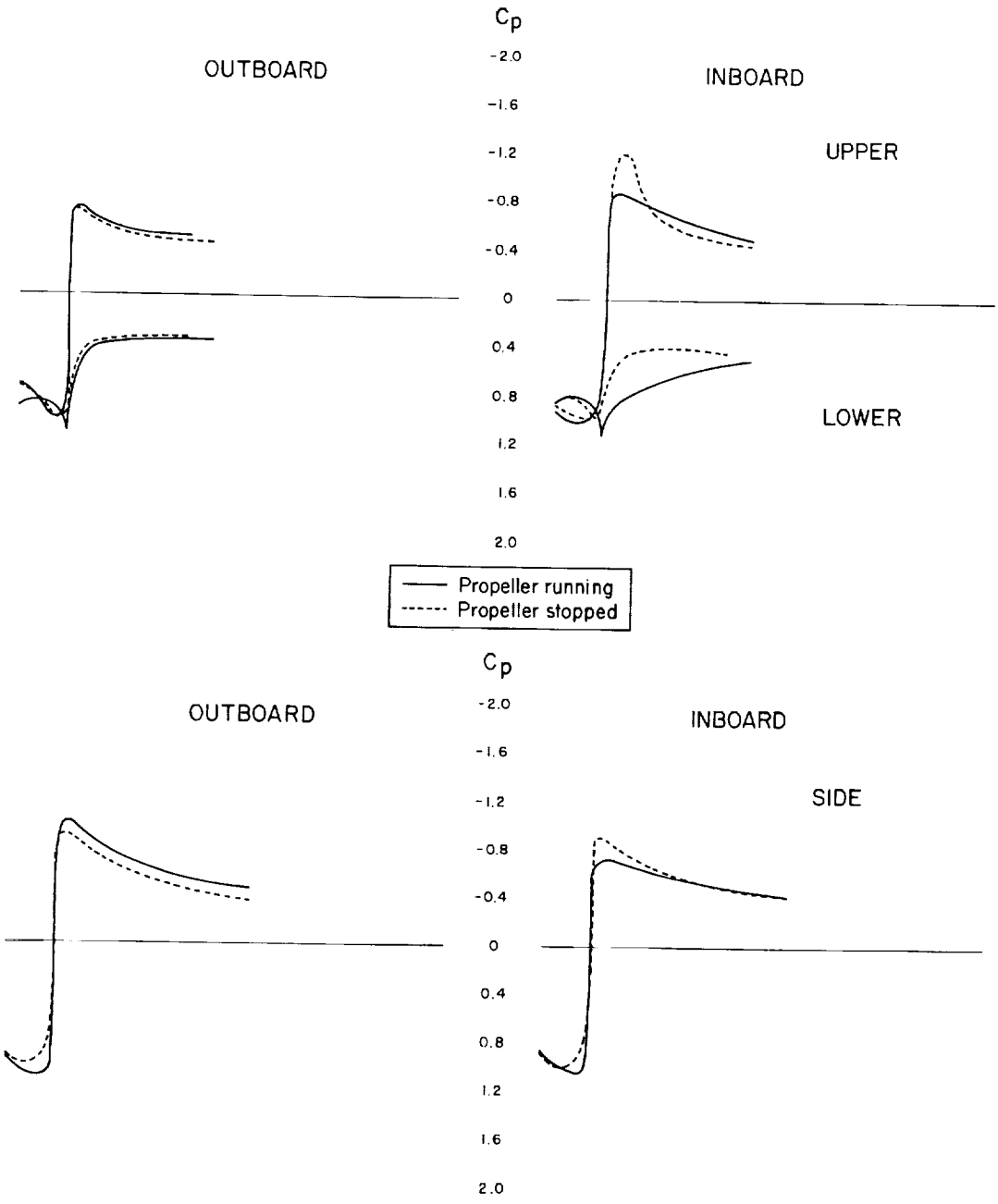

Figure 61. - External pressure distributions for 0.3A inlet.

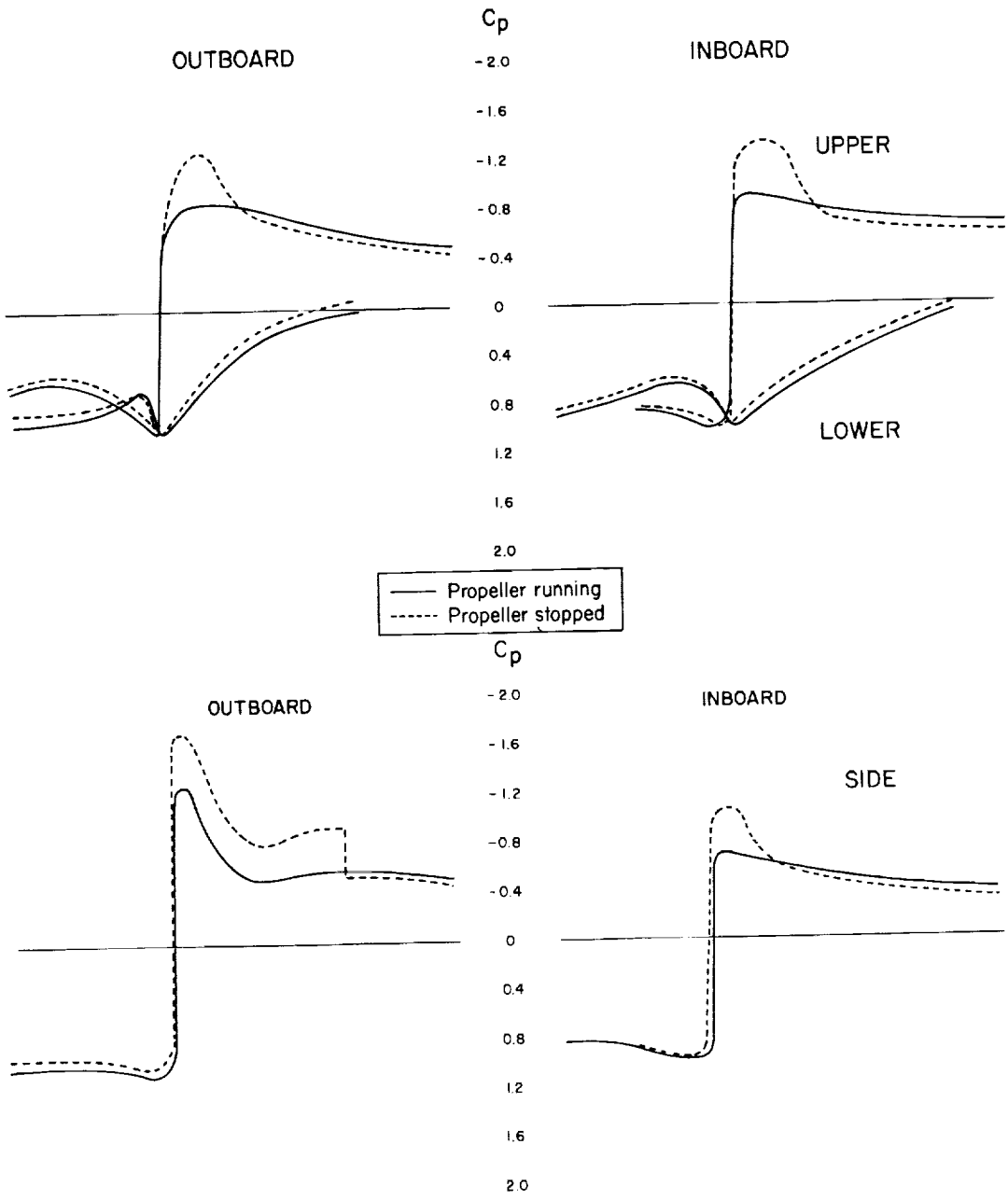

Figure 62. - External pressure distributions for GAC inlet.

Figure 63. - Original PA-41P exit configuration.

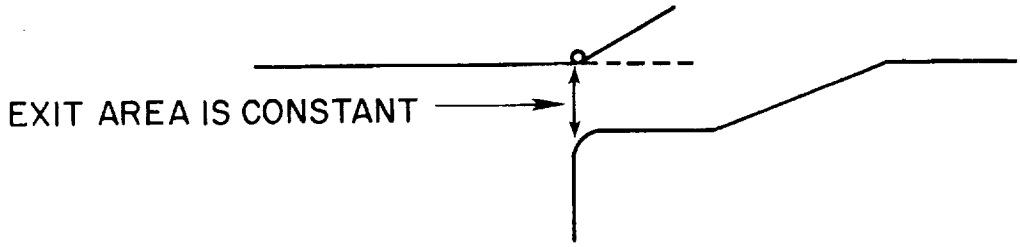

(a) exit area constant

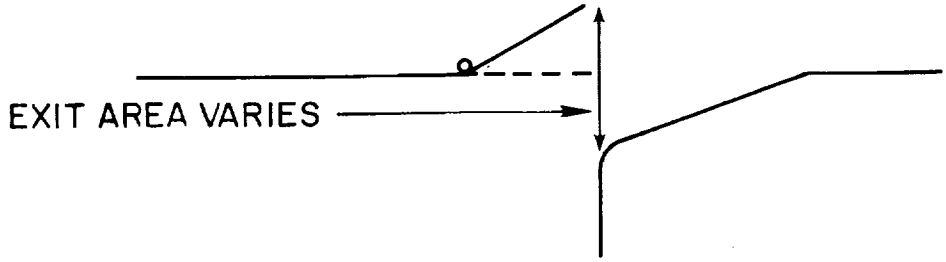

(b) exit area variable

Figure 64. - Cowl flap arrangements.

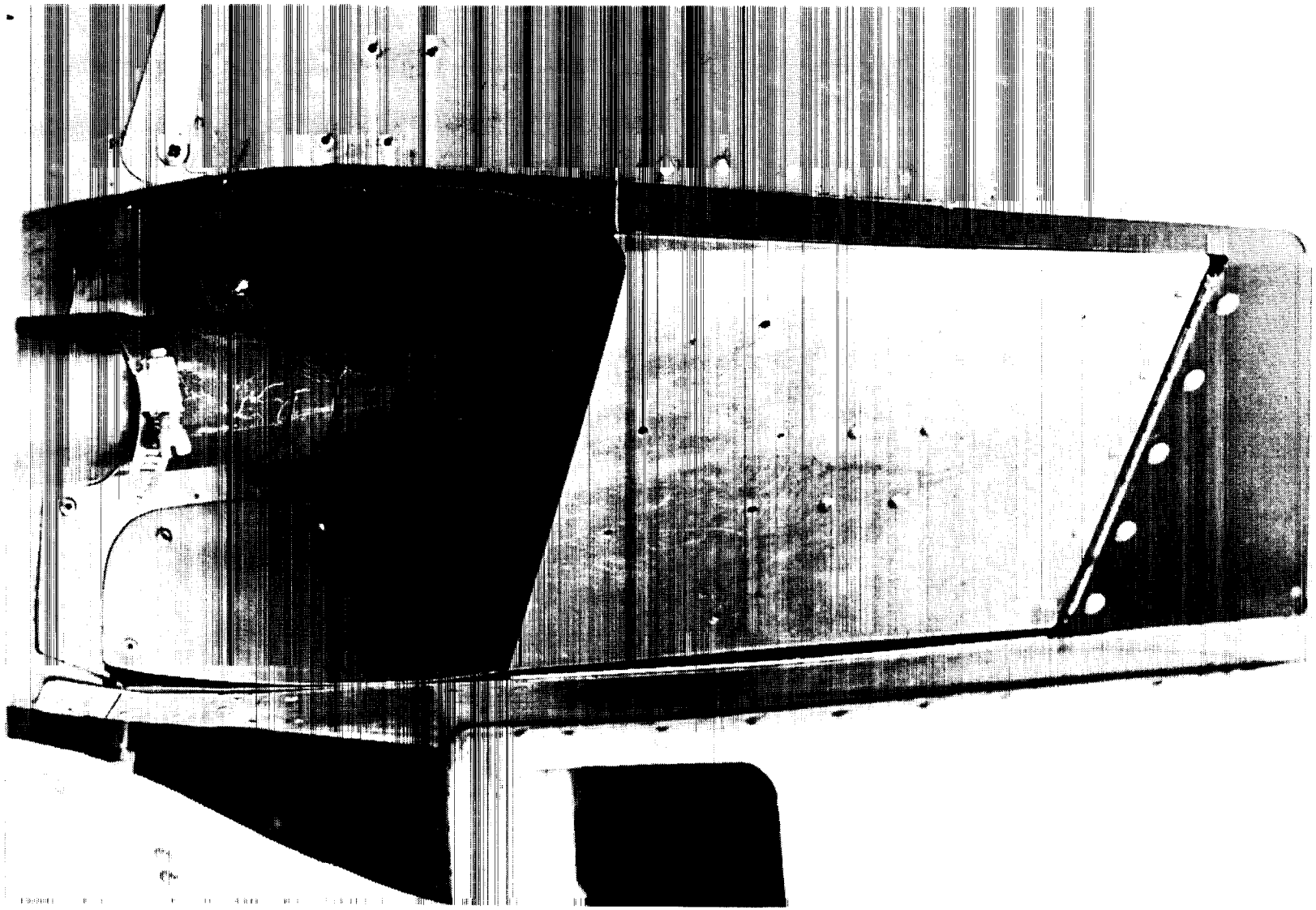

(a) no restriction, 150% original.

Figure 65. - Exit area variation.

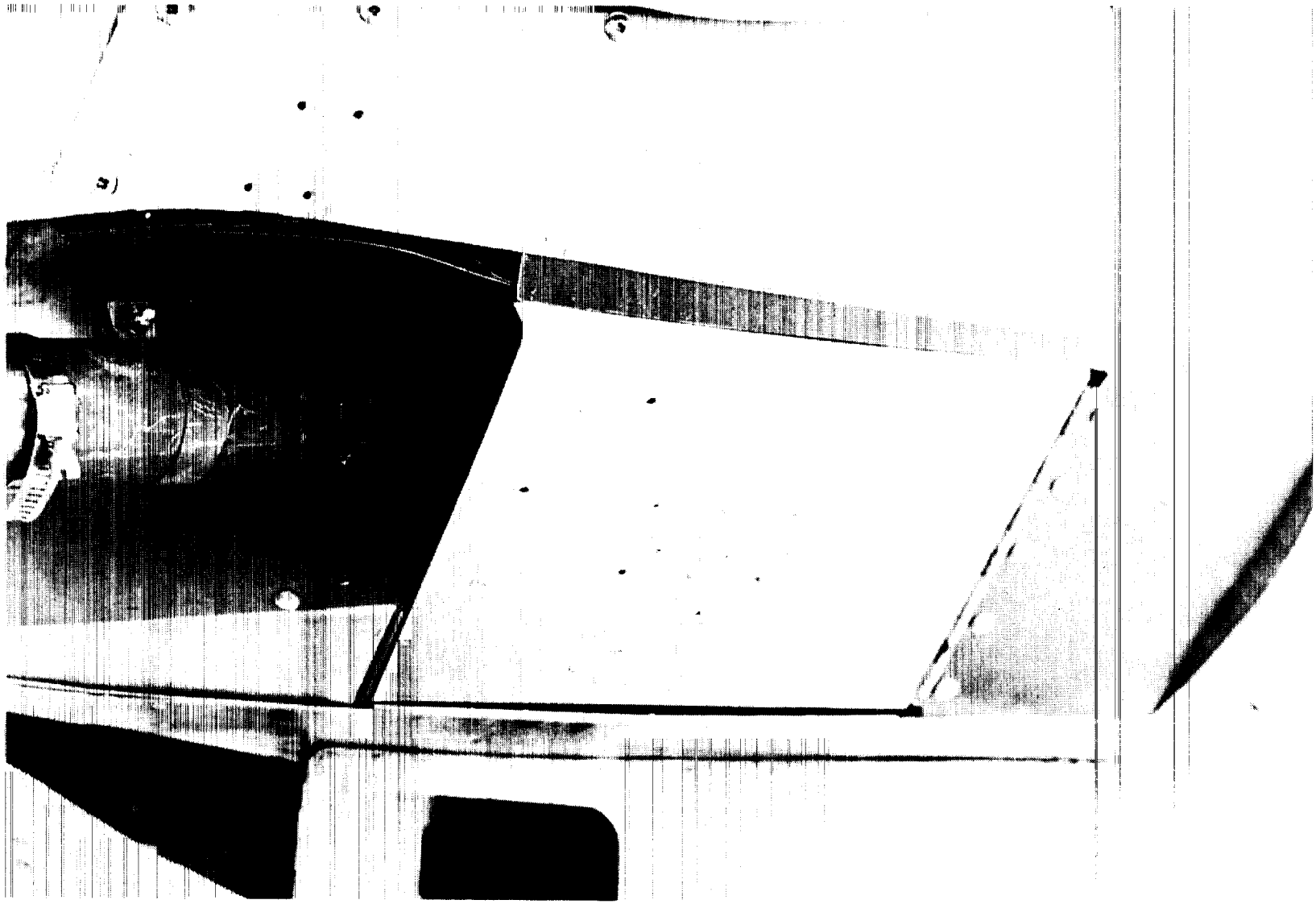

(b) partial restriction, 100% original.

Figure 65. - Continued.

(c) full restriction, 50% original.

Figure 65. - Concluded.

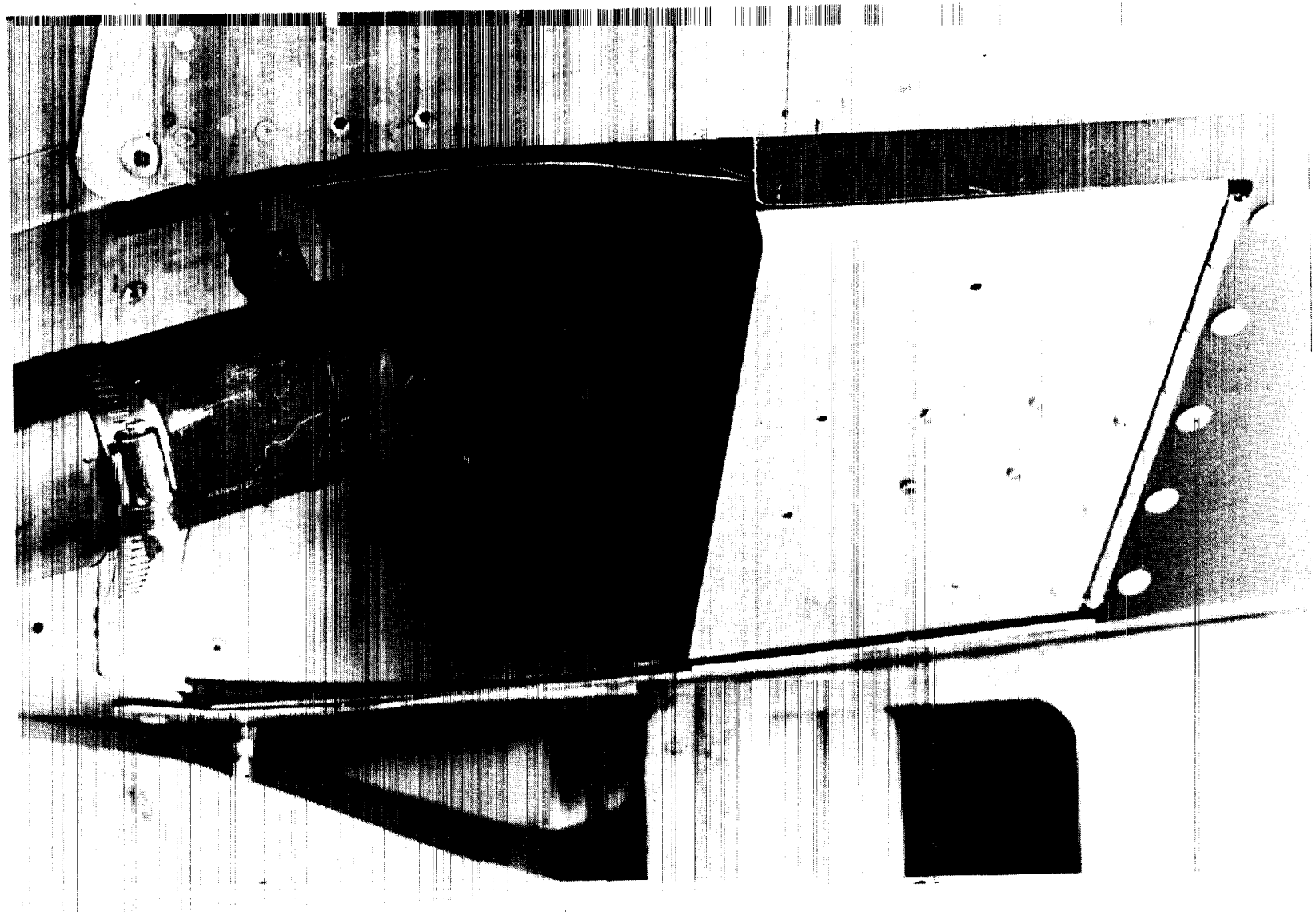

(a) short, 1.5 aspect ratio.

Figure 66. - Cowl flap variation.

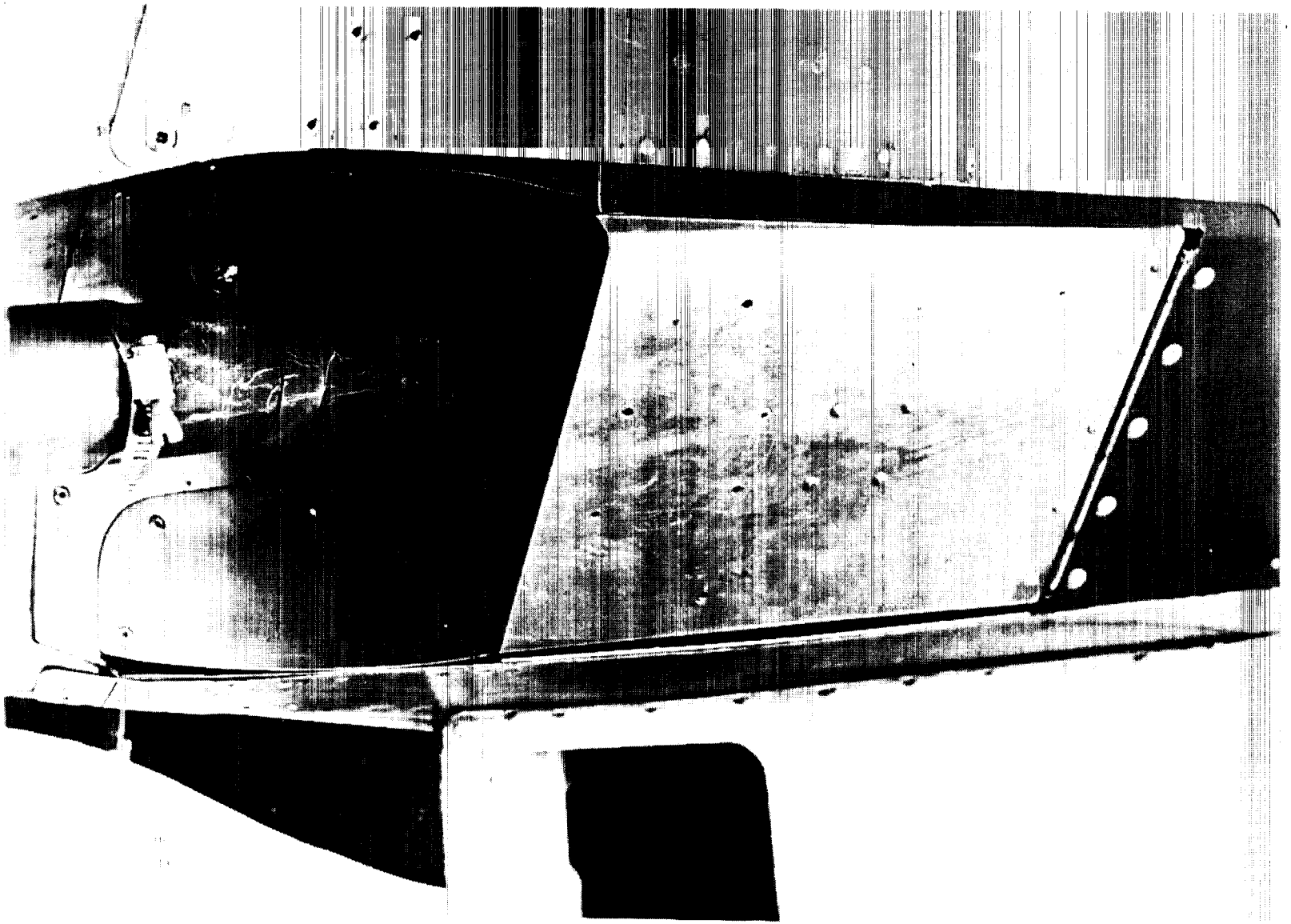

(b) medium, 0.75 aspect ratio.

Figure 66. - Continued.

(c) long, 0.55 aspect ratio.

Figure 66. - Concluded.

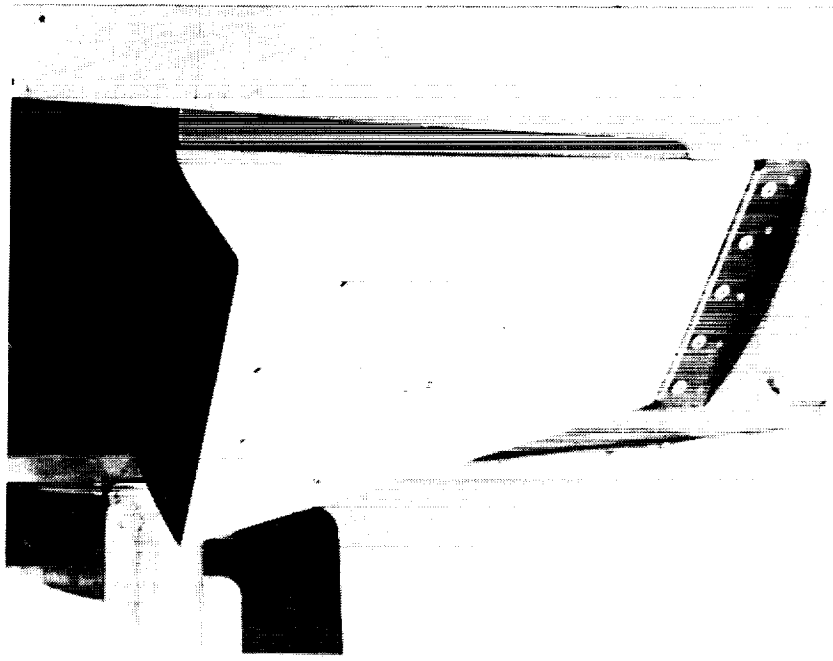

(a) long cowl flap.

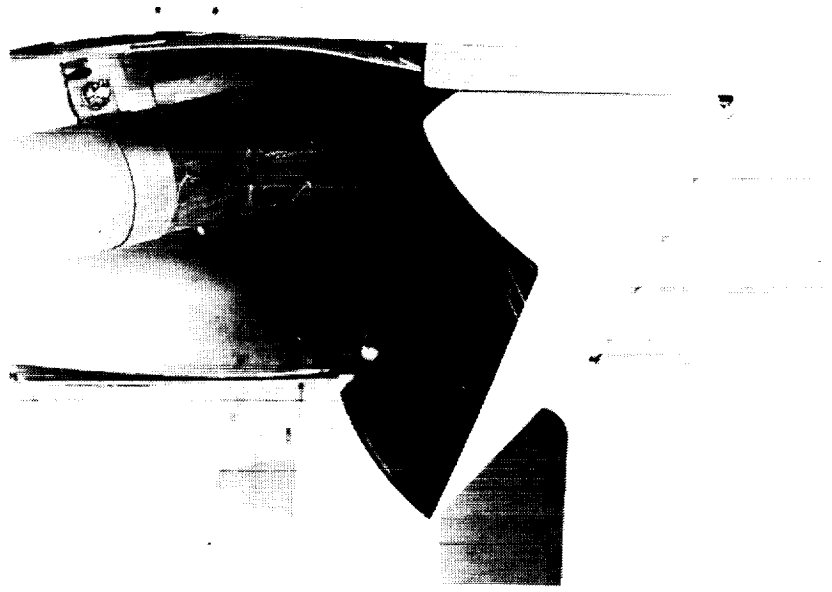

(b) short cowl flap.

Figure 67. - Maximum cowl flap deflection.

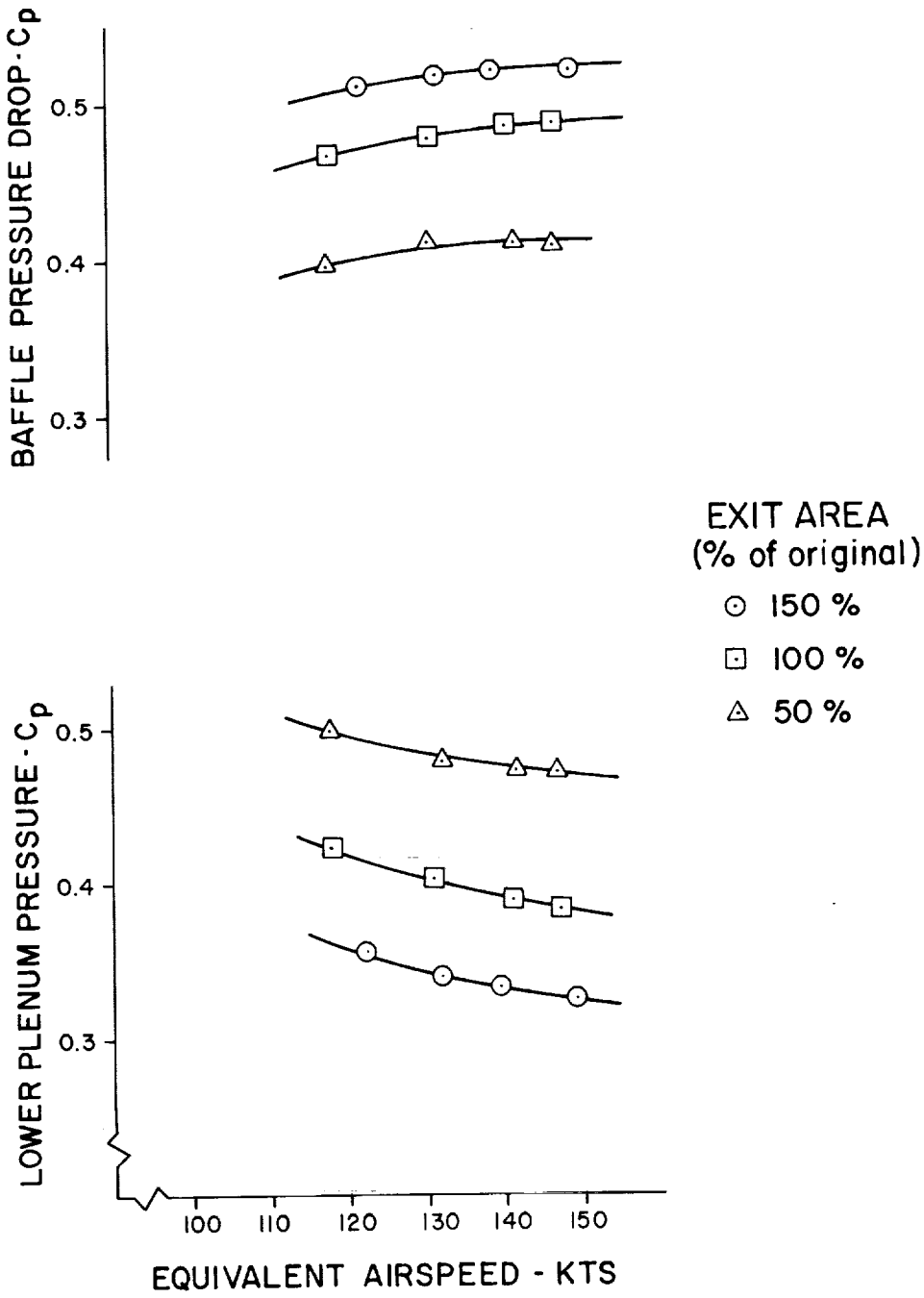

Figure 68. - Effect of exit area on lower plenum pressure and engine baffle pressure drop.

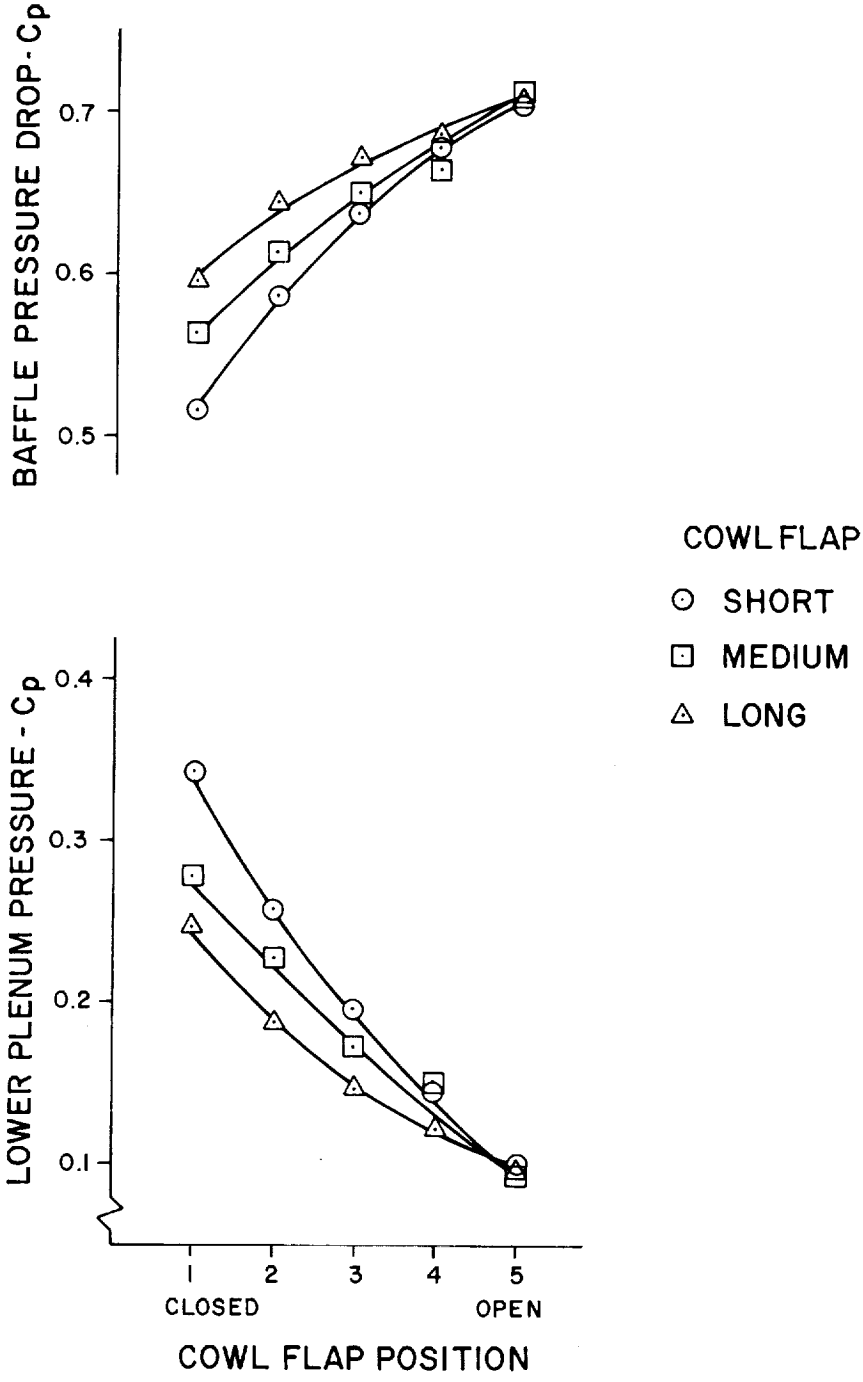

Figure 69. - Effect of cowl flap aspect ratio on lower plenum pressure and engine baffle pressure drop for low speed cruise power flight condition.

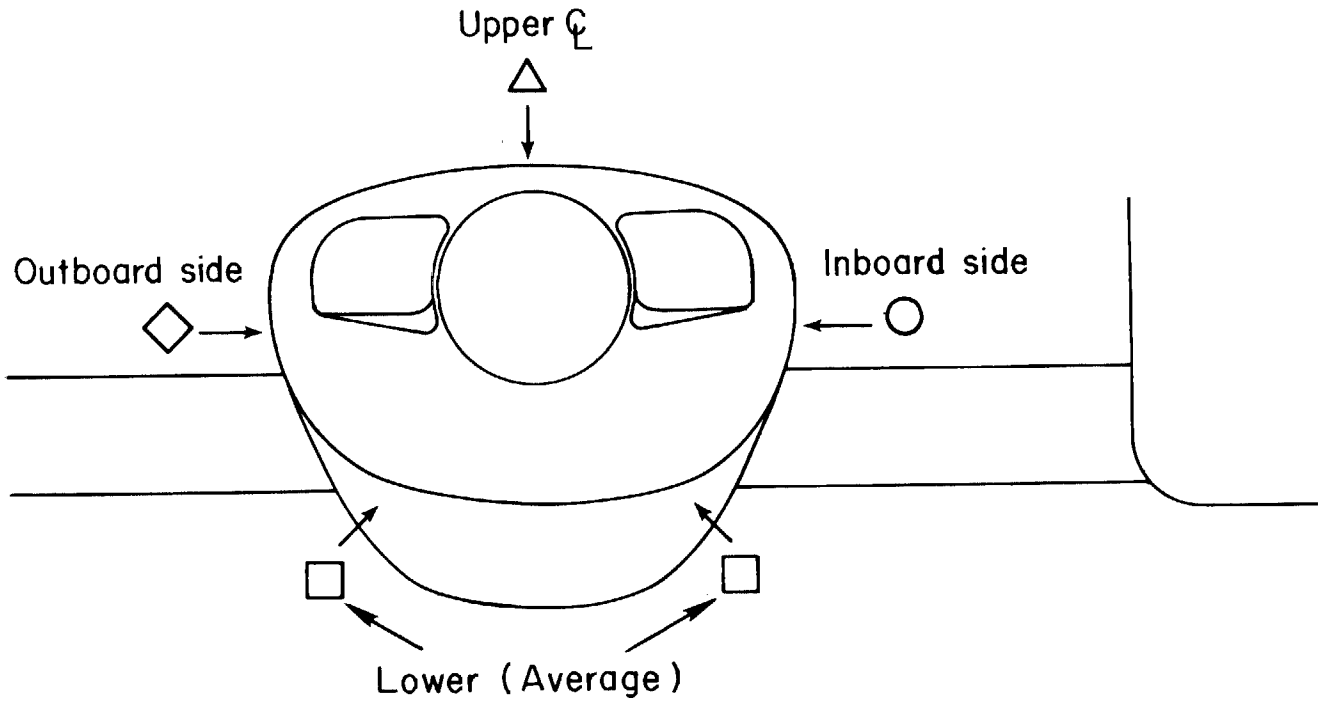

Figure 70. - Static pressure belt locations on the nacelle.

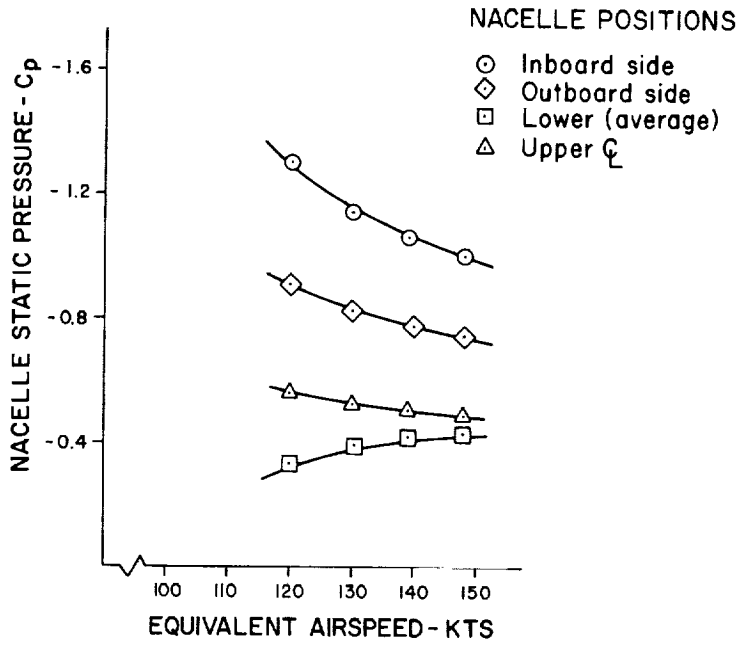

Figure 71. - Nacelle static pressure for cruise condition.

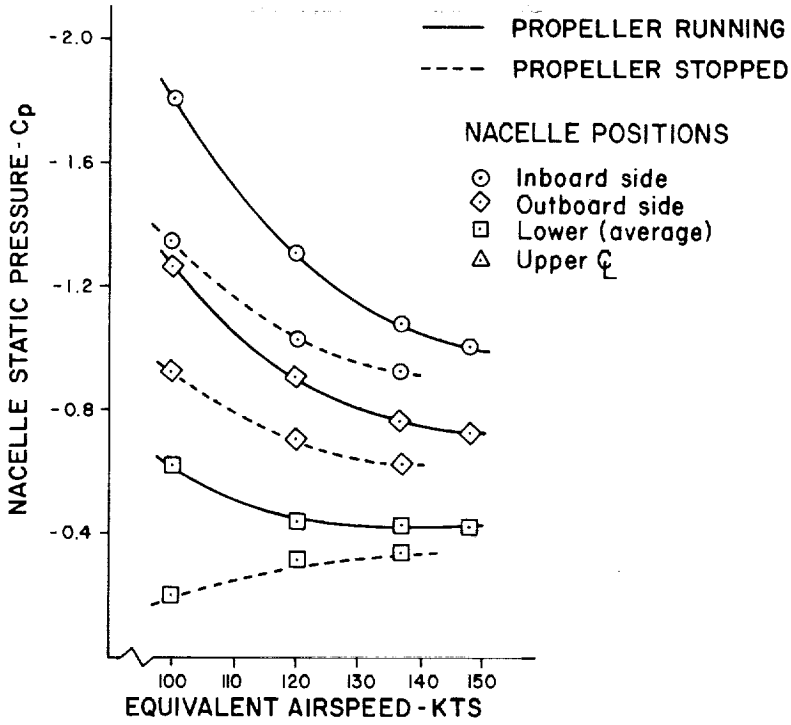

Figure 72. - Nacelle static pressure for climb power.

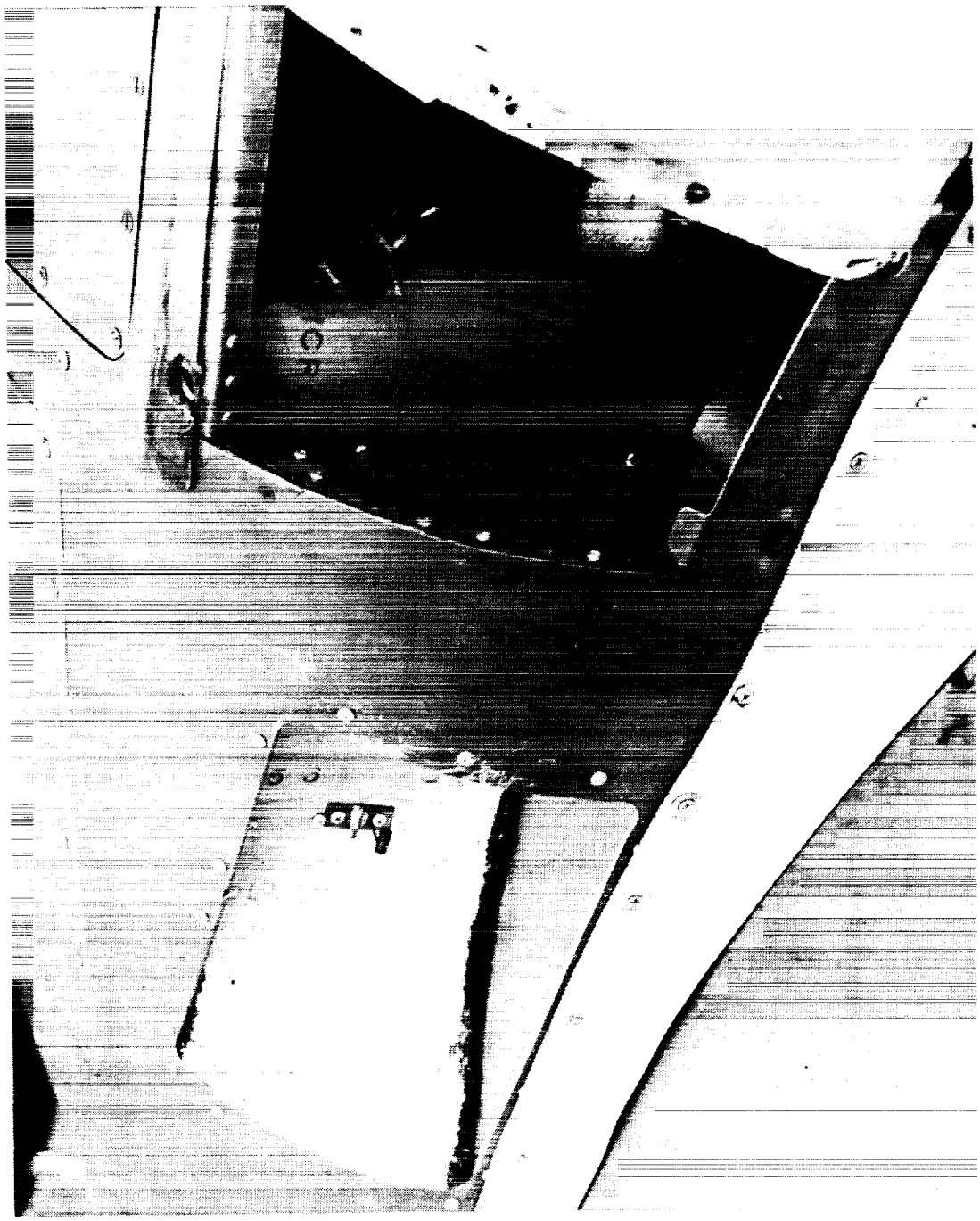

Figure 73. - Installation of upper surface exits.

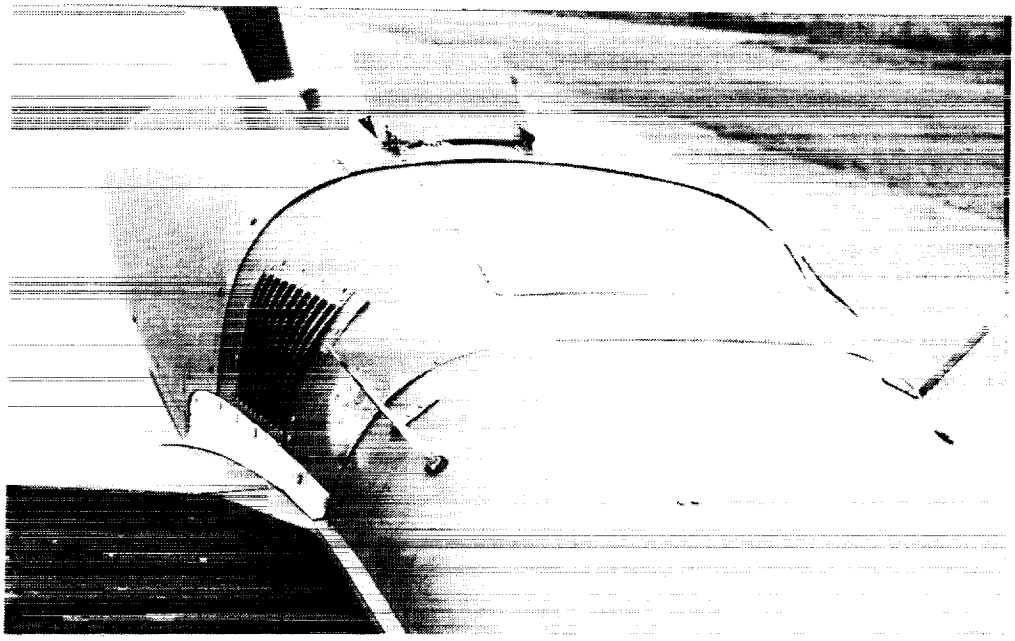

(a) inboard side

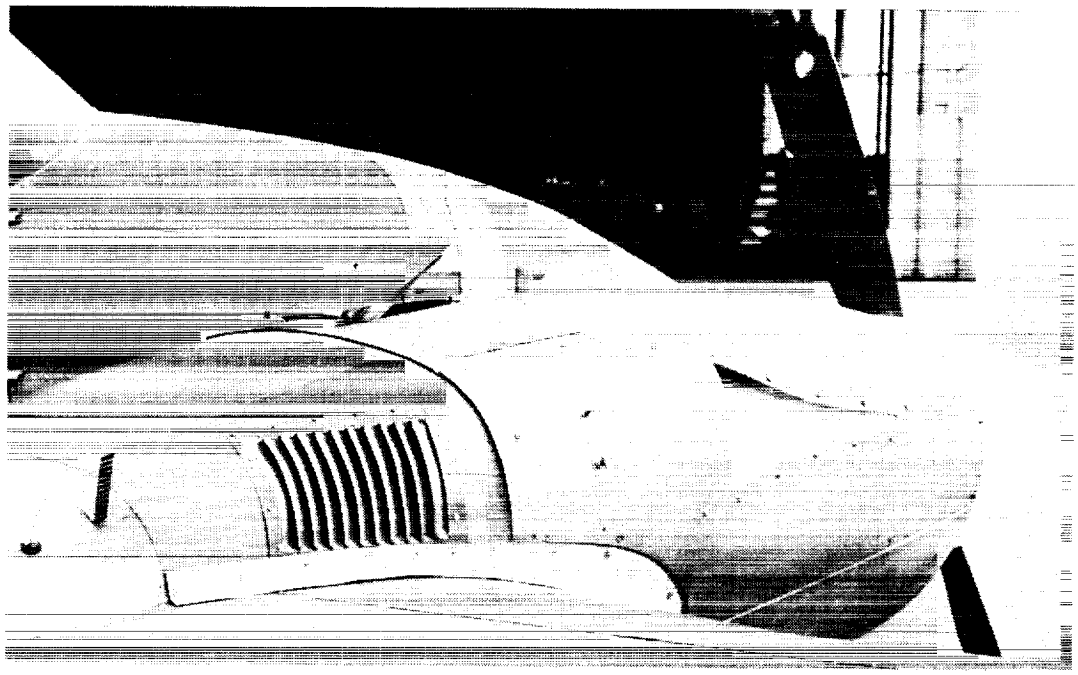

(b) outboard side

Figure 74. - Upper surface exits.

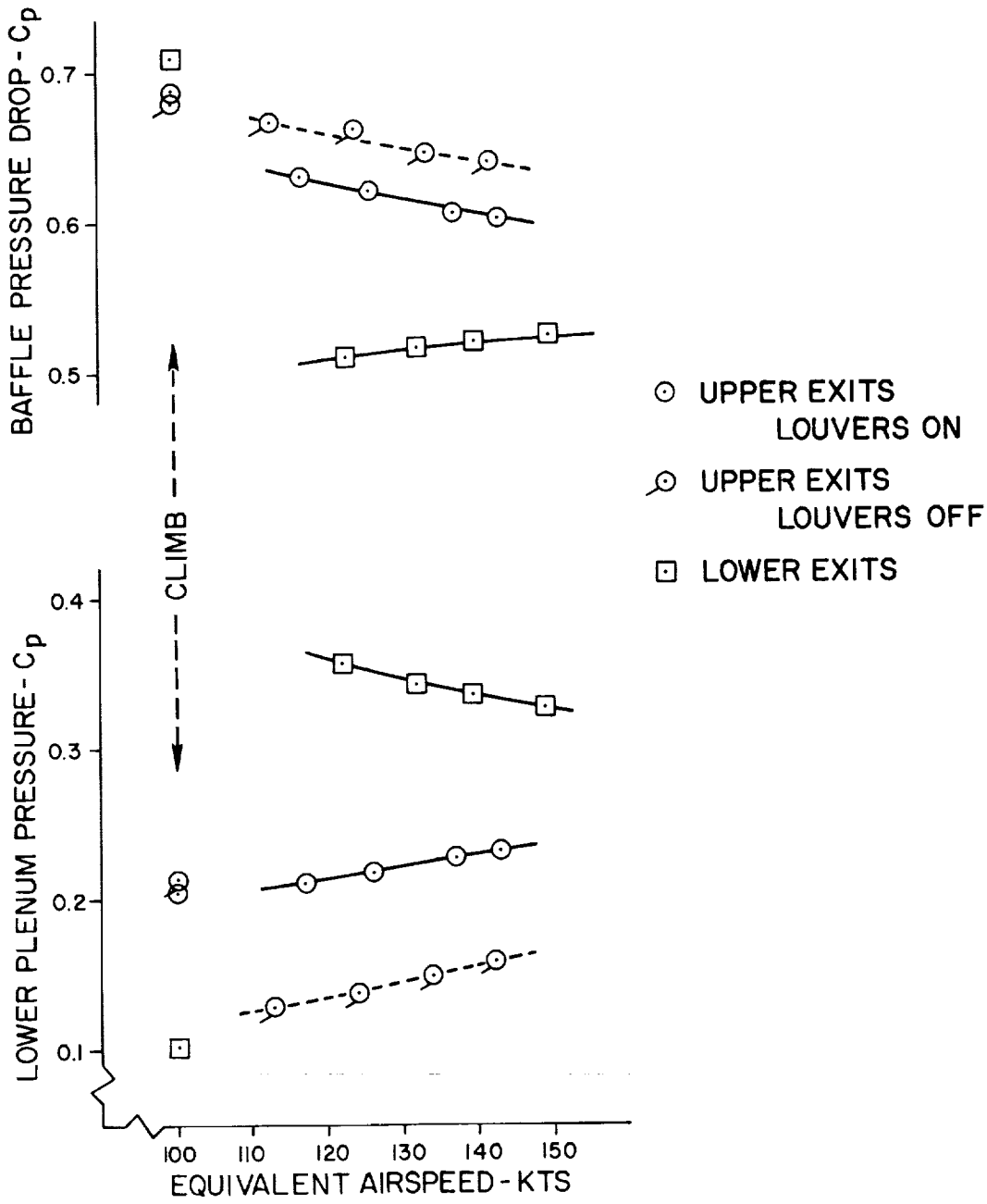

Figure 75. - Upper surface exit location effects on lower plenum pressure and engine baffle pressure drop.

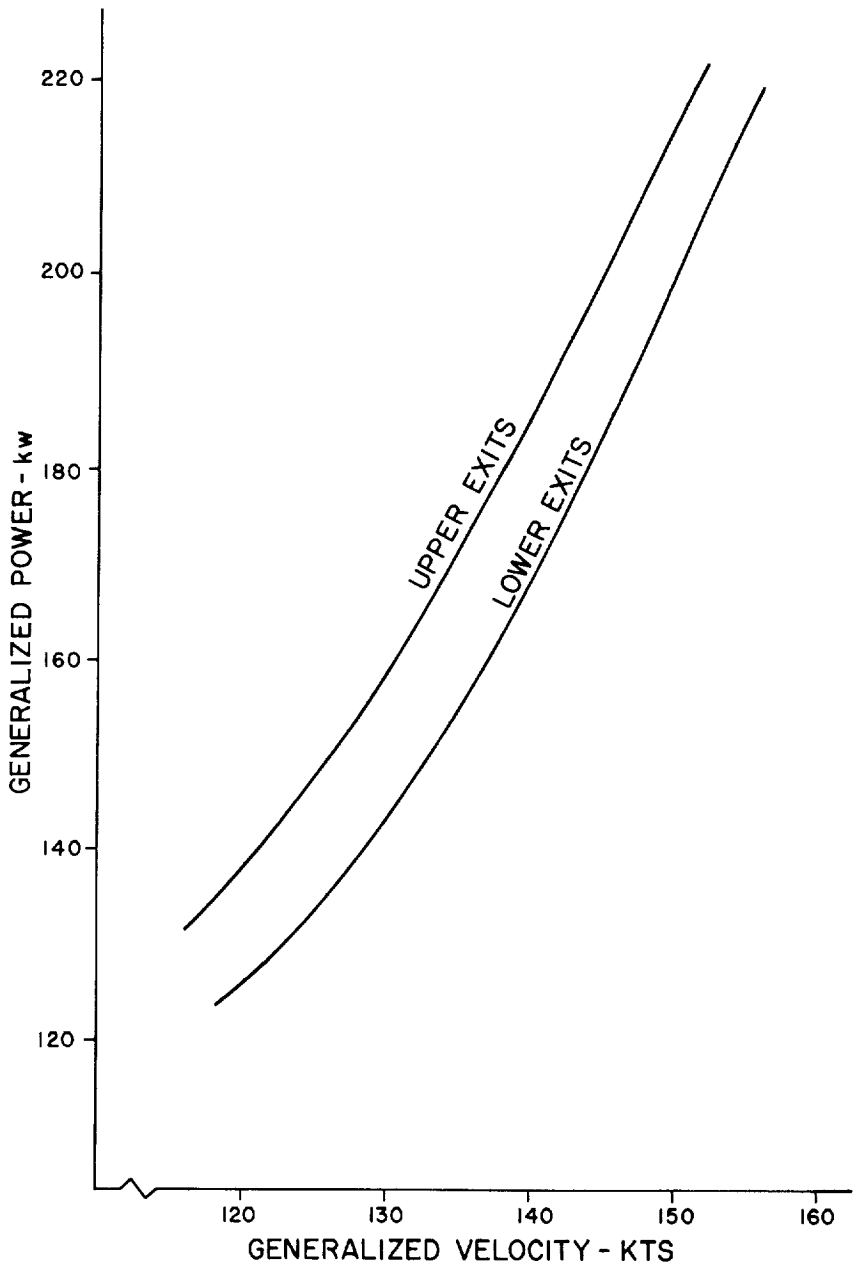

Figure 76. - Effect of upper surface exits on aircraft drag.

1. Report No.	2. Government Accession No.	3. Recipient's Catalog No.
NASA CR-3405		

4. Title and Subtitle	5. Report Date
AN EXPERIMENTAL INVESTIGATION OF THE AERODYNAMICS AND COOLING OF A HORIZONTALLY-OPPOSED AIR-COOLED AIRCRAFT ENGINE INSTALLATION	March 1981
	6. Performing Organization Code

7. Author(s)	8. Performing Organization Report No.
Stan J. Miley,* Ernest J. Cross, Jr.,* John K. Owens,** and David L. Lawrence***	
	10. Work Unit No.

9. Performing Organization Name and Address	11. Contract or Grant No.
Mississippi State University Aerophysics and Aerospace Engineering P. O. Drawer A or AP Mississippi State, MS 39762	NSG-1083
	13. Type of Report and Period Covered
12. Sponsoring Agency Name and Address	Contractor Report
National Aeronautics and Space Administration Washington, DC 20546	14. Sponsoring Agency Code 505-41-13-01

15. Supplementary Notes

Langley Technical Monitor: Albert W. Hall. Final Report.
*Stan J. Miley and Ernest J. Cross, Jr., Texas A&M University, College Station, Texas 77843; **John K. Owens, Mississippi State University, Mississippi State, Mississippi 39762, ***David L. Lawrence, Turbo West Corporate Aircraft Center, Broomfield, Colorado 80020.

16. Abstract

A flight-test based research program was performed to investigate the aerodynamics and cooling of a horizontally-opposed engine installation. Specific areas investigated were the internal aerodynamics and cooling mechanics of the installation, inlet aerodynamics, and exit aerodynamics. The applicable theory and current state-of-the-art are discussed for each area. Flight-test and ground-test techniques for the development of the cooling installation and the solution of cooling problems are presented.

The results show that much of the internal aerodynamics and cooling technology developed for radial engines are applicable to horizontally-opposed engines. Correlation is established between engine manufacturer's cooling design data and flight measurements of the particular installation. Also, a flight-test method for the development of cooling requirements in terms of easily measurable parameters is presented. The impact of inlet and exit design on cooling and cooling drag is shown to be of major significance.

17. Key Words (Suggested by Author(s))	18. Distribution Statement
Cooling drag Aircraft performance Horizontally opposed engines Subsonic inlets and exits	Unclassified - Unlimited Subject Category 02

19. Security Classif. (of this report)	20. Security Classif. (of this page)	21. No. of Pages	22. Price
Unclassified	Unclassified	151	A08

For sale by the National Technical Information Service, Springfield, Virginia 22161

NASA-Langley, 1981